Radial glia synchronous activity modulates visual responses and functional connectivity in the zebrafish optic tectum

Sergio Alejandro Uribe

PSL UNIVERSITÉ PARIS

THÈSE DE DOCTORAT
DE L'UNIVERSITÉ PSL

Préparée à L'École normale supérieure

L'activité synchrone de la glie radiale régule les réponses visuelles et la connectivité fonctionnelle dans le toit optique du poisson zèbre

Soutenue par

Sergio Alejandro Uribe

Le 29 Septembre 2022

Ecole doctorale n° ED158

Cerveau, cognition, comportement (ED3C)

Spécialité

Neurosciences

Composition du jury :

Cendra, AGULHON CR-HDR, Université Paris Cité	*Présidente*
Gertrudis, PEREA DR, The Cajal Institute-CSIC	*Rapporteure*
Takashi, KAWASHIMA PU, The Weizmann Institute of Science	*Rapporteur*
Glenn, DALLERAC CR, Institut des Neurosciences Paris	*Examinateur*
German, SUMBRE DR, Ecole Normale Supérieure	*Directeur de thèse*

1794

ENS

ÉCOLE NORMALE SUPÉRIEURE

Abstract

Initial observations of astrocytes confined these cells to just passive elements that served to fill the gaps between neurons with merely secondary or supportive roles. However, over the past decades, recent studies suggest that astrocytes are involved in several brain functions once considered specific to neurons. Astrocytes and neurons have a reciprocate communication in which astrocytes sense neuronal inputs mainly by Ca^{2+} signaling and in turn, influence neuronal activity. This bilateral dialogue has important implications for synaptic functions including synaptic transmission and plasticity. Most recently, studies *in vivo* have highlighted the astrocytes' roles in more complex functions such as memory, learning, perception processing, sleep-wakefulness cycle, and arousal states among others. Despite these advances, the role of glia in visual processing remains elusive. Here, I addressed this open question through a comprehensive *in vivo* approach using the visual system of an intact, non-anesthetized, non-paralyzed vertebrate. We use transgenic zebrafish larvae expressing genetically encoded calcium indicators (GECIs) in neurons and radial glia cells (functional analogous to mammalian astrocytes), two-photon microscopy, optogenetics, and motor behavior. These approaches enabled monitoring with single-cell resolution of the neuronal and radial glia cells (RGCs) dynamics in the zebrafish's main visual center, the optic tectum (OT) while simultaneously the tail behavior was recorded.

My findings are organized along 5 main axes:

1. **Tectal RGCs synchronize their Ca^{2+} transients following an escape behavior.** We found that individual RGCs displayed synchronous Ca^{2+} transients across the RGC population only in the ventral layers of the optic tectum. These synchronous events were followed specifically by escape behaviors and not by other types of movements.

2. **Muscle proprioception does not play a role in RGC Ca^{2+} synchronization.** Paralyzed larvae still showed the RGC synchronization.

3. **Tectal RGC synchronization is mediated by the locus Coeruleus (LC).** We observed that LC projections innervate the optic tectum neuropil. Furthermore, LC optogenetic stimulation induced RGC synchronous Ca^{2+} events without triggering any type of tail movement responses. On the other hand, LC ablation suppressed the Ca^{2+} synchronization without affecting tail movements. These results suggest that LC activity is necessary and sufficient for tectal RGC synchronization. However, the escape behaviors and tectal RGC synchronization share a common input rather than having a causal relationship. The latter is also supported by ablations of the motor circuits which did not affect the tectal RGC synchronizations.

4. **RGC synchronization modulates the directional selectivity of tectal neu-**

rons. We found that RGCs did not respond to visual stimuli (small light dots and moving bars). However, the neuronal responses to the moving bars but not to the small light dots were significantly reduced during the RGC synchronizations. Notably, the number of direction-selective neurons to moving bars decreases after the onset of RGCs Ca^{2+} synchronization events.

5. **RGC synchronous events modulate the functional correlations between tectal neurons.** To understand the interactions between RGCs and tectal neurons, we analyzed spontaneous neuronal Ca^{2+} dynamics after laser ablation of the LC. We observed that the pair-wise correlations between the spontaneous activity of tectal neurons (functional connectivity) were significantly reduced only between distant neurons during periods of RGC synchronizations (correlations between nearby neurons remained unchanged).

Overall, our results suggest the following scenario: a switch to an arousal state induces the activity of the LC. LC-NE projections to the tectum generate synchronous Ca^{2+} events among the ventral population of RGCs. The RGC synchronous events modulate the directional selectivity of tectal neurons and prune their functional correlations to adapt the larva's visual system to cope with the environmental context associated with an arousal state. This multidisciplinary approach provides a comprehensive view of how neuro-glia interactions adapt the visual system to an arousal state.

Résumé en français

0.1 Introduction

Les astrocytes jouent un rôle important dans le soutien des neurones (par exemple, la clairance des neurotransmetteurs, le tampon ionique, la régulation du flux sanguin et l'apport de métabolites). Bien qu'ils n'affichent pas de potentiels d'action, ils présentent d'important dynamique du Ca^{2+} en réponse à l'activité neuronale, à la stimulation sensorielle et à la locomotion. Ce Ca^{2+} dynamique peuvent déclencher la libération de plusieurs gliotransmetteurs tels que le glutamate, l'ATP et la D-sérine, qui sont capables de moduler la transmission synaptique neuronale.

Des études récentes ont montré que les astrocytes de l'hippocampe induisent une potentialisation synaptique, améliorant l'acquisition de la mémoire et améliorant le comportement cognitif chez la souris. De plus, les astrocytes déclenchent des transitions synchronisées vers des états supérieurs dans les neurones corticaux voisins chez la souris et assurent la transition entre les états de travail et de repos. Ces changements d'état globaux impliquent la libération de noradrénaline (NE) à l'échelle du cerveau, qui est associée à des états d'éveil et de vigilance. En outre, le comportement moteur déclenche l'augmentation de Ca^{2+} dans les astrocytes en réponse à une stimulation visuelle. Ces études et plusieurs autres suggèrent que les astrocytes jouent un rôle important dans les calculs cérébraux.

Chez le poisson zèbre, il a été proposé que les astrocytes radiaux (AR) aient une fonction analogue à celle des astrocytes de mammifères. Contrairement aux mammifères, les RA chez le poisson zèbre ne dégénèrent pas; ils ont élaboré des processus et expriment des protéines considérées comme des marqueurs spécifiques des astrocytes (par exemple, l'aquaporine-4, les marqueurs des jonctions serrées, les transporteurs de la glutamine synthétase et du glutamate). Des études récentes montrent que les RA dans le cerveau postérieur des larves de poisson zèbre fonctionnent comme des intégrateurs de réponses de nage futiles au flux visuel lorsqu'ils sont privés de rétroaction visuelle. Cette intégration permet aux larves de passer à un état comportemental quiescent. De plus, dans le cerveau antérieur du poisson zèbre, l'activité des RA est anti-corrélée avec des rafales d'activité neuronale, ce qui suggère que les RA peuvent réguler l'activité neuronale. Au cours de l'épilepsie induite, des perturbations de ces interactions glie-neurones conduisent à l'apparition de crises d'épilepsie. Cependant, le rôle fonctionnel des RA dans le système visuel est inconnu.

Ici, nous avons utilisé la microscopie de deux photons et des larves de poisson zèbre transgéniques exprimant des indicateurs de Ca^{2+} génétiquement codés dans les RA et les neurones, pour étudier le rôle des cellules gliales durant les transitions de comportement.

Nous avons découvert que les neurones du locus coeruleus (LC) qui produit NE et sont associés aux états d'éveil déclenchent des événements de synchronisation du Ca^{2+} dans les RA dans le toit optique (TO). Ces synchronisations du RA modulent la sélectivité en direction des neurones et sa connectivité fonctionnelle du circuit dans le TO. Nous proposons que les synchronisations du Ca^{2+} dans le RA induites par LC sont fondamentales pour adapter le système visuel aux nouvelles contraintes contextuelles et comportementales.

0.2 Résultats

0.2.1 RA synchronise son Ca^{2+} activité dans le TO suite à un comportement d'échappement

Pour étudier le rôle fonctionnel des RA dans le traitement visuel, nous avons d'abord caractérisé l'activité Ca^{2+} spontanée des RA dans le TO. À cette fin, nous avons utilisé la microscopie par excitation à deux photons pour imager 6 à 7 jours après la fécondation des larves de poisson zèbre exprimant l'indicateur Ca^{2+} génétiquement codé GCaMP-7a ou GCaMP6m sous un promoteur glial. Nous avons constaté que les RA individuels affichaient sporadiquement de l'augmentation synchrone de Ca^{2+} sur l'ensemble de la population de RA imagée. En utilisant de une caméra de vidéo à grande vitesse en combinaison avec le microscope à deux photons, nous avons observé que les événements synchrones du RA sont suivaient pour les mouvements de la queue. L'amplitude moyenne du Ca^{2+} associés aux comportements d'échappement était significativement plus grande que celle associée aux petites déviations de la queue. De plus, nous avons trouvé que pendant les 10 première secondes après le début d'événements de synchrones du Ca^{2+} la probabilité d'observer des comportements moteurs supplémentaires a diminué de manière significative.

Les RA se trouvent dans tout le volume de le TO. Cependant, l'imagerie Ca^{2+} à deux photons de l'activité RA à différents plans optiques du TO a révélé que les événements du synchronisation du Ca^{2+} dans les RA sont spécifiques à la région ventrale (90-100 µm de la surface dorsale). Les régions du TO à moins de 60-80 µm de la surface dorsale ont montré du Ca^{2+} synchrone avec une fréquence significativement plus court. Dans l'ensemble, ces résultats suggèrent que les RA dans les régions ventrales de le TO synchronisent leurs augmentation du Ca^{2+}, agissant comme une seule unité suivant les comportements moteurs d'échappement.

0.2.2 La proprioception musculaire ne joue aucun rôle dans les synchronisations du Ca^{2+} dans les RA

Étant donné que les synchronisations des RA se produisent quelques secondes après un mouvement d'échappement, il est possible que la proprioception musculaire de la queue soit impliquée dans ce phénomène. Pour tester cette hypothèse, nous avons effectué une imagerie Ca^{2+} à deux photons du RA dans le TO chez les larves paralysées. Dans ces conditions, les RA affichaient toujours des événements synchrones spontanés au Ca^{2+}. Pour tester si ces événements synchrones au Ca^{2+} dans les RA spontanés étaient associés

à des comportements d'échappement, nous avons stimulé les larves paralysées à l'aide de stimuli électriques légers qui induisent des comportements d'échappement. Nous avons constaté que les RA des larves paralysées présentaient des événements synchrones au Ca^{2+} robustes. Ceci suggère que la synchronisation des RA ne dépend pas de la proprioception musculaire. Par conséquent, la synchronisation RA peut être déclenchée par une copie efférente d'un centre moteur ou médiée par un processus parallèle à la génération du comportement moteur de la queue.

0.2.3 La synchronisation au Ca^{2+} des RA dans le TO est médiée par le locus coeruleus

Chez les vertébrés, le LC est la source principale de NE. Étant donné que les RA dans le cerveau postérieur du poisson zèbre répondent à NE, nous avons étudié le rôle du LC dans la synchronisation des RA tectales. À cette fin, nous avons donc réalisé une imagerie du Ca^{2+} des neurones du LC tout en surveillant simultanément les mouvements de la queue. Nous avons observé que les neurones du LC présentaient une activité synchrone de Ca^{2+} suite à des comportements d'échappement spontanés et induits. L'activité maximale des neurones du LC a précédé celle de la synchronisation des RA dans le TO. L'ablation au laser à deux photons du LC a supprimé les événements de synchronisation du Ca^{2+} des RA dans le TO. Nous avons ensuite effectué une stimulation optogénétique de LC tout en surveillant la dynamique du Ca^{2+} des RA. Pour cela, nous avons utilisé des doubles larves transgéniques exprimant ChR2 sous un promoteur spécifique du LC et GCaMP6m sous un promoteur glial à l'aide d'une fibre optique couplé à une LED de 455 nm, nous avons stimulé le LC en utilisant des impulsions lumineuses de 1 s. La stimulation optogénétique du LC a induit des événements synchrones du Ca^{2+} dans les RA du le TO. Pour tester si les comportements d'échappement précédant les événements synchrones au Ca^{2+} sont médiés par le LC, nous avons surveillé les mouvements de la queue chez les larves avec les nuerons du LC ablatées. Nous avons observé que les ablations LC n'affectaient pas les mouvements spontanés ni induits de la queue. De même, la stimulation optogénétique n'a induit aucun type de mouvement de la queue. Dans l'ensemble, ces résultats suggèrent que l'activité du LC est nécessaire et suffisante pour la synchronisation des RA tectales. Cette synchronisation est médiée par le LC. Cependant, les comportements d'évasion et la synchronisation tectale de semblent être deux processus parallèles indépendants avec une entrée commune plutôt que d'avoir une relation causale.

0.2.4 Les événements synchrones au Ca^{2+} chez le RA modulent les corrélations fonctionnelles entre les neurones du TO

Pour mieux comprendre les interactions entre les RA et les neurones dans le TO, nous avons analysé les corrélations par paires entre l'activité spontanés du Ca^{2+} des RA et ceux des neurones. Nous n'avons observé aucune corrélation significative par paires entre l'activité spontanés de Ca^{2+} des RA et ceux des neurones. Ce manque de corrélations suggère que les RA n'excitent pas les neurones. Nous avons ainsi testé l'hypothèse que les RA pourraient inhiber l'activité neuronale, et donc empêcher la suractivation des neurones lors de la génération des comportements d'échappement. À cette fin, nous avons effectué une ablation au laser du LC et nous avons analysé la dynamique neuronale spontanée

du Ca^{2+} des neurones du TO. Nous n'avons trouvé aucune augmentation significative de l'activité spontanée des neurones par rapport aux larves témoins lors de l'induction de comportements d'évasion. Nous proposons donc que les synchronisations des RAs n'inhibent pas l'activité neuronale dans le TO.

Nous avons précédemment montré que la connectivité fonctionnelle neuronale dans le TO est adaptée pour améliorer la détection visuelle des stimuli vitaux. Ainsi, nous avons demandé si les événements synchrones du RA peuvent affecter la connectivité fonctionnelle entre les neurones afin de moduler la détection visuelle. Pour cela, nous avons calculé les corrélations par paires entre l'activité spontané de Ca^{2+} des neurones, dans des conditions de contrôle et pendant les périodes d'activation répétitive des RA. L'activation répétitive des RA a été induite par des stimuli électriques légers qui ont activé de manière robuste les synchronisations LC et RA dans le TO. Les événements synchrones Ca^{2+} chez le RA n'ont pas eu d'impact sur les corrélations globales par paires entre les neurones. Cependant, lorsque nous avons analysé la relation entre les corrélations par paires entre les neurones et la distance euclidienne entre eux, nous avons constaté une diminution significative des corrélations par paires spécifiques entre les neurones distants. Cela suggère que les RA peuvent moduler la connectivité fonctionnelle à longue portée entre les neurones. Dans l'ensemble, ces résultats montrent que les événements Ca^{2+} synchrones de les RA n'excitent ni n'inhibent les neurones, mais modulent plutôt les corrélations fonctionnelles en élaguant celles entre les neurones distants dans le TO, un mécanisme qui peut moduler le traitement visuel.

0.2.5 La synchronisation du RA module la sélectivité de la direction visuelle dans le TO

Pour en savoir plus sur le rôle fonctionnel des RA dans le traitement visuel, nous avons d'abord demandé si les RA dans le TO présentaient des événements Ca^{2+} en réponse à des stimuli visuels. Pour cela, nous avons présenté dans l'hémichamp droit de la larve, des stimuli visuels constitués de taches lumineuses de 13°, 23° et 44°, et de barres lumineuses qui déplaçant dans les directions rostro-caudale ou caudo-rostrale, tout en surveillant RA Ca^{2+} dynamique dans la région ventrale du TO. Dans cette région, les RA n'ont répondu à aucun des stimuli visuels présentés. Cependant, il est toujours possible que les RA modulent les réponses visuelles des neurones pour les adapter à l'état comportemental actuel de l'animal. Nous avons donc présenté les mêmes taches lumineuses et barres lumineuses mobiles avant les synchronisassions au Ca^{2+} du RA, à leur pic d'activité, et à la fin de leur activation. Nous avons constaté que l'amplitude moyenne et le pourcentage de neurones qui répondaient aux stimuli visuels n'étaient pas significativement différents avant , pendant et après les événements synchrones du Ca^{2+}. Les réponses neuronales aux taches lumineuses de différentes tailles pour les 3 conditions différentes n'ont montré aucun changement significatif. Cependant, les réponses neuronales aux barres mobiles affichaient des amplitudes significativement plus petites pendant les périodes de synchronisation du RA. La diminution de la réponse n'était significative que pour les barres se déplaçant dans la direction rostro-caudale. Nous avons donc calculé l'indice de sélectivité directionnelle de tous les neurones enregistrés avant, pendant et à la fin des événements synchrones du Ca^{2+} dans le RA. Nous avons observé que cet indice était significativement plus faible pendant et à la fin des événements synchrones du Ca^{2+} dans le RA. Ce dernier suggère que les synchronisations des RA tectales modulent la sélectivité directionnelle des

neurones. Pour tester si la modulation des neurones sélectifs en direction était induite par la synchronisation des RA ou si elle représente plutôt une modulation directe des neurones par la libération du NE pour le LC, nous avons réalisé la même expérience mais cette fois en activant directement les RA dans le TO au moyen de l'optogénétique. À cette fin, nous avons utilisé des larves exprimant ChR-2 sous un promoteur RAs. Nous avons constaté que l'activation directe des RA était suffisante pour diminuer la sélectivité de direction des neurones. Ces résultats montrant que la sélectivité directionnelle des neurones est modulée par la synchronisation des RA sont également étayés par le fait que l'étendue de l'effet modulateur des neurones sélectifs en direction correspond à celle des événements synchrones du Ca^{2+}. Dans l'ensemble, ces résultats démontrent que la synchronisation RA module spécifiquement la sélectivité directionnelle des neurones.

0.3 Discussion

Des études récentes soutiennent l'hypothèse que les calculs cérébraux ne dépendent pas exclusivement de l'activité neuronale, mais plutôt des interactions coordonnées entre les astrocytes et les neurones. Ici, nous avons étudié l'interaction neuro-glie dans le système visuel des larves de poisson zèbre. Ici, nous avons spécifiquement étudié les interactions entre les neurones et les RA dans le TO. Nous avons constaté que les RA dans les régions ventrales de le TO synchronisent son activité de Ca^{2+}, après de un comportement moteur d'échappement. Cette synchronisation ne dépend pas de la proprioception musculaire, mais plutôt de l'activation du LC.

De plus, nous avons observé que l'activation optogénétique des LC ne déclenchait pas de mouvements de queue ni de comportements d'échappement, mais qu'elle induisait l'activité synchrone des RA tectales. En revanche, l'ablation de LC a empêché l'activité synchrone des RA sans affecter la génération de comportements d'échappement. Ces résultats suggèrent que : 1) L'activation de LC est suffisante et nécessaire pour les synchronisations RAs tectales, et 2) L'association entre la synchronisation RAs et les comportements d'échappement n'est pas causale, mais très probablement le résultat de processus parallèles déclenchés par un source en amont du LC. Chez les mammifères et les poissons zèbres, la NE augmente les niveaux de Ca^{2+} dans les astrocytes, et sa libération est associée à la vigilance, à l'attention, à l'éveil ou aux réponses de combat ou de fuite. Nous suggérons ainsi que la synchronisation des RA dans le TO est induite par un passage en état de vigilance, qui en parallèle déclenche un comportement de fuite. Dans ce scénario, le LC est impliqué dans le passage à un état d'éveil, tandis que la dynamique lente du Ca^{2+} dans les RA médie l'évolution temporelle de l'état d'éveil. Cela suggère que la glie peut prolonger la constante de temps des réseaux cérébraux jusqu'à des dizaines de secondes. Ainsi, les interactions neuro-gliales peuvent sous-tendre des états comportementaux soutenus tels que l'éveil.

Même si les RA tectaux n'excitent ni n'inhibent les neurones, nous avons observé que les événements synchrones RA modulent la connectivité fonctionnelle entre les neurones tectaux en éliminant les corrélations entre l'activité spontanée des neurones distants. Ceci est biologiquement pertinent car le circuit du TO est organisé selon des assemblages de neurones hautement corrélés avec une dynamique de type attracteur qui améliore la détection visuelle des stimuli vitaux. La modulation des connexions fonctionnelles à longue distance créera des assemblages neuronaux plus compacts et améliorera ainsi la

détection des objets visuels vitaux (par exemple les proies). Alternativement, il est possible que la diminution des corrélations distales élague les neurones à fonctions spécifiques comme les neurones cholinergiques. Dans ce cas, l'élagage va démêler les assemblages neuronaux d'éventuelles modulations cholinergiques.

Contrairement aux études précédentes qui ont montré que les astrocytes du cortex visuel primaire répondent aux stimuli visuels pendant le comportement moteur, les RA de la région ventrale de l'OT des larves de poisson zèbre ne répondent pas aux stimuli visuels. Cependant, lorsque les RA synchronisent leurs événements Ca^{2+}, ils modulent fortement la sélectivité directionnelle des neurones sans influencer leurs courbes de réglage de taille. Les événements synchrones RA se produisent uniquement dans les régions ventrales de TO, qui représentent la partie inférieure du champ visuel (le lit de la rivière dans des conditions naturelles). Ainsi, il est possible que la modulation neuronale RA réduise la réponse optomotrice sans affecter fortement les autres types de réponses visuelles. Ce mécanisme peut prendre en charge le comportement de congélation 3 s. suite à un passage en état d'alerte. En effet, lors de la présentation de facteurs de stress, le poisson zèbre nage rapidement pendant quelques secondes puis se fige. Cette hypothèse est étayée par nos résultats montrant qu'à la suite d'un événement synchrone Ca^{2+} dans les RA, les larves entrent dans une période de passivité comportementale (la probabilité d'observer un comportement moteur diminue).

Dans l'ensemble, nos résultats suggèrent le scénario suivant : un passage à un état d'éveil induit l'activation de LC. Le LC génèrent des événements Ca^{2+} parmi la population ventrale des RA. Les événements synchrones RA modulent la sélectivité directionnelle des neurones tectaux et élaguent leurs corrélations fonctionnelles pour adapter le système visuel de la larve pour faire face au contexte environnemental associé à un état d'éveil. Bien que nous ayons observé que l'activation optogénétique directe des RA est suffisante pour moduler la sélectivité de direction des neurones tectaux, il est possible que le NE libéré par le LC dans le neuropile tectal soit également détecté par les récepteurs β2-adrénergiques dans les neurones. Dans ce cas, les adaptations observées du système visuel pendant les états d'éveil peuvent être étayées par les interactions étroites entre les RA tectales et les neurones sécréteurs de NE du LC. Chez le poisson zèbre, les RA affichent différents rôles fonctionnels. Par exemple, Dans la moelle épinière rostrale, des stimuli acousto-vestibulaires induisent des ondes du Ca^{2+} dnas le RA voyageant de manière bidirectionnelle vers le cerveau postérieur et la moelle épinière caudale. Dans le cerveau postérieur, les RA intègrent des erreurs de rétroaction visuelle lors de comportements visuo-moteurs pour déclencher la futilité. Contrairement à nos résultats, ce dernier phénomène n'est pas médié par LC, mais plutôt déclenché par le cluster noradrénergique du bulbe rachidien (NE-MO). Cette découverte indique que les événements synchrones tectal RA Ca^{2+} médiés par LC et les activations RA du cerveau postérieur médiées par NE-MO sont deux phénomènes indépendants avec une pertinence biologique différente (futilité vs passage à un état d'éveil). Ici, nous avons observé un rôle fonctionnel supplémentaire des RA dans le TO du poisson zèbre capable de moduler les calculs cérébraux et la connectivité fonctionnelle pour faire face à différents états comportementaux du cerveau. Cette étude ajoute à la preuve émergente que les calculs cérébraux et les états comportementaux dépendent des interactions coordonnées entre les astrocytes et les neurones.

Acknowledgements

First of all, I would like to thank Germán for having taken me in the lab, and for having been available and helpful whenever I needed. Also, many many thanks to the best team in the universe, my family support, and my friends.

Contents

List of Figures

Nomenclature

ACh Acetylcholine

ATP Adenosine triphosphate

ChR2 Channelrhodopsin

dpf Days post-fertilization

DS direction selectivity

ECBs Endocannabinoidse

ER Endoplasmic reticulum

GABA γ-Aminobutyric acid receptors

GECI Genetically encoded Ca^{2+} indicator

GPCR G-protein coupled receptor

hpf Hours post-fertilization

LC Locus coerueleus

LTD Long-term depression

LTP Long-term potentiation

mGluR Glutamate receptors

mGluR Metabotropic glutamate receptor

NAR Norepinephrine receptors

NCX Na^{+}/Ca^{2+} exchanger

NE Norepinephrine

OMR Optomotor response

OT Optic tectum

PC Principal component

PCA Principal component analysis

RGC Radial Glial Cell

ROI Region of interest

1

Introduction

Astrocyte-neuron interactions is an emerging and rapidly expanding field. The recent discoveries on the function of astrocytes provide new insights into the mechanisms underlying brain computations and brain diseases. Since their discovery more than 150 years ago [Rajadhyaksha and Manghani, 2002], astroglial cells were considered a cohesive substance that provides support to nerve cells. However, recent studies suggest that astrocytes and neurons form complex interactions necessary for information processing and synaptic input integration. The zebrafish larvae is a unique animal model to study neuro-glia interactions as it enables monitoring *in vivo* the spontaneous and the sensory-evoked activity of large neuro-glial networks in an intact behaving vertebrate.

In this introduction, I present an overview of neuroglia biology describing the astrocytes morphology, their spatial organization, and function. Then, I review the physiology of the synapse tripartite, how astrocytes activity is influenced by neurons, their Ca^{2+} dynamics, and their effect on neural networks. In the following section, I discuss the new findings regarding the role of astrocytes in behavior and information processing. Afterward, I discuss recent evidence demonstrating the role of astrocytes in noradrenaline neuromodulation and their potential role in behavior. Finally, I describe the zebrafish larva experimental model, its uniqueness for systems neuroscience research, and the most recent studies on glial functional roles in zebrafish.

1.1 Glial Cells

The brain has a notable complexity and an intricate structural diversity, with many different cell types. The most common are neuroglia and neurons each with its particular properties. In the human brain, more than 200 billion neural cells are packed within a restricted volume (1200–1400 cm^3) forming complex networks and connected through trillions of synapses that provide the computing power of this organ. In the brain, neuroglial cells are represented by astrocytes, oligodendrocytes, polydendrocytes, and microglia. Although neurons are the most studied brain cells, both neurons and neuroglial cells are necessary for proper brain function [Verkhratsky et al., 2019c].

Glial cells were first reported by Robert Remak and Heinrich Müller in peripheral nerves and the retina, respectively. However, the term neuroglia was first introduced by Rudolf Virchow in 1858. According to his observations neuroglia formed part of the connective tissue of the nervous system. Since then, in the second part of the 19th century, many other forms of glial cells were extensively described. For instance, Michael Von Lenhossek proposed the term 'astrocyte' in 1893. At that time, it was obvious that the non-neuronal cells were quite diverse. However, just in 1919 oligodendrocytes and microglia were considered separate cell types and recognized such as neuroglia by Pio del Rio-Hortega. Since then, several theories have considered the functional role of neuroglia in brain homeostasis, blood flow modulation, metabolic and structural support, as well as neuropathologycite [Kettenmann and Verkhratsky, 2008, Hubbard and Binder, 2016].

In the human brain, the total number of non-neuronal cells and neurons is about the same (between 80–100 billion) with substantial variations between different brain regions. If the population of endothelial cells is subtracted from the non-neuronal cells the proper number of glial can be estimated at 60 billion therefore the total glia-neuron rate for the whole brain is less than 1:1 [Azevedo et al., 2009, von Bartheld et al., 2016]. The evolution of the nervous system is parallel with an increase in the glia-neuron ratio, however, it was not always linear and was not directly related to brain size, here I cite some examples:

- `In invertebrates`, the nervous system has relatively fewer glial cells, with a glia-neuron rate between 0.01:1 and 0.2:1. In Caenorhabditis elegans 56 glial cells per 302 neurons. 10 glial cells per 400–700 neurons in every ganglion of the leech. In the central nervous system of Drosophila 9000 glial cells per 90,000 neurons. Nevertheless, the buccal ganglion of the great ramshorn snail Planorbis corneus contains 298 neurons and 391 glial cells, thus having a glia-neuron rate of 1.3, very similar to that of humans[Verkhratsky et al., 2019c].

- `In vertebrates` there is not a clear correlation between the glia-neuron rate and

the brain size; for example, in the cortex, the glia-Neuron rate is about 0.3–0.4 in rodents, 1.1 in cats, 1.2 in horses, 0.5–1.0 in the rhesus monkey, 2.2 in Göttingen minipig, 1.5 in humans and as high as 4–8 in elephants and the fin whale [Verkhratsky et al., 2019a]

Taking into account these trends, the glia-neuron ratio does not reflect the evolutionary advance. However, it has been reported substantial changes in glial function and morphology in parallel with the evolution of the nervous system. This advance in glial complexity is specifically prominent in the cortex of higher primates, especially humans which also contains several highly specialized types of glial cells which are absent in the brains of lesser vertebrates [Verkhratsky et al., 2019c].

Initial observations of neuroglia confined these cells to just passive elements that served to fill the gaps between neurons with merely secondary or supportive roles. However, new findings over the past decades have shown that neuroglia has a crucial involvement in brain functions and is implicated in neurological diseases such as Alzheimer's and Parkinson's disease [Kettenmann and Verkhratsky, 2008, Verkhratsky et al., 2019b]. Neuroglia of the Central Nervous system is narrowly subdivided into four different types of cells astrocytes, oligodendrocytes, polydendrocytes, and microglia, in the following section I describe the main functions and characteristics:

1. `Astroglia or astrocytes` are a heterogeneous population of cells encompassing a broad structural diversity. Representing, on average, 20 to 40 % of all glial cells. Astrocytes execute pivotal supportive functions, including maintaining brain homeostasis, neurotransmitter clearance, ion buffering, blood flow, and metabolite delivery [Curreli et al., 2022]. Astrocytes are critical components of neuroplasticity and aid the continual remodeling of neural connections [Perez-Catalan et al., 2021]. They can also influence neuronal activity by releasing gliotransmitters in response to intracellular transients. Recent findings have proposed that their Ca^{2+} signaling encodes information [Guerra-Gomes et al., 2018]. *a more detailed description is given in the section* 1.2.

2. `Oligodendroglia or oligodendrocytes` are the myelinating cells of the central nervous system. Their main function is to increase the neuron transmission rate of the electrical impulses [Bradl and Lassmann, 2010].

3. `NG2 glia also known as polydendrocytes` is a heterogeneous cell population, which plays a role in neuroprotection and cell regeneration after injury, contributes to homeostasis, and participates in neural circuit physiology and plasticity, albeit their functions are yet to be better-characterized [Dimou and Gallo, 2015]

4. `Microglia` are cells of mesodermal/mesenchymal origin that migrate into the CNS to become resident macrophages within the brain microenvironment. Microglia are highly dynamic cells that interact with neurons and non-neuronal cells. Microglia patrols the brain parenchyma playing a crucial role in the brain's health as regulators of synaptic functions phagocyting cellular waste and dead cells. In disease conditions, their phagocyte power is also neuroprotective. However, their malfunction is constantly found to be involved in neurodegeneration [Davalos et al., 2020].

1.2 Astrocytes

1.2.1 Overview

Astrocytes exhibit noteworthy heterogeneity in their morphology, organization, and functions. Astrocytes display remarkable plasticity and they are largely integrated into neural networks modulating neuronal activity. Astrocytes are hyperpolarized cells with low membrane resistance and do not generate action potentials. Besides supportive and homeostatic roles, their intercommunication with neurons is gaining more and more relevance [Dallérac et al., 2018]. Astrocytes have a high dynamic intracellular Ca^{2+} signaling which is influenced by neuronal network activity. These Ca^{2+} transients trigger the release of neuroactive molecules, called gliotransmitters, that regulate synaptic and neuronal functions at diverse timescales. Recent studies support a paradigm shift in neuroscience, in which information processing and behavior are not the exclusive outcomes of neuronal activity, but rather the interactions between neurons and astrocytes [Kofuji and Araque, 2021a, Lines et al., 2020]. In this section, we described the general physiology of astrocytes and the functional implication in the dialog between both neurons and astrocytes.

1.2.2 Astrocytes morphology

Astroglia encompasses plenty of cell subpopulations with heterogeneous morphology and functions. Broadly, the two most well-known astrocyte types are protoplasmic and fibrous. On the one hand, the protoplasmic are found in gray matter, they exhibit a small round cell body from which the main primary processes emerge. These processes ramify extensively to develop a remarkable and dense arborization of countless peripheral short and fine processes with high plasticity properties. [Oberheim et al., 2012, Zhou et al., 2019, Verkhratsky et al., 2017] In the rodent cortex, for instance, a single protoplasmic astrocyte interacts with 4-8 neurons, contacts 300-600 dendrites, and surrounds between 20,000-120,000 synapses. Remarkably, human protoplasmic astrocytes are larger and dis-

play a more complex morphology interacting with more neurons and synapses [Oberheim et al., 2009]. *see figure* 1.1. Protoplasmic astrocytes organize into extensive networks forming territorial domains where the overlapping between them is restricted to interdigitations between the most distal processes.This intercommunication allows a high level of cell-to-cell interchange [Bushong et al., 2002, Pannasch and Rouach, 2013] *see section* 1.2.3. On the other hand, the fibrous astrocytes are located in white matter. they project long processes and exhibit a diverse morphology. Nevertheless, they have much fewer processes as compared to those of protoplasmic. Therefore, their morphology is less complex. In Addition, the processes of the fibrous astrocytes overlap, thus lacking domain organization, characteristic of protoplasmic cells. [Oberheim et al., 2012, Zhou et al., 2019, Verkhratsky et al., 2017].

Furthermore, there are plenty of specialized astroglial cells, characterized by specific functions, particular structures, or anatomical distribution. Some of the most known are the Müller cells, Bergmann glial cells, and radial glial cells:

- `The retina contains Müller glial cells`, which are organized in parallel with the line of cones and rods. Müller cells combine a radial morphology with fine processes characteristic of protoplasmic astrocytes. These processes enwrap synapses and form an endfeet, which plaster blood vessels [Fischer and Reh, 2003].
- `The Bergmann glia cells are found in the cerebellum`, they have a small cell body and between 3-6 highly elaborated processes which are in close interaction with hundreds of synapses of Purkinje dendrites. Several (8 in rodents) of their processes surround a single Purkinje neuron covering their dendritic arborization [Müller and Kettenmann, 1995].
- `The radial glial are bipolar cells` that populate the neural tube exhibiting two main processes that can communicate the ventricular wall and the pial surface. In the early stages of development, they are neural and glial progenitors and serve as a scaffold to support cell migration. In mammalians, these cells disappear after birth, whereas they remain in lower vertebrates such as teleost fish for their whole life span [Rakic, 2009].

The morphology of astrocytes is different among vertebrates. For instance, The volume of human astrocytes is 15 to 20-fold larger than that in rodents covering many more synapses in the brain [Oberheim et al., 2009]. To address if a more complex structure could affect synaptic performance and behavior, chimeric mice were generated by brain implantation of human astrocytes progenitors. These cells developed and populated in the mice brain displaying their typical morphology as in the human brain. Then, these mice showed a lower threshold for induction of long-term potentiation (LTP) in hippocampal

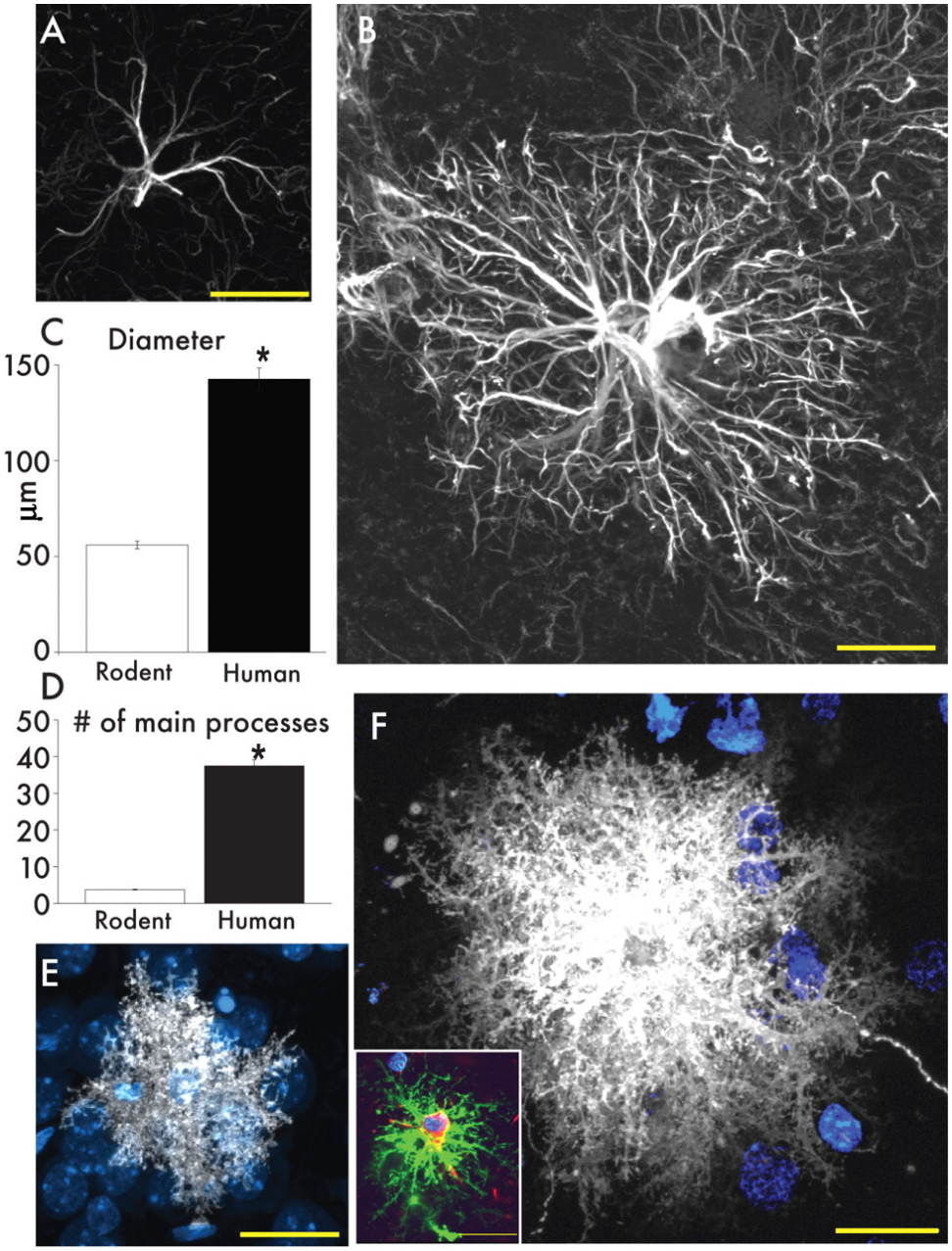

Figure 1.1: **Human protoplasmic astrocytes are larger and more complex than the rodent counterpart. (A)** Mouse protoplasmic astrocyte immunostained using GFAP antibody. **(B)** human protoplasmic astrocyte immunostained using GFAP antibody. **(C and D)** C, astrocytes diameter in µm; D, Number of processes immunostained using GFAP antibody; white bars, mouse; black bars human. Human protoplasmic astrocytes are 2.55-fold larger and have 10-fold more main GFAP processes than mouse astrocytes (human, n = 50 cells from 7 patients; mouse, n = 65 cells from 6 mice; mean ± SEM; * p 0.005, t test). **(E and F)** protoplasmic astrocyte diolistically labeled with DiI (white) and sytox for nucleus (blue) revealing the full structure of the astrocyte including its numerous fine processes. E, mouse; F, human. F inset, Human protoplasmic astrocyte diolistically labeled as well as immunolabeled for GFAP (green) demonstrating colocalization. Scale bar, 20 µm. textitreproduced from [Oberheim et al., 2009].

neurons, memory enhancement, and improved cognitive tasks [Han et al., 2013]. From

these experiments, it has been hypothesized that astrocytes could constitute an essential part of the processing power of the brain.

1.2.3 Astrocytes networks

Astrocytes are organized into extensive networks forming anatomical domains which allow a high level of intercellular communication. This interconnection is mediated by gap junctions that are made by connexins (the most important are connexins 30 and 43). These gap junction subunits form intercellular channels between adjacent cells allowing direct cytoplasmic coupling, and the exchange of several molecules such as ions, neuromodulators, and other metabolites. Astrocytic gap junctions contribute to Ca^{2+} transient propagation and can also modulate neurotransmission through metabolites trafficking, and by providing ion and neurotransmitter homeostasis. [Giaume et al., 2010, Mazaud et al., 2021] The astroglial networks are, in turn, controlled by neuronal activity. For instance, it has been shown in hippocampal astrocytes an increase in the trafficking of bioactive molecules such as glucose through gap junctions as a response to the Neuronal release of glutamate [Rouach et al., 2008]. Remarkably, The use of connexin 30 and 43 KO mice has revealed that dysfunction in the astroglial domains generates impairment in spatial memory and motor behavior. Moreover, it was reported that human brains of patients with psychiatric disorders such as autism and major depression display altered expression of astroglial connexins [Pannasch and Rouach, 2013].

1.3 Synapse tripartite

Astrocyte functions go beyond their role as scaffold or neuronal homeostatic regulation. Due to their unique morphological and functional features, it is nowadays accepted that they play a fundamental role in neurotransmission. Astrocytes have complex processes that are found in close physical contact with many synapses sometimes wrapping around them [Witcher et al., 2007]. This anatomical proximity exposes the astroglia cells to neurotransmitters released by synaptic terminals. Astrocytes express a large variety of receptors of neurotransmitters, metabotropic receptors and ionotropic receptors, capable of triggering several intracellular molecular pathways. One of the most reported outcomes is the glia Ca^{2+} elevations followed by the release of neuroactive molecules named gliotransmitters, such as glutamate, D-serine, and adenosine triphosphate (ATP) [Kofuji and Araque, 2021b, Agulhon et al., 2008]. These gliotransmitters influence synaptic function, including basal synaptic transmission and synaptic plasticity [Santello et al., 2012]. Remarkably, recent evidence using 3D-STED microscopy showed a nanoscale organization between dendritic spines and adjacent astrocytes processes displaying a high

correlation between their Ca^{2+} signaling and their structural remodeling [Arizono et al., 2020]. This bidirectional communication between neurons and astrocytes has been termed the synapse tripartite. According to this concept, a synapse is composed of presynaptic and postsynaptic terminals surrounded by astrocyte processes. Under these conditions, the information does not exclusively flow between the pre and postsynaptic neurons, but rather a more complex process where astrocytes exchange information with neurons, responding to synaptic inputs and, in turn, influencing the neuronal activity [Araque et al., 1999, Perea et al., 2009, Noriega-Prieto and Araque, 2021]. *see figure* 1.2

In this section, I briefly review recent results on the neuron–astrocyte communication properties. Firstly, I discuss the mechanisms associated with astrocytes' excitability by neurons. Then we focus on their Ca^{2+} signaling and their internal dynamics. Finally, we discuss the role of astrocytes in synaptic physiology through the release of gliotransmitters.

1.3.1 Astrocytes excitability and glial receptors

Pioneer studies showed that astrocytes display spontaneous intracellular Ca^{2+} fluctuation in cultured hippocampal explants [Cornell-Bell et al., 1990]. It was also shown that the Ca^{2+} dynamics of astrocytes can be modulated by neuronal activity [Khakh and McCarthy, 2015, Kofuji and Araque, 2021b]. For example, a neuronal discharge of neurotransmitters can induce a cytosolic increase in Ca^{2+} concentration [Bernardinelli et al., 2011]. Remarkably, Ca^{2+} elevations in astrocytes can be triggered not just by excitatory neurotransmitters (e.g. glutamate), but also by inhibitory neurotransmitters [Mederos and Perea, 2019]. For instance, The activation of γ-Aminobutyric acid (GABA) and Glutamate receptors, main inhibitory and excitatory neurotransmitters respectively, lead to an intracellular Ca^{2+} increase in astroglia [Doengi et al., 2009, Matos et al., 2018, Rose et al., 2018]. Therefore, although astrocytes are non-electrically excitable cells, they are highly responsive to neurotransmitters, displaying intracellular Ca^{2+} transients in their processes and soma. This astrocytic calcium-based excitability depends on the expression of a wide variety of membrane glial receptors which can sense the synaptic activity through the specific detection of neurotransmitters. Such heterogeneity of receptors confers on astrocytes a wide spectrum of responses to multiple neuronal signals [Kofuji and Araque, 2021b, Noriega-Prieto and Araque, 2021]. *In further sections I discuss, in more detail, these different Ca^{2+} responses and their downstream effects. See section* 1.3.3.

The main type of astrocyte receptors involved in the tripartite synapse is the G-protein coupled receptor (GPCR) class which is a metabotropic receptor with seven-(pass)-transmembrane domains that initiates the intracellular signaling by coupling to G-proteins. The binding of a particular neurotransmitter to the GPCR leads to a confor-

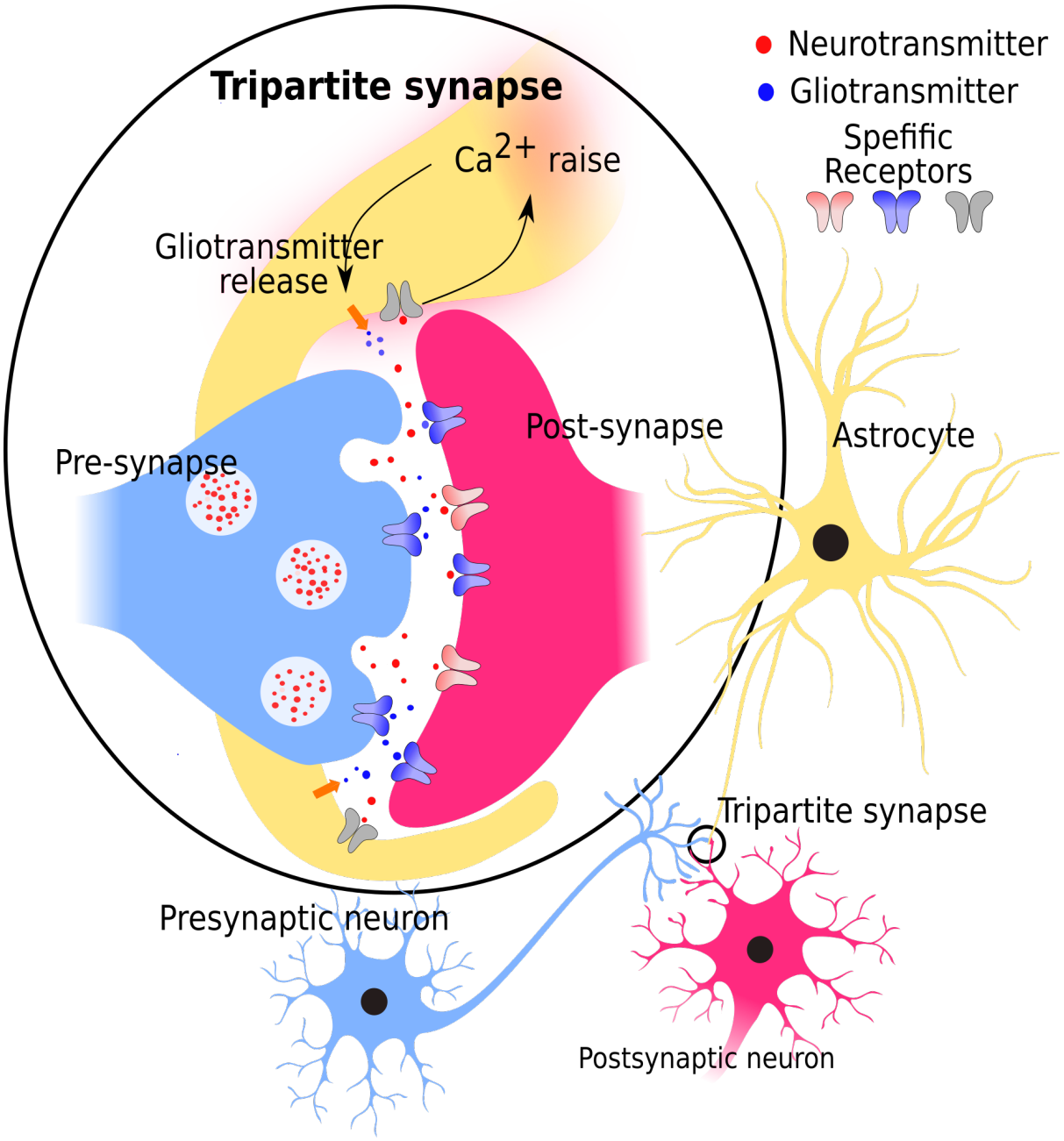

Figure 1.2: **Tripartite synapse** The tripartite synapse is composed of presynaptic neurons (blue), postsynaptic neurons (red), and astrocyte processes (Yellow) forming a functional unit. the neurotransmitters released from neurons also bind receptors on the adjacent astrocyte process, activating signaling pathways, mainly Ca^{2+} signaling which in turn influence synaptic function through the release of gliotransmitters

mational change to active the phospholipase C (PLC) that catalyzes the hydrolyzation of the membrane lipid phosphatidylinositol 4,5-bisphosphate to generate inositol 1,4,5-trisphosphate (IP3) and diacylglycerol (DAG). Then the activation of the IP3 receptor by IP3 leads to the Ca^{2+} spillover from the Endoplasmic Reticulum (ER), the main internal Ca^{2+} store in astrocytes [Agulhon et al., 2008, Perea et al., 2009, Noriega-Prieto

and Araque, 2021]. Although typically the GPCR activation in astrocytes triggers intracellular Ca^{2+} elevations, some reports have indicated its decrease. For example, it has been shown, *in vitro* and *in vivo* that the astrocyte intracellular Ca^{2+} concentration is dynamically modulated by dopamine signaling which can either elevate or decrease Ca^{2+} concentration depending on the receptors involved and the specific regional circuitry [Jennings et al., 2017, Xin et al., 2018].

A single astrocyte integrates the neurotransmitter signals coming from several synapses, some features of GPCRs contribute to this integration process. For instance, GPCRs in astrocytes show, in general, high affinity for their binding ligand displaying KDs in the nanomolar range. This characteristic allows the astrocytes to sense low concentrations of neurotransmitters. In addition, GPCRs are characterized to be slowly desensitized for their ligands which implies that astrocytes respond to low concentrations of neurotransmitters for long periods. GPCRs are broadly expressed in the astrocyte membranes rather than focally. This allows the astrocytes to simultaneously respond to several synaptic contacts. Therefore, the properties of GPCRs to sense low concentrations of neurotransmitters to avoid rapid desensitization and their broad expression along the whole membrane, allows astrocytes to have efficient temporal integration from multiples neurotransmitters signals even from different neurons [Kofuji and Araque, 2021b, Noriega-Prieto and Araque, 2021, Araque et al., 2014].

In addition to GPCRs, astrocytes express multiple classes of intramembrane ionotropic receptors which are ligand-gated ion channels. Several protein subunits form a pore in the receptor that can be activated and opened by neurotransmitter binding, the ion channel overture, in turn, permits the ions to flow into or outside the cell depending on the equilibrium potential [Meriney and Fanselow, 2019]. These receptors are activated by ongoing synaptic transmission. It has been proven that astroglia cells express ionotropic receptors of glutamate, ATP, GABA, and glycine. The activation of astroglial ionotropic receptors mediates localized and rapid neuronal-glial communications by inducing changes in intracellular Ca^{2+} concentration, but also other ions such as Na^{+} and K^{+} [Verkhratsky and Steinhäuser, 2000, Lalo et al., 2011]. For example, astroglia cells express Ca^{2+} permeable receptor channels such as NMDA and P2X, glutamate, and ATP-gated receptors. Application of agonist or direct synaptic stimulation trigger intracellular Ca^{2+} transients. On the contrary, the specific inhibition of NMDA and P2X receptors reduced the amplitude of astroglial Ca^{2+} transients by 40 to 50%. That implies that ionotropic receptors contribute to intracellular Ca^{2+} signaling by ion flux through the receptor channel providing a specific mechanism for fast neuronal-glial communication [Palygin et al., 2010]. Glioreceptors have then a highly functional heterogeneity resulting in intracellular Ca^{2+} dynamics of different temporal scales, however, their functional role remains unknown. Neurotransmitters capable of triggering astrocytes responses are glutamate, GABA, ATP,

endocannabinoids (ECBs), norepinephrine (NE), and acetylcholine (ACh):

- `Glutamate, the most important excitatory neurotransmitter`, plays a role in astrocyte signaling. The most relevant in astrocyte physiology, reported so far, are mGlu3 and mGlu5 receptors displaying different levels of expression relying on developmental stage or brain region [Sun et al., 2013, Kofuji and Araque, 2021b]. The main role attributed to mGluR induces the release of Ca^{2+} from the internal store by triggering the G-protein pathways [Rose et al., 2018].

- `The main inhibitory neurotransmitter GABA` acts on astrocytes inducing the generation of Ca^{2+} signaling through the activation of the ionotropic GABA A and the metabotropic GABA B receptors [Kofuji and Araque, 2021b]. For example, in mice, the striatal medium spiny neurons trigger astrocytic ca^{2+} transients by the activation of GABA B receptor, and the chemogenetic activation of this pathway leads to an impairment in attention and hyperactivity in rodents [Nagai et al., 2019].

- `ATP is released as a neurotransmitter` and its breakdown products ADP, AMP, and adenosine bind and activate astrocyte receptors. The most cited are the P2X and P2Y which are ionotropic and metabotropic, respectively. Both receptors have been found in different brain areas. The expression of purinergic receptors in the astroglial cell has been associated with intracellular Ca^{2+} transients [Abbracchio and Ceruti, 2006, Kofuji and Araque, 2021b]. For example, in rodents, stimulation of PY receptors induces Ca^{2+} transients in the hippocampus [Shigetomi et al., 2018].

- `The most known retrograde signaling system is mediated by ECBs` that are synthesized and released by the postsynaptic neurons to travel backward to modulate presynaptic inputs. This endogenous system regulates synaptic transmission and neuronal plasticity [Ohno-Shosaku and Kano, 2014, Winters and Vaughan, 2021]. ECBs act in the astrocytes by the G-couple ECBs receptor CB1R, triggering the discharge of internal Ca^{2+} stores. Nevertheless, CB1Rs are less expressed in astrocytes than in neurons [Navarrete and Araque, 2008]. Despite its moderate expression, CB1Rs are associated with some forms of synaptic plasticity. For instance, astroglial CB1 receptors KO mouse displays decreased LTP and impairment in object recognition memory [Robin et al., 2018].

- `NE is mainly produced and released from the locus Coerueleus (LC)`, NE is associated with arousal and alertness states. Astrocytes located in multiple brain areas respond to this neurotransmitter by the expression of $\alpha 1$, $\alpha 2$ and $\beta 1$ adrenergic receptors increasing the intracellular Ca^{2+} concentration. Electrical stimulation

and locomotion induce astrocyte activation leading to the release of NE by the LC [Bekar et al., 2008, Paukert et al., 2014]. *In further sections I discuss in more detail the NE biological relevance and its implications to neuron-astrocytes communication see section* 1.5.

- `ACh has several roles in synaptic communication`. It has been shown that cholinergic agonists and ACh neuronal release mediate the astrocytic intracellular Ca^{2+} rise via muscarinic and nicotinic receptors [Araque et al., 2002]. Remarkably as it was demonstrated in mice, the LTP in the hippocampus required the astrocytic muscarinic receptors activation. That implies that ACh signaling in astrocytes is associated with synaptic plasticity [Navarrete et al., 2012].

1.3.2 Astrocytes calcium dynamic

Since the very first findings on Ca^{2+} fluctuation in cultured hippocampal astrocytes [Cornell-Bell et al., 1990] many other studies have observed these intracellular Ca^{2+} transients under multiples conditions. Intracellular Ca^{2+} variations have been extensively associated with synaptic activity but they also occur spontaneously. An outstanding finding is that locomotion and sensory stimulation has proved to evoke astrocyte Ca^{2+} responses. For instance, in rodents, astroglial cells located in the cerebellum and other brain regions respond to motor behavior by exhibiting an increase in Ca^{2+} during locomotion [Nimmerjahn et al., 2009, Paukert et al., 2014]. Moreover, coupling motor behavior with light stimulation enhanced intracellular Ca^{2+} concentration in astrocytes of the visual cortex [Paukert et al., 2014] *see figure* 1.3. Furthermore, several protocols inducing sensory stimulation *in vivo* such as air-puff-elicited startle reflex, mild electric shocks, or whisker stimulation have triggered Ca2+ signaling in astrocytes [Bekar et al., 2008, Oe et al., 2020, Wang et al., 2006].

A single astrocyte may contact thousands of different synaptic terminals that also may release several types of neurotransmitters. That implies that astrocytes integrate the activity of several synapses via their Ca^{2+} responses. However this integration is not linear, on the contrary, it appears to be governed by nonlinear excitability [Perea et al., 2009]. Namely, it has been shown in rat hippocampal slices that the astrocytic Ca^{2+} response to different synaptic inputs could be a sublinear or supralinear summation. Thus, the astrocytic Ca^{2+} variations obey a nonlinear dynamic depending on neuronal activity [Perea and Araque, 2005].

Astrocytes display complex intracellular Ca^{2+} signaling exhibiting very diverse temporal-spacial properties. Firstly, there is a global Ca^{2+} response detected mainly in the soma and main processes. These Ca^{2+} elevations can propagate beyond single astrocytes

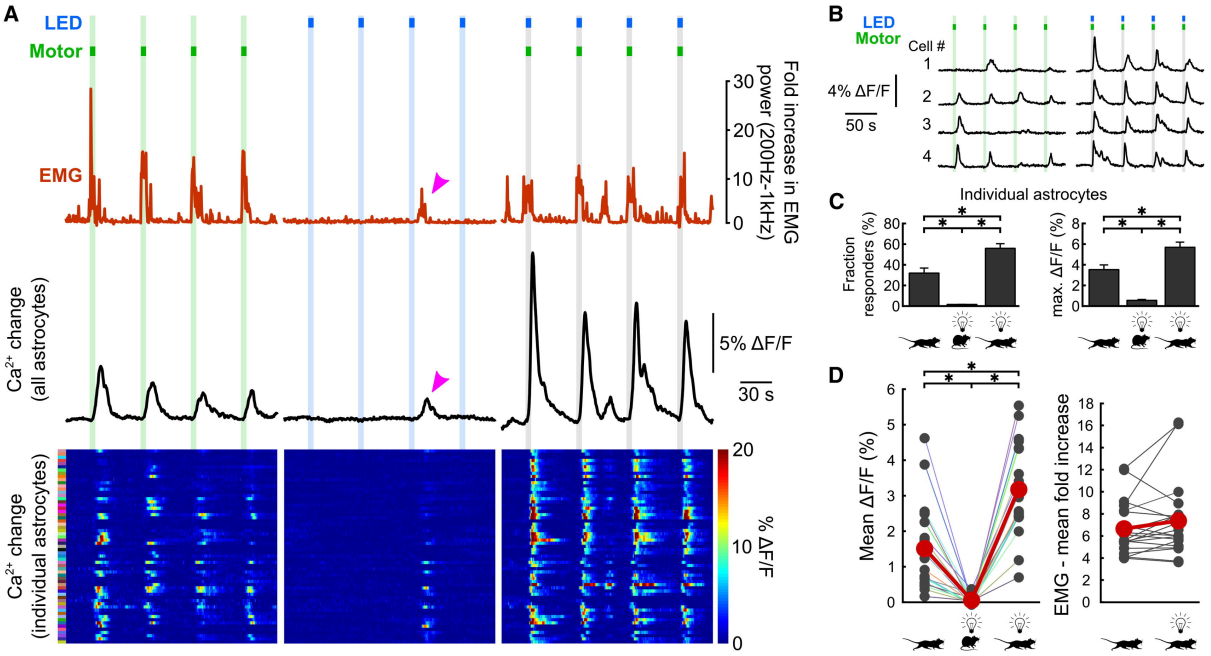

Figure 1.3: **Visual stimuli enhance astrocyte responses (A)** Mouse astrocytes located in visual cortex V1 Ca^{2+} responses to enforced locomotion (green bars), visual stimulation (blue bars) or simultaneous enforced locomotion and visual stimulation (gray bars). Red traces represent electromyography (EMG) activity; black traces represent mean Ca^{2+} variation in all astrocytes. Bottom: Raster of astrocytes Ca^{2+} activity. pseudocolor scale bar: $\Delta F/F$. Arrowhead highlights Ca^{2+} elevation associated with spontaneous locomotion. **(B)** Ca^{2+} transients in four representative cells during four consecutive trials of enforced locomotion (green bars) or simultaneous enforced locomotion and visual stimulation (gray bars). **(C)** Left: average fraction of astrocytes responding with a mean Ca^{2+} elevation exceeding 1% $\Delta F/F$. Right, average maximum Ca^{2+} responses in individual astrocytes (16–20 trials). Error bars represent mean ± SEM; n = 20 mice; asterisks indicate a significant difference (one-way ANOVA with Bonferroni post hoc test). **(D)** Left: mean Ca^{2+} elevations in all astrocytes (16–20 trials). Colored lines connect data points from individual mice. Asterisks indicate a significant difference (one-way ANOVA with Bonferroni post hoc test). Right: change in EMG power during enforced locomotion or simultaneous enforced locomotion and visual stimulation. Each point represents the average response in 16–20 trials. Red circles indicate the mean of all trials. *reproduced from* [Paukert et al., 2014]

spreading intercellularly via gap-junctions, forming an astrocytic network with complex spatiotemporal Ca^{2+} patterns *see section* 1.2.3. Moreover, in astrocyte processes, it is possible to observe compartmentalized Ca^{2+} traces with diverse kinetics [Guerra-Gomes et al., 2018].

Frequently, it has been reported that several neurotransmitters induce the release of Ca^{2+} from internal stores, mainly from ER via the activation of IP3 pathway [Perea et al., 2009, Guerra-Gomes et al., 2018] *see section* 1.3.1. However, this represents just a global response within the astrocyte. Formerly, certain technical restrictions prevented the study of Ca^{2+} dynamics across the entire astrocyte's morphology, limiting the observations only to the bulk Ca^{2+} changes occurring mostly in the cell soma. Most recently, the

noteworthy development in multiphoton microscopy and the advent of more sensible *in vivo* Ca^{2+} sensors such as the genetically encoded Ca^{2+} indicators (GECI) have meant the possibility of tracking efficiently Ca^{2+} in the fine astrocyte processes. This led to the detection of a local Ca^{2+} activity which often differs from Ca^{2+} variations in the soma in terms of frequency, kinetics, and spatial spread. This localized Ca^{2+} events are named microdomains [Lia et al., 2021].

Astrocytic microdomains often refer to the Ca^{2+} variations confined to a restricted area normally detected in astrocyte processes [Lia et al., 2021]. Notably, these events have been registered at nano-scale in the thinner processes showing a high functional correlation with neighbor synaptic partners in which even the fine morphological remodeling of both cells (in astrocytes processes and dendritic spines) are also correlated [Arizono et al., 2020]. Notably, these Ca^{2+} signals can be faster than in the soma displaying frequently a timescale closer to that of neurons [Stobart et al., 2018]. The use of IP3R2 knockout mouse to block the PLC/IP3 pathway in astrocytes significantly abolished the Ca^{2+} response in the soma. In contrast, in the microdomains, it was reduced only partially. This implies that there are other additional Ca^{2+} sources beyond those of the ER [Stobart et al., 2018]. For example, it has been reported that intracellular stores in the mitochondria, which are abundant in the astrocytes processes, play a pivotal role in these Ca^{2+} microdomains [Agarwal et al., 2017]. Additionally, the extracellular Ca^{2+} entry via transmembrane Ca^{2+} influxes traveling through channels such as TRPC1 and TRPA1 also contribute to the microdomains of Ca^{2+} activity [Malarkey et al., 2008, Shigetomi et al., 2013]. Furthermore, the Na^{+}/Ca^{2+} exchanger (NCX), which removes elevated Ca^{2+} concentration from the cell, can also reverse this flux. Indeed, it has been shown that Ca^{2+} elevations via NCX occur as a response to GABA stimulation[Boddum et al., 2016].

Overall, the astrocytic Ca^{2+} dynamics are more complex and diverse than previously believed, and this active signaling between astrocytes and neurons may contribute to the brain's information processing.

1.3.3 Astrocytes down-stream synapse effects

The bidirectional relationship between astrocytes and neurons is an intricate phenomenon that includes a plethora of mechanisms to lead reciprocal communication. As described above, astrocytes sense and integrate neural inputs via their intrinsic Ca^{2+} dynamics and other mechanisms. In turn, astrocytes influence neuronal activity through a multiplicity of mechanisms in which gliotransmission is the most studied. For example, the increase of intracellular Ca^{2+} promotes the Na^{+}/Ca^{2+} exchange increasing the intracellular concentration of Na^{+}. Then, the sodium pump is activated via the Na^{+}/K^{+}-ATPase lowering

the presynaptic K^+. As a result, the nearby neurons are hyperpolarized reducing the frequency of excitatory postsynaptic currents and the synaptic failure rate, promoting the enhancement of synaptic efficacy [Wang et al., 2012].

Gliotransmission refers to the mechanisms and the outcomes of the astrocyte release of the neuroactive molecules (gliotransmitters) that module synaptic physiology in many different ways [Durkee and Araque, 2019]. A single astrocyte can release one or more than one type of gliotransmitters that can have either inhibitory or excitatory effects in neurons depending on the properties of the gliotransmitter receptor that the neurons express [Kozlov et al., 2006, Martín et al., 2007, Pascual et al., 2005]. The set of mechanisms involved in the gliotransmitter release has been under debate [Hamilton and Attwell, 2010, Savtchouk and Volterra, 2018]. Nevertheless, numerous studies suggest that SNARE protein-dependent vesicular discharge is one of the most important [Schwarz et al., 2017, Araque et al., 2000, Bezzi et al., 2004]. Astrocytes release multiple gliotransmitters such as glutamate, ATP, and GABA, D-serine. In the next section, I summarise some of their effects on neurons.

- `Glutamate` was the first gliotransmitter associated with astrocyte-neuron communication. Its release has been related to enhancing slow inward currents, hippocampal synaptic transmission, and neuronal excitability acting on NMDA receptors [Araque et al., 1998, Angulo et al., 2004, Perea and Araque, 2005]. Furthermore, metabotropic glutamate receptors (mGluRs) activation has been involved in the modulation of the synaptic efficacy by inducing enhancement or suppression depending on the specific neuronal circuit [Fiacco and McCarthy, 2004, Nedergaard et al., 2004, Jourdain et al., 2007]. Additionally, astrocyte glutamatergic signaling has been involved in synaptic plasticity capable of modulating LTD and LTP [Park et al., 2015, Min and Nevian, 2012].

- `ATP` is initially hydrolyzed extracellularly by ATPases getting as a result adenosine. Adenosine binds to the GPCR receptors A1 and A2A located in the presynaptic terminal modulating synaptic transmission in diverse ways. While the activation of the A1 receptor by astrocytic ATP/adenosine depress the synaptic transmission [Pascual et al., 2005, Zhang et al., 2003], the A2A receptor enhances neurotransmission [Gordon et al., 2005, Panatier et al., 2011]. Noticeably, ATP/adenosine released by a single astrocyte can impact neuronal circuits in different manners according to the type of receptor expressed in the presynaptic terminal.

- `Astrocytic GABA` impacts the synaptic activity in different ways. For example, Astroglia cells release GABA exerting a tonic inhibition in the cerebellum [Lee et al., 2010]. Furthermore, in mice, the activation of the GPCR GABAB receptor

by astrocyte GABA release induces a disinhibitory effect on dentate granule neurons [Yarishkin et al., 2015]. Moreover, GABA gliotransmission regulates the tonic inhibition in the cerebellum influencing motor coordination [Woo et al., 2018].

- `D-serine gliotransmission` has been involved in neuronal plasticity, an amino acid known as the main NMDAR coagonist at the postsynaptic terminal. More, specifically, D-serine is involved in LTP induction [Kartvelishvily et al., 2006]. For example, D-serine and its vesicles release machinery have been found in the astrocytes' cytoplasmic processes [Ehmsen et al., 2013, Kang et al., 2013]. Additionally, the discharge of D-serine by astrocytes promotes the NMDA-dependent LTP which is blocked by the extracellular or intracellular Ca^{2+} depletion or by a D-serine pharmacological inhibitor [Henneberger et al., 2010].

1.4 Astrocytes and neuronal functions

The bilateral communication between neurons and astrocytes has important implications in several levels of synaptic functions, influencing the transmission, formation, and plasticity of the synapse. *see section* 1.3.3. Recent evidence *in vivo* has shown the role of astrocytes in more complex functions such as memory, learning, sleep, sensory processing, and behavior. In this section, I summarized some evidence in this regard.

In the nematode *C. elegans* the cephalic sheath glia (CEPsh) is an astrocytes-like cell that extends its processes contacting synapses and displaying Ca^{2+} responses [Nagai et al., 2021]. Experimental approaches have shown that after the ablation of CEPsh glia the animal displays abnormal neuronal Ca^{2+} signaling, impairment in the sleep cycle, and locomotion imbalance [Katz et al., 2018]. The fruit fly *Drosophila melanogaster* exhibits astrocyte-like glia cells that are functionally analogous to mammal astrocytes. It has been reported that the fruit fly glia has functional roles modulating synaptic formation and plasticity. Drosophila astrocyte-like cells express protein transporters to glutamate and GABA to control the balance between excitation and inhibition of neural signals. Their function has been associated with long-term memory and locomotion [Nagai et al., 2021].

At first glance, the first approaches to prove the involvement of astrocytes' Ca^{2+} dynamics in learning and memory were not conclusive due to the lack of memory impairment in IP3R2 KO mice [Agulhon et al., 2010, Petravicz et al., 2014]. Accordingly, later examination using the same model confirmed that recent memory was not affected. However, after 2-4 weeks, the IP3R2 KO mice exhibited memory consolidation deficits [Pinto-Duarte et al., 2019]. Besides, the chemogenetic activation of hippocampal astrocytes facilitates NMDA-dependent LTP and enhanced memory in fear conditioning and

T-maze [Adamsky et al., 2018]. These findings support previous studies showing that optogenetic activation of hippocampal astrocytes increases excitatory synaptic transmission, synaptic plasticity, and enhances episodic-like memory [Mederos and Perea, 2019]. Moreover, The astroglia cell release of D-serine via the activation of CB1Rs has been associated with the modulation of LTP and object recognition memory [Robin et al., 2018]. These studies highlight astrocytes as an integrative component of learning and memory processes.

Accumulating data have proposed that astrocytes appear fundamental in the physiology of sleep and wakefulness. Namely, the inhibition of adenosine gliotransmission via the conditional over-expression of a dominant-negative domain of the vesicular SNARE (dnSNARE) shows an attenuated accumulation of sleep pressure, represented by a decreased slow-wave activity during NREM (non-rapid eye movement) sleep [Florian et al., 2011]. Moreover, astrocyte activation using optogenetics in the posterior hypothalamus of mice increased both REM (rapid eye movement) and NREM sleep [Pelluru et al., 2016]. Monitoring the astrocytic Ca^{2+} signaling in mice neocortex has shown lower intracellular Ca^{2+} concentration during sleep, and a large surge preceding the transition to wakefulness. Finally, astrocytic IP3R KO mice exhibited impaired slow-wave associated activity [Bojarskaite et al.,]. These results highlight the relevant role of astrocytes in the sleep/wake cycle.

Recent evidence indicates that astrocyte signaling plays a fundamental role in sensory responses. For example, astrocyte Ca^{2+} imaging in mice revealed an odor map in the olfactory bulb. Furthermore, chemogenetic modulation of Ca^{2+} signaling indicates that astrocytes contribute to odor detection and discrimination [Ung et al., 2020]. Moreover, the impairment in astrocyte glutamate transport via genetic deletion of transcription the factor Sox9 led to aberrant olfactory behaviors and altered neuronal sensory response maps [Ung et al., 2021]. Furthermore, it has been found that thalamic astrocytes' release of GABA results in tonic inhibition in thalamocortical neurons. Finally, genetic manipulation to inhibit GABA gliotransmission showed lower tactile discrimination in a touch-based novel object recognition test. On the contrary, enhanced GABA release resulted in a high discrimination performance [Kwak et al., 2020]. These findings suggest the potential role of astrocyte-neuron communication in sensory processing.

1.5 Astrocytes and noradrenaline-depended neuromodulation

NE is one of the main neuromodulators in the central nervous system exerting widespread influence over many brain regions. NE is released from axonal varicosities and spread

throughout the parenchyma. It is known that the LC is the main source of NE in the brain. Although LC is constituted by a few neurons (3,000 neurons in rodents) it sends projections throughout the CNS innervating the hippocampus, spinal cord, prefrontal cortex, cerebellum, thalamus, cortex, and amygdala [Sara, 2009, Breton-Provencher et al., 2021]. LC neurons respond to external stimuli and internal states by exhibiting phasic and tonic firing activity patterns which differ in the NE release properties. The phasic activity consists of brief 10–20 Hz bursts of a few action potentials that are normally followed by a sustained suppression of spontaneous activity. On the other hand, tonic discharges comprise slow firing rates (0.1–5.0 Hz) [Devilbiss and Waterhouse, 2011]. Fluctuations in these firing patterns are correlated with arousal responses, sleep, and wakefulness. For example, LC-NE neurons activity increases during arousal states and displays low firing rates during non-REM sleep and silent activity during REM sleep [Breton-Provencher et al., 2021]. Additionally, using optogenetic manipulations, it has been shown that sleep/wakefulness states are modulated by LC-NE activity and its stimulation promotes arousal responses in rodents [Carter et al., 2010, Hayat et al., 2020]. Beyond the roles in arousal states and sleep, the LC-NE system is involved in higher cognitive functions such as learning and memory [Nguyen and Connor, 2019].

Recent studies suggested that astrocytes are highly involved in LC-NE neuromodulation. NE triggers robust Ca^{2+} elevations in astrocytes via the activation of NE receptors (NAR) which is coupled to G proteins signaling [Wahis and Holt, 2021]. It has been shown that in rodents, cortical astrocytes respond to LC electrical stimulation, NA discharge following air-puff startle, footshock stimuli and NE-dependent high vigilance fear conditioning [Bekar et al., 2008, Ding et al., 2013, Oe et al., 2020]. In the mouse cerebellum, the Bergmann glia activation by enforced locomotion has been associated with NE release [Paukert et al., 2014]. Furthermore, the visual cortex astrocytes do not respond to visual stimulation during animal quiet wakefulness. Nevertheless, pairing visual stimuli and locomotion induces NE-depended rise in astrocyte Ca^{2+} concentration [Paukert et al., 2014, Slezak et al., 2019]. Notably, the amplitudes of astrocytic visual responses are correlated with variations in pupil size, indicating changes in arousal state [Slezak et al., 2019]. Recently, astrocytes activity and their LC-NE system modulation have been associated with mechanosensory behavior in rodents: Astrocytes located in the superficial laminae of the spinal dorsal horn, the core region associated with receiving and processing somatosensory inputs, respond to mechanical pain in mice via LC-NE system activation. NE intrathecal stimulation induces pain hypersensitivity in the animal, this effect is replicated by chemogenetic activation of G protein signaling in astrocytes [Kohro et al., 2020]. Moreover, It has been shown that cortical astrocytic NAR activation triggers ATP and D-serine gliotransmission inducing synaptic plasticity by facilitation of LTP. Transgenic mice (dnSNARE mice) characterized by impairments in gliotransmitter

exocytosis abolished this effect [Pankratov and Lalo, 2015].

1.6 The zebrafish model

1.6.1 Overview

The zebrafish *Danio rerio* is a tropical teleost fish of the Cyprinidae family (freshwater fish) that owes its name to the horizontal blue stripes that run along its body (see Figure 1.4. B) [Hamilton, 1822]. In the wild, they live in rice fields, shallow streams, or ponds in Nepal, India, Pakistan, Bangladesh, and possibly Myanmar [Parichy, 2015] (see Figure 1.4. They usually live in clear but can also cope with turbid waters (in particular after rain). They are found across a large range of environmental conditions (temperatures, pH, or salinity can vary greatly between the different places they live in). It is a gregarious species that usually form shoals of tens of individuals (see Figure 1.4.C). They eat mostly insect larvae and plankton and grow up to approximately 4 cm and become sexually mature at 3 months old [Parichy, 2015].

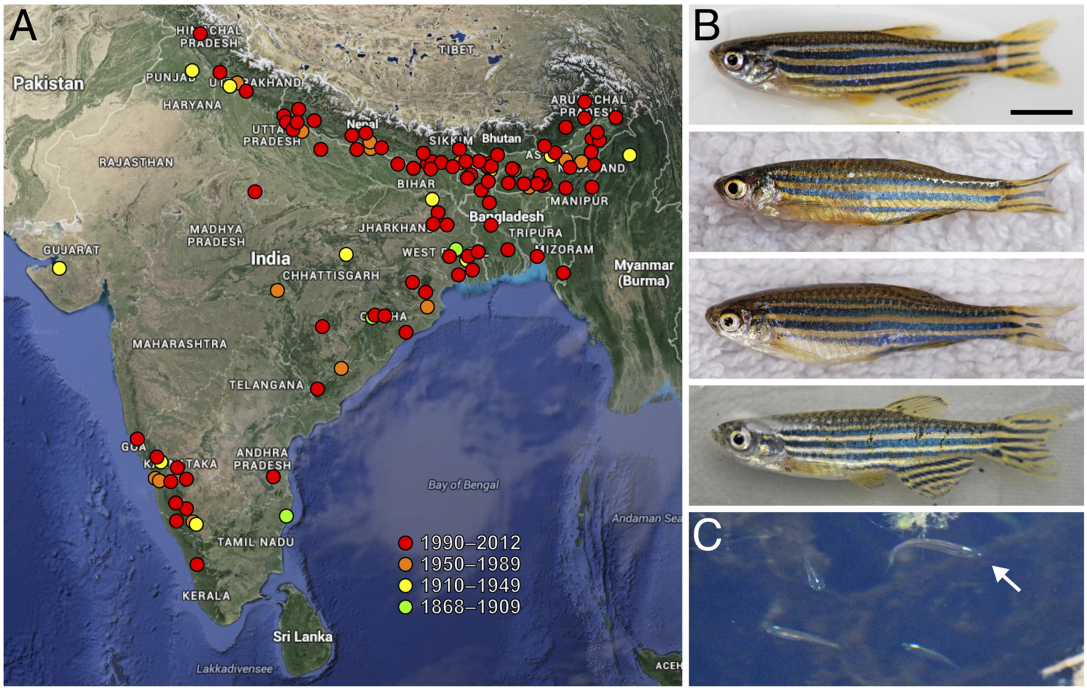

Figure 1.4: **Geographical range of zebrafish. (A)** Sites where zebrafish have been reported between 1868 and 2012. **(B)** Zebrafish from northeastern India. The upper two fish are males and the lower two fish are females. Scale bar: 5 mm. **(C)** A group of fish, with a single fish pointed out by the arrow. Reproduced from [Parichy, 2015]

1.6.2 Advantages of using zebrafish as an experimental model

In recent years, the zebrafish has become a valuable vertebrate model for systems neuroscience research. First, zebrafish tolerate a broad range of environmental conditions, the adults are small and prefer to be housed in shoals. As a result, they require much less space than mice and they are relatively inexpensive to maintain. Zebrafish produce hundreds of offspring (around 200 to 300 eggs per week per female) providing scientists with an abundant supply of embryos to study [Harper and Lawrence, 2010]. Due to the external development and the transparency of the eggs, this model is ideal for developmental studies and live imaging. Moreover, Its genome has been completely sequenced and approximately 70% of the human genes have at least one zebrafish orthologue [Howe et al., 2013].

The Zebrafish model offers a set of advantages that are particularly notable in neuroscience research. Namely, its larva hatches at around 3 days post-fertilization (dpf) losing the nutritive support of the yolk sac. This implies a strong ecological pressure that forces the larvae at very young stages to develop sensory-motor systems and appropriate behaviors to catch prey and avoid predators to survive. Therefore, within just one just week zebrafish larvae display a wide set of motor behaviors that are mainly guided by the visual system. Notably, it has been shown that zebrafish larvae exhibit similar visuomotor functions to those observed in adults. See Figure 1.5 for a picture of the larva at 6 dpf [Friedrich et al., 2010, Portugues and Engert, 2009]. The use of *nacre* zebrafish lines that lack melanophores facilitates the use of live-imaging techniques to monitor brain cells due to the transparency of its skin and skull at the larval stage [Lister et al., 1999]. In addition, the larva's brain at 6 dpf is relatively small, about 0.5 mm thick and 1.5 mm long, making virtually all brain cells accessible for functional imaging. Moreover, at the larval stage (before scales are formed and before the functional development of the gills), respiration is mainly performed by osmosis through the skin, enabling to immobilize of the larva in low-melting agarose for long periods without affecting the larva's health. In addition, there is a wide range of available transgenic fish, such as GECI and Channelrhodopsin (ChR2) expressing lines that make this model ideal for ca^{2+} imaging and optogenetic manipulation. The fast development of functional sensory systems, the large repertoire although discrete motor behaviors, and recent advances in optics for functional imaging (two-photon microscopy or selective-plane illumination microscopy (SPIM)), have remarkable importance in neuroscience research since allow studying the dynamics of large neuro-glia networks and motor behavior with single-cell resolution, in an intact

Figure 1.5: **Zebrafish larva at 6 dpf** from: [Easter and Nicola, 1997]

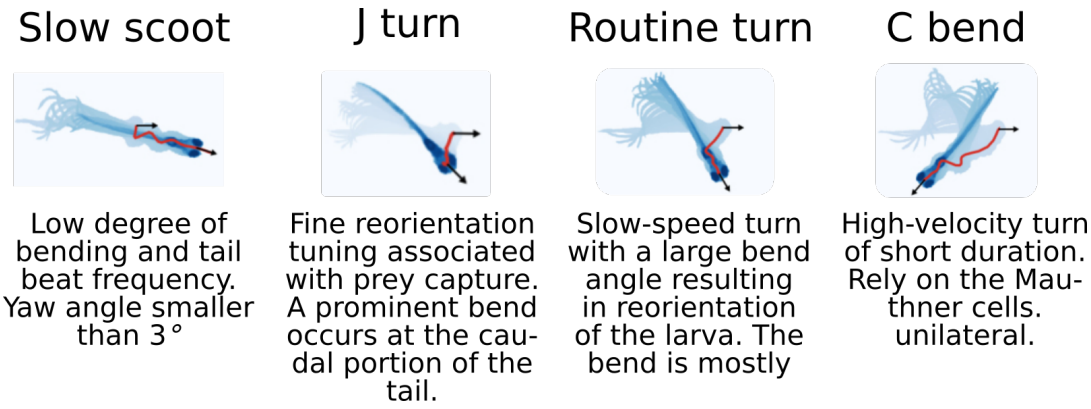

Figure 1.6: **Tail movements repertoire**. Each column represents a typical tail movement and its characteristics. superimposition of the images of the larva during the tail bout. The trajectory of the head is shown by a red line, the black arrows represent the head orientation at the beginning and end of the bout. Adapted from [Jouary et al., 2016].

non-anesthetized, non-paralyzed behaving vertebrate [Panier et al., 2013, Romano et al., 2015, Pérez-Schuster et al., 2016, Ahrens and Engert, 2015, Mu et al., 2019].

1.6.3 Zebrafish motor behavior

The zebrafish larvae swim in discrete episodes of body undulations involving the coordinated locomotion between the tail and pectoral fins. Zebrafish swimming is intercalated with non-swimming episodes. These locomotor patterns have been termed ”bouts”. These bouts are discrete and simplify behavioral analysis and classification. These discrete segments of activity called tail bouts have a range of duration between 80-400 ms [Buss and Drapeau, 2001]. By the use of high-speed video recording and taking into account the characteristics of tail locomotion and the kinematics of the trajectories. Several categories of tail bouts have been described: slow scoots (also called forward swim), routine turns, J turns or C bends *see figure* 1.6 [Mirat et al., 2013, Borla et al., 2002, Budick and O'Malley, 2000, Marques et al., 2018]. As the vitellus lipids reserves are consumed by 6 dpf, larvae zebrafish are forced to catch prey in their natural habitat This implies a strong ecological pressure for the early development of functional sensory-motor circuits thus displaying a rich behavioral repertoire in the early stages. I will thus focus on visually induced behaviors in zebrafish larva.

Visuomotor behaviors

After hatching at 3 dpf, zebrafish larvae first lie on the bottom of the tank moving forward or circling occasionally. Then, the first visuomotor behavior that emerges is the visual startle response: a sudden decrease in brightness (interpreted as a threat) leads to an escape response. This avoidance behavior could also be triggered by abrupt stimuli

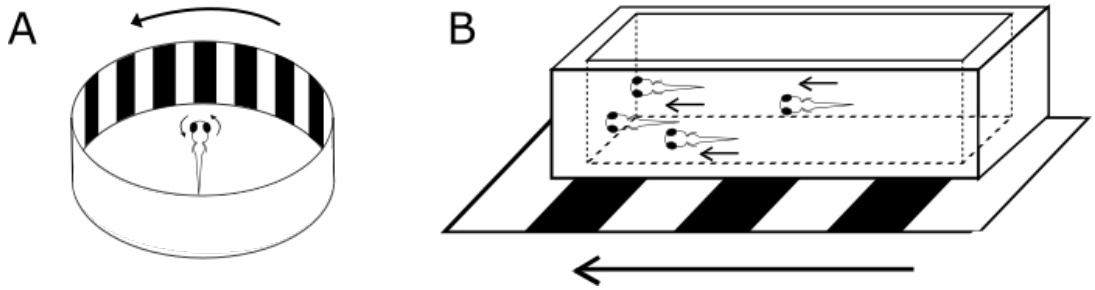

Figure 1.7: **OKR and OMR in zebrafish larva. (A)** Optokinetic response: a rotating vertical grating creates a large coherent moving visual stimulus around the immobilized fish, that responds with following eye movements. **(B)** Optomotor response: the larvae swim to follow a moving grating below their tank. The direction of motion is indicated by arrows. Adapted from [Roeser and Baier, 2003].

such as touch, sounds, or water flow. At 4 dpf, when their swim bladder becomes inflated, larvae begin to swim reliably. At this stage, larvae can follow moving objects with their eyes developing the optokinetic response (OKR). This is the earliest visual behavior requiring pattern vision and directionality [Easter and Nicola, 1996, Easter and Nicola, 1997, Colwill and Creton, 2011]. Slightly after, the optomotor response (OMR) also emerges. See Figure 1.7 for a schematic view of the optokinetic and the optomotor responses.

Both the OKR and the OMR serve to compensate for self-motion and stabilize the external world on the retina. The OMR refers to a form of visual taxis whereby animals follow the whole-field motion through tail-flip bouts generating swimming in the direction of the perceived environmental movement. This behavior enables the larva to avoid being carried downstream by the current and to stay in the same region using the visual cues present in the riverbed. OMR can be accurately generated from 5 dpf and is maintained throughout adulthood. The OKR is very robust and stereotyped. It is due to the coherent-moving environment around the fish's visual field that evokes slow eye rotations (pursuits) in the direction of perceived movement followed by rapid saccades in the opposite direction to reset the eyes' position. It should be noted that in the absence of visual cues, zebrafish larvae also move their eyes, by making regular spontaneous saccades in opposite directions [Portugues and Engert, 2009]. Because both OKR and OMR can be reliably evoked in the laboratory at early larval stages, these behaviors have been largely used to study visuomotor behaviors [Neuhauss et al., 1999, Huang and Neuhauss, 2008].

Hunting is critical for survival and relies on several decision-making processes. The first step is visual recognition. Larvae rely mostly on vision to capture prey, as demonstrated by the dramatic decrease in the number of prey eaten in the dark [Gahtan, 2005].

Small moving stimuli elicit specific locomotor and oculomotor movements intended

to position the larva in front of its prey. On the contrary, larger stimuli will elicit turns away from the stimulus [Bianco et al., 2011]. After recognition, the larva will initiate a tail bout to bring the paramecia in front of it. Successive bouts will bring the paramecia progressively closer. The capture itself will occur via suction or bitting depending on the relative position of the prey [Patterson et al., 2013, Borla et al., 2002]. The rapid maturation of sensory and motor systems also allows zebrafish to detect and avoid threatening or unpleasant stimuli by evoking escape and avoidance behaviors. In the face of an aversive stimulus such as a looming object (an expanding disk miming the approaching of a predator), head touching, air-puff, or acoustic stimuli. Trigger by these stimuli, larvae perform a C-bend movement to turn away from them followed by an immediate fast-forward swim. The time from the onset of tail bending to the moment of maximum tail curvature ranges between 9-18 ms [Temizer et al., 2015, Colwill and Creton, 2011]. Thus, zebrafish larvae display a variety of complex behaviors during the first 7 dpf.

1.6.4 *The optic tectum*

As for all vertebrates, the main excitatory and inhibitory neurotransmitters of the zebrafish are glutamate and GABA. While serotoninergic, dopaminergic, cholinergic, and norepinephrinergic neurotransmitters act as modulators. The gross architecture of many brain areas, e.g., retina, olfactory bulb, cerebellum, and spinal cord, and their main projection pathways are conserved as for all other vertebrate classes [Friedrich et al., 2010]. The optic tectum (OT), homologous to the superior colliculus in mammals, is the main visual center of zebrafish (see Figure 1.8 for its location in the brain). It is involved in receiving and processing multiple sensory inputs which are integrated to generate goal-directed motor behaviors via the tectal projections to motor centers in the hindbrain [Thompson et al., 2016]. Apart from the projections from the retina, the OT receives direct or indirect inputs from several sensory organs, the opposite tectal hemisphere, and other brain regions such as the telencephalon, thalamus, and nucleus istmi among others. The OT is composed of a large number of GABAergic and glutamatergic neurons (similar proportions) and a smaller number of cholinergic neurons [Nevin et al., 2010].

The projections from the retina are retinotopic and non-overlapping in the tectum. This means that neighboring retinal ganglion cells in the retina project to neighboring positions in the tectum. Indeed, evidence the tectal circuit contains a functional retinotopic tectal map of the contralateral visual field in which the dorsal-ventral visual hemifields are represented dorso-ventrally in the OT, and the nasal-temporal hemifields are mapped rostro-caudally in the tectal axis [Niell and Smith, 2005, Romano et al., 2015]. Moreover, The retinotectal projections have fine sublaminar divisions in which the OT receives multiple inputs from different combinations of the retinal ganglion cell terminals forming each

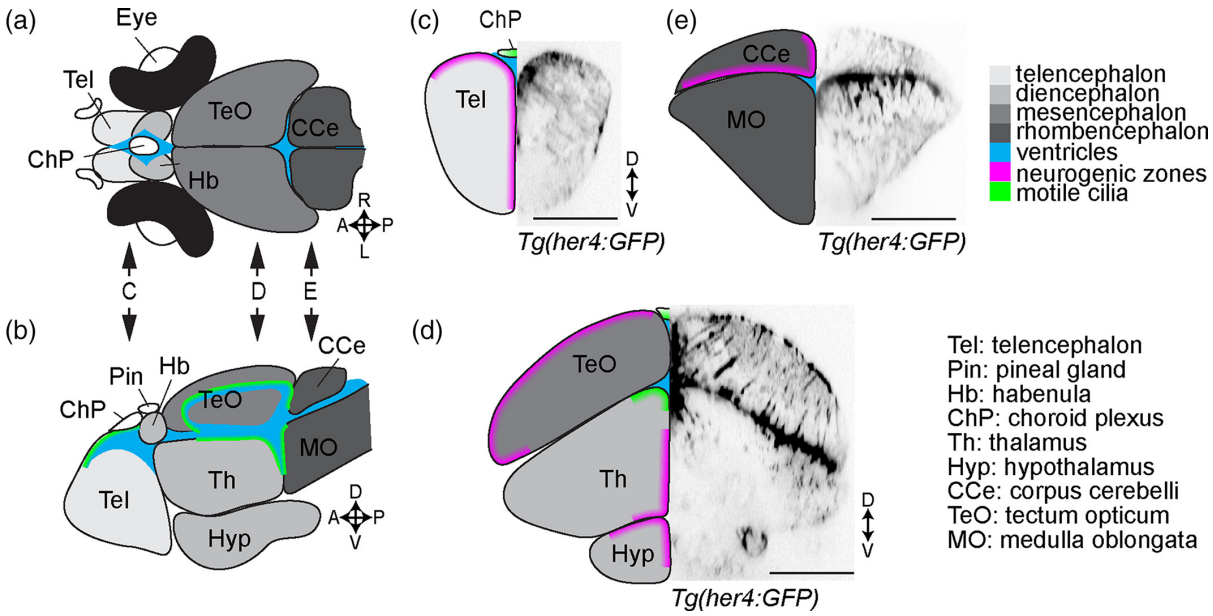

Figure 1.8: **Anatomy of the larval zebrafish brain.** Schematic representation of a 4–5-day-old larval zebrafish brain seen from dorsal (a), lateral (b), or transverse (c–e) views. Brain areas are represented in different shades of grey, ventricles in blue, neurogenic zones in magenta and motile cilia generating CSF flow in green. (c–e) Transverse sections through the telencephalon (c), di/mesencephalon (d), and rhombencephalon (e) as indicated in panels (a) and (b) show the various brain regions and the distribution of Tg(her4:GFP) positive radial glia obtained by confocal microscopy. Note the radial organization of radial glia with their nuclei located along the ventricles and processes reaching the pial surface. A: anterior, P: posterior, D: dorsal, V: ventral, R: right, L: left. Scale bar: 100 µm. Reproduced from [Jurisch-Yaksi et al., 2020].

sublamina by heterogeneous afferents. This implies that OT integrates different types of inputs in a multilayered organization associated with different functional responses to visual stimuli [Robles et al., 2013].

It has been shown that OT ventral regions have a preferential response to small visual stimuli while GABAergic interneurons in the dorsal layers are tuned to large ones. Notably, the selective ablation of these GABAergic neurons reverts this size filtering in the deep layers revealing an interesting mechanism that has been associated with prey capture processes [Bene et al., 2010]. Along the same lines, tectal ablation significantly affects prey capture of paramecia [Gahtan, 2005]. Moreover, a population of glutamatergic tectal interneurons, tuned to small-size stimuli, was proven to be required for larvae approach towards small objects [Barker and Baier, 2015]. Similarly, it was also shown by volumetric ca^{2+} imaging that tectal neurons located more caudally tend to respond more efficiently to prey-like visual stimuli than more rostral neurons [Förster et al., 2020]. Furthermore, OT has been also associated with the detection of predator-like stimulation, in which tectal neurons respond selectively to looming stimuli [Colwill and Creton, 2011]. These results imply that the tectal organization and its internal dynamics are adapted for processing object features relevant for triggering appropriate behavior.

Accumulating data has suggested that the direction of object motion is also processed by the OT. Visual stimulation and simultaneous Ca^{2+} imaging in intact larva experiments show that tectal neurons exhibit direction selectivity (DS), which means that they display a preferred response to stimuli moving toward a particular direction [Niell and Smith, 2005]. It was demonstrated by electrophysiology recordings of DS tectal neurons that their inhibitory inputs display significant selectivity toward the direction of motion while their excitatory inputs exhibit are less biased to moving stimuli [Grama and Engert, 2012]. Nevertheless, opposite results were also reported in which the excitatory inputs were more tuned by the direction of motion [Gabriel et al., 2012]. This discrepancy between the data is complementary since both studies focused on different neuronal subpopulations [Hunter et al., 2013].

Functional Ca^{2+} imaging in intact zebrafish larvae experiments revealed that the ongoing spontaneous activity of the OT is organized in neuronal functional assemblies composed of highly correlated neurons. These neuronal assemblies are spatially organized reflecting the functional tectal retinotopic map. They are tuned to biologically relevant visual stimuli (e.g., prey), and their activation predicted orienting tail movements. Moreover, the tectal assemblies show attractor-like dynamics (all-or-none activations and winner-takes-all dynamics), mechanisms that offer an advantage during prey detection in noisy environments. Overall, this suggests that the spatiotemporal functional connectivity of the OT is adapted for its vital functional roles such as the detection of prey [Romano et al., 2015].

1.6.5 Radial Glia Cell in Zebrafish is analogous cells to mammalian's astrocytes

The zebrafish brain cells repertoire contains diverse glial cell types, such as the radial glia cell (RGC) also called astroglia, microglia, and oligodendrocytes, each having a specific function in the brain [Jurisch-Yaksi et al., 2020, Lyons and Talbot, 2015]. In this section, I focus on the physiology of RGCs in zebrafish and how these cells in many aspects display homologous roles to the mammalian astrocytes

It has been widely described that RGCs are neuronal progenitors in the CNS of a variety of vertebrates, including zebrafish. During neural development, RGCs extend from the apical ventricular end to the basal layer establishing a radial morphology that also serves as such scaffold to help the migration of neurons. In mammals, RGCs differentiate to astrocytes generating a stellate morphology in the parenchyma at early post-natal stages, althougth these cells lost the neurogenic capacity, they can divide and populate the entire central nervous system [Jurisch-Yaksi et al., 2020, Lyons and Talbot, 2015]. Nevertheless, some astrocytes keep the neurogenic progenitor potential in restricted re-

gions of the brain throughout the entire life span of the animal [Steiner et al., 2019] . Intriguingly, In zebrafish, RGCs keep their morphology and their function as progenitor cells throughout their entire life [Kroehne et al., 2011].

The absence of star-shaped glial cells in zebrafish raises the possibility that RGCs become specialized in fishes to serve many of the specific roles of astrocytes in mammals. Accumulative evidence indicates that zebrafish RGCs have additional features in common with mammalian astrocytes despite their morphological differences. Namely, RGCs responses after an injury contribute to the formation of the glial scar and increase the neural stem cell proliferation rate [Becker and Becker, 2014]. Moreover, RGCs express proteins relevant to astrocytes' functions. For example, the water-transporting protein aquaporin-4 is associated with the regulation of ionic and water homeostasis [Grupp et al., 2010]. RGCs express the glutamate transporter Eaat2b suggesting their contribution to the neurotransmitters' equilibrium [Niklaus et al., 2017]. Recently, it has been reported that RGCs also express glutamine synthetase, an enzyme that participates in the metabolic regulation of glutamate [Chen et al., 2020]. Furthermore, as was described before *see section* 1.2.3, Astrocytes are organized in extensive domains via gap junctions. Equivalently, zebrafish RGCs establish functional territories via gap junction coupling and express connexin 43 [Chen et al., 2020, Verdugo et al., 2019]. A recent study reported the close association between RGCs and neuronal synapses [Chen et al., 2020]. Altogether these findings propose the zebrafish as an appealing model to study astrocyte biology *in vivo*.

Functional interaction between RGCs and neurons in Zebrafish

One of the most striking features of RGCs is their functional interactions with neurons. Recent evidence has confirmed the Ca^{2+} signaling as a response to NE discharge in the hindbrain and the spinal cord [Mu et al., 2019, Orts-Del'Immagine et al., 2022]. Intriguingly, RGCs also display microdomain Ca^{2+} transients [Chen et al., 2020]. RGCs Ca^{2+} elevations in the hindbrain of zebrafish larvae induce a transient cessation of neural activity, functioning as error integrators of futile optomotor responses when larvae are deprived of visual feedback. This integration enables larvae to switch to a quiescent behavioral state. This phenomenon is mediated by NE neurons located in the medulla oblongata leading to the RGCs activation of GABAergic neurons [Mu et al., 2019]. During induced epilepsy, perturbations of glia-neuron interactions lead to the emergence of epileptic seizures, in which, RGCs in the telencephalon are involved in the transition from the preictal period to seizures after the excessive release of glutamate [Verdugo et al., 2019]. In the rostral spinal cord, acousto-vestibular stimuli induce RGCs Ca^{2+} waves traveling bi-directionally to the hindbrain and the caudal spinal cord [Orts-Del'Immagine et al.,

2022]. All these studies reveal a clear parallel between zebrafish RGCs and mammalian astrocytes and highlight the outstanding RGCs-neuron functional dialogue associated with brain computation and behavior. Follow-up work using zebrafish may complement the studies made in mammals and will contribute to unveiling additional functional roles of astroglia underlying brain computations and behavior [Jurisch-Yaksi et al., 2020].

1.7 Objectives of the thesis

For many years, astrocytes were thought to mainly play a role in supporting neurons (e.g., neurotransmitter clearance, ion buffering, blood flow regulation, and metabolite delivery). However, more recent studies suggest that astrocytes are involved in several brain functions once considered specific to neurons. Astrocytes and Neurons have a reciprocate communication in which astrocytes sense neuronal inputs mainly by Ca^{2+} signaling and in turn, influencing neuronal activity, namely, via the gliotransmitters release. This bilateral dialogue has important implications in several levels of synaptic functions, sensory processing, and behaviour.

Despite these advances, the role of glia in visual processing remains elusive. Here, I addressed this open question through a comprehensive *in-vivo* approach using the visual system of an intact, non-anesthetized, non-paralyzed vertebrate. We used two-photon microscopy, transgenic zebrafish larvae expressing GECs in neurons and radial glia, optogenetics, and motor behavior. This approach enabled monitoring with single-cell resolution of the neuronal and radial glia dynamics in the zebrafish's main visual center, the OT.

During my thesis, I focused on these main topics:

1. I monitored the tectal RGCs Ca^{2+} transients and their correlation with tail behavior.

2. I investigated the tectal RGCs synchronization mechanisms and their relationship with proprioception and LC activity.

3. I explored the visual processes influence of tectal RGC Ca^{2+} signaling in the OT by evaluating neuron responses in the OT to visual stimulation during RGCs synchronization.

4. I studied the functional interactions between RGCs and tectal neurons by calculating the functional connectivity between RGCs and neurons and how RGCs

synchronization affects the pair-wise correlations between the spontaneous activity of tectal neuron.

I will detail the methods I used to conduct this project and the results I obtained in the following chapters.

2

Methods and techniques

In this chapter, I will present the different methods and techniques I used in this project. First, I describe the zebrafish husbandry and the transgenic lines I used. then, I explain the setup for the simultaneous Ca^{2+} imaging and behavioral recording, how the glia and neuronal activity was monitored using the two-photon microscope, and the data analysis for both Ca^{2+} imaging and tail behavior. Further, I detail the experiments in which larvae received different types of stimulation (Electric, Visual, and Auditory stimulation) and how the LC ablation and LC optogenetic activation were performed. Also, I describe cell labeling experiments and confocal imaging finally I describe the statistical methods applied.

2.1 Zebrafish lines and husbandry

Zebrafish develop rapidly in eggs and hatch at approximately 3 days dpf. They are then free-swimming larvae and start to be autonomous at 5 dpf (visual behavior is functional and they can hunt for food). They undergo at approximately one month of age a metamorphosis, including fins development, ossification of the skeleton, and scale development, among other changes, and are then called juveniles. Afterward, they reach

sexual maturity at 3 months of age and can live up to 5 years.

For all experiments, zebrafish larvae from 6 to 7 dpf were used. All experiments were approved by the *comité d'éthique en expérimentation animale* n°005 (reference number APAFIS#27495-2020100614519712 v14).

2.1.1 Crossings and care

In our zebrafish facility, adult fish are maintained in fish tanks whose water is running in a closed loop, with filters that keep the water clean and in a good chemical and physical state. They are fed with Artemia salina (crustaceans) or rotifers, and dry powder containing algae. The light/dark cycle is set at 14:10 hours with the lights on at 9:15 AM. Fish from 4 to 18 months can be crossbred up to twice a week. Each mature female can produce between 50 to 200 eggs in one crossing so we can easily and quickly obtain a high number of larvae for the experiments.

For the crossings, one adult male and one adult female are placed at the end of the day in a fish tank, with a physical vertical separation between the two to allow them to see and smell each other but not touch them. The next day, as soon as the lights go on, fish are put together above a horizontal grid. The eggs are produced and fall across the grid to the bottom of the tank where they are protected from the adults (that would otherwise eat them).

Embryos are then collected and placed in Petri dishes in a 28°C incubator, in an embryo medium (NaCl 5.0 mM, KCl 0.17 mM, CaCl2 0.33 mM, MgSO4 0.33 mM pH 7.2 in distilled water with 0.1% methylene blue as an antifungal) until they hatch. This medium is changed twice a day and the abnormal or unfertilized eggs are removed. After the hatching, the composition of the medium is the same except for the methylene blue. Once they have reached 5 dpf, the larvae are fed with paramecia twice a day.

2.1.2 Fish lines

We used *nacre* background zebrafish: mutants that lack melanophores (black pigmentation) except in the non-crest-derived retinal pigment epithelium (meaning they have a normal retina) [Lister et al., 1999]. Therefore, *nacre* larvae have transparent skin enabling monitoring brain activity in an intact organism without the need to open the skin or use 1-phenyl 2-thiourea (PTU) to reduce pigmentation, as what was done before, but it was highly inconvenient and teratogenic [Karlsson et al., 2001].

Ca^{2+} is a second messenger for neurotransmitter reception and membrane depolarization. After a neuron spike, there is an intracellular Ca^{2+} concentration increase. In

astrocytes Ca^{2+} signaling has been accepted as an functional link between the neuronal-glia communication *see section* 1.3.2. Therefore, following the Ca^{2+} dynamic enables monitoring the neuro-glia circuits activity. For this end, the genetically encoded calcium indicator (GECI) binds to Ca^{2+} and emits fluorescence visualizing intracellular Ca^{2+} concentration *in vivo*. Intracellular Ca^{2+} variations induce conformational changes of the GECIs proteins which in turn are correlated with different emission fluorescence levels [Chen et al., 2013]. The use of GECI presents many advantages, notably the possibility to sample sub-populations of cells by the use of promoters, the stability of their expression over time, or the fact that optical imaging, contrary to electrophysiology, can capture the activity of thousands of neurons at the same time [Lin and Schnitzer, 2016].

In this project we use a different set of GECI zebrafish expressing lines under the control of different promotors:

- Ca^{2+} functional imaging experiments of RGCs were performed using the GECIs GCaMP (Green fluorescent protein-CalModulin Protein sensor) and RCaMP (Red fluorescent protein-CalModulin Protein sensor) for green and red fluorescence emission respectively under the control of the RGCs promoters gfap or her4.1. We use tg(gfap:GAL4; uas:GCaMP7a), tg(gfap:GAL4; uas:RCaMp1b) or tg(her4.1: GCaMP6m) zebrafish larvae. The transgenic line tg(gfap:GAL4) [Shimizu et al., 2015] (kindly provided by Dr. Ohshimar, Waseda University, Japan and National Bioresource Project, Japan) was cross with (uas:GCaMP7a) and (uas:RCaMp1b) [Muto et al., 2013, Zada et al., 2019].

- Neuronal Ca^{2+} dynamics were recorded using larvae pan-neuronally expressing the GCaMP6f indicator tg(huc:H2B-GCaMP6f). Huc promoter targets all neurons and the H2B protein is a histone attached to the GCaMP6f to direct its expression to the nucleus [Dunn et al., 2016]. The use of the H2B protein allows a high signal-to-noise ratio because neurons can be separated from each other easily in dense regions such as the OT [Shemesh et al., 2020]. The nucleus uses the Ca^{2+} signals for the regulation of gene expression for example [Hardingham et al., 2001], but it was proven in hippocampal neurons that the nuclear envelope does not block Ca^{2+} signals coming from the soma, and thus the intracellular wave of Ca^{2+} increase can be detected in the soma as well as in the nucleus [Eder and Bading, 2007]. Nevertheless, the nuclear localization of the fluorophore slows the kinetics of the fluorescence [Shemesh et al., 2020].

To study the projections of LC to the OT we cross two different lines: the tg(her4.1: mCherry) to express a red fluorescence protein in RGCs and tg(dbh:Gal4; uas:EGFP-caax) to express GFP under an LC promoter (dbh) [Admati et al., 2020, DeMarco

et al., 2020, Zada et al., 2019]. Additionally, for tracking the LC efferents we use the photoactivatable fluorescent protein Kaede expressing under LC-specific promotor dbh tg(dbh:Gal4; uas:Kaede) [Bergeron et al., 2012]. *In section 2.4 I give a detail explanation of the method I used.* Finally, to activate specifically NE-LC neurons we performed optogenetic experiments by the use of the larvae expressing ChR2 under dbh as a LC promotor tg(dbh:Gal4; uas:ChR2-mCherry) [Helmbrecht et al., 2018]. tg(uas:ChR2-mCherry) was kindly provided by Herwig Baier and Harold Burgess; National Institute of Child Health and Human Development, Bethesda, MD, USA). *see section 2.3.3.*

2.2 Functional Ca^{2+} imaging

2.2.1 Two-photon Ca^{2+} imaging

To study the Ca^{2+} activity and the behavior at the same time, we combined a two-photon point scanning microscope with a behavioral set-up where the tail recording was done by using an infrared camera filming from below (see Figure 2.1. A). Two-photon Ca^{2+} imaging in combination with transgenic zebrafish larvae described before 2.1.2, makes it possible to study the dynamics of large neuronal networks, with single-cell resolution, while presenting the stimuli. The two-photon microscopy relies on a laser that produces pulses of light of extremely short duration (10^{-12} to 10^{-15} seconds) containing a very high density of photons.

The larvae were embedded in 2% low-melting agarose and placed in the center of a chamber filled with E3 embryo medium. Agarose was gently removed from the tail. For tail recording, we added to the system a high-speed camera (Baumer HXG20NIR, 200 Hz.) and an infrared LED for illumination purposes (920nm). The two-photon microscope consisted of a modified version of the MOM (Sutter Instruments) controlled by the software package scanimage 3.8. We used a NA 1.05, 25X objective (Olympus), and a Ti:Sapphire laser (Spectra-Physics Mai Tai DeepSee) tuned at 920 nm for GCaMP and 980 nm for RCaMP. The output power at the focal plane was less than 3 mW. The emission signal passed through a FF705 dichroic filter, then it was separated by a FF562-Di03 dichroic mirror. Two band-pass filters FF01-512/25 (green) or FF01-630/92 (red) (all semrock) were positioned before the photomultiplier tubes (H1070 GaAsP from Hamamatsu, Japan). The current signals were then pre-amplified with a SR-570 (Stanford Research Systems) and reconstituted and saved using ScanImage 3.8 software [Pologruto et al., 2003] (in Matlab (MathWorks). The acquisition rate was 1.95 Hz with 256x256 pixels resolution. An arduino board was used to synchronize the Ca^{2+} imaging with the

behavior recordings. (see Figure 2.1.A)

This method leads to the precise localization of the excitation in the focal volume, thus optimizing the signal-to-noise ratio and limiting the phototoxicity of the laser to the living tissue, allowing longer recordings without damaging the tissue in and outside of the focal plane. An additional advantage is that the 920 nm wavelength can penetrate deeply into the tissue and does not stimulate the visual system of the larva, thus not interfering with the presented stimulus. With this method of point-scanning microscopy, we can have a very precise spatial resolution, however scanning each point is a relatively slow process, so it is at the expense of temporal resolution.

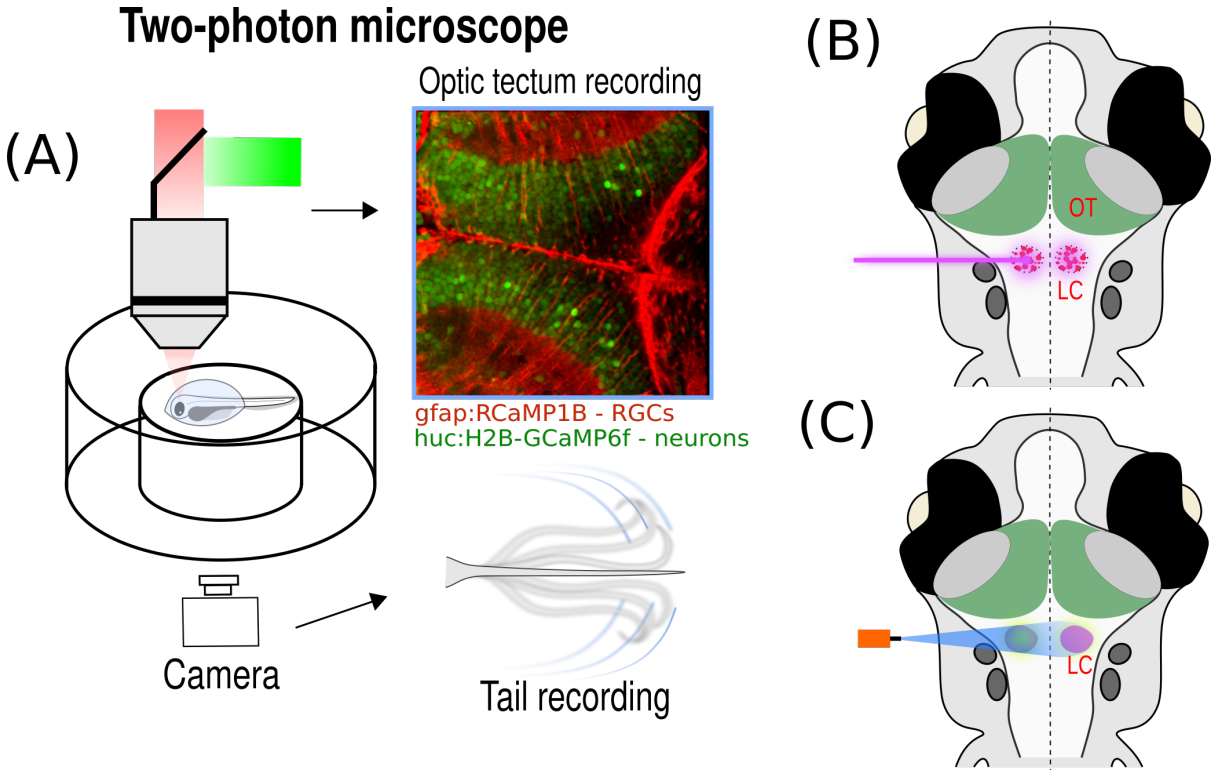

Figure 2.1: **Experimental set-up. (A)** Two-photon point-scanning calcium imaging was used for recording the neuronal and astroglia activity while simultaneously the tail behavior was recorded. The larvae were embedded in 2% low-melting agarose and placed in the center of a chamber. Agarose was gently removed from the tail. For tail recording, we added to the system a high-speed camera and an infrared LED for illumination purposes. blue square, Optical section of the optic tectum of a zebrafish larva expressing GCaMP under a neuronal promoter (HuC:GCaMP6f, green) and RCaMP under the control of a glia promoter (GFAP:RCaMP, red). **(B)** I performed the ablations using a two-photon laser in transgenic larvae expressing a red fluorescence protein under the control of a noradrenergic neurons promoter (dbh:nfsb-mCherry) for identifying the LC. To confirm neuronal death following the laser ablations, we used the apoptosis marker acridine orange. **(C)** For optogenetic stimulation a 100 µm optic fiber (455 nm) was directed towards the LC from the side of the larva. The LC was identified according to its red fluorescence (dbh:nfsb-mCherry). The stimulation consisted of a 1-sec pulse of 1 mW/cm2.

2.2.2 Ca^{2+} imaging data analysis

The extraction of significant events from the acquired ca^{2+} imaging data was performed using custom-made programs in Matlab (The MathWorks, Inc.), as well as a Matlab toolbox developed by Sebastian A. Romano in the lab [Romano et al., 2017]. Several steps are needed to obtain the fluorescence traces from every cell across time.

- **Image registration**. A ScanImage custom-made plugin allowed us to compensate drifts in the Z plane by calculating in real time the correlation between every 50 frames and three recorded planes in advance (The registration plane, as reference, and two other planes 2.2 µm dorsal and ventral from it). If the correlation was higher with another plane than with the reference one, the objective was moved up or down accordingly by 0.44 µm until the correlation of the running average was again maximal with the reference plane. If this compensation failed, the experiment was discarded. The images series were saved as TIFF files. To compensate for potential mild XY shifts, we registered the stacks offline using the Image J plugin Template Matching, in combination with a custom-made algorithm (Matlab, The MathWorks, Inc.) to further smooth the registration.

- **Movement artifacts**. Movement artifacts were detected according to the successive frames' cross-correlation. All frames with large discrepancies (z-score smaller than -3) were manually examined and discarded if necessary. If after a movement artifact the imaged plane did not return to its original position, the experiment was not taken into account.

- **RGCs segmentation and detection of significant Ca^{2+} events**. Based on RGCs morphology and their anatomical distribution, their corresponding Regions of interest (ROIs) were manually segmented. The calcium changes were estimated by averaging the pixel values inside the ROIs, across frames. The relative change in fluorescence corresponded to the difference between each point in time and the baseline ($\Delta F/F$). To calculate the baseline of each RGC a 7.5 sec running average was applied to the data. Then, the 8th percentile in a 30 sec long running time window was computed. Due to the slow Ca^{2+} dynamics of RGCs, we applied to the $\Delta F/F$ time series a filter based on an exponentially weighted moving average. We considered a RGC significant Ca^{2+} transient if its $\Delta F/F$ exceeded two standard deviations above baseline and a population synchronous Ca^{2+} event when at least 33% of RGCs were simultaneously active in at least 8 frames in a row.

- **Neuron segmentation** We created ROIs corresponding to the nucleus of the imaged neurons based on their morphology using a watershed algorithm [Romano

et al., 2017]. The algorithm identified the nucleus of neurons finding local fluorescence intensity peaks, then it generated ROIs layouts which were later manually curated. Analysis was done in time-averaged registered stacks. Averaged pixel values within the ROIs were used to estimate the Ca^{2+} dynamic associated with the activity of each neuron.

- **Neuron detection of significant Ca^{2+} events**. The time series baseline of each neuron was computed as the 8th percentile in a 30 sec long running time window to obtain the slow fluctuations unrelated to the fast Ca^{2+} transients associated with the neuronal activity [Romano et al., 2017]. The relative change in fluorescence ($\Delta F/F$) corresponded to the difference between the fluorescence at each point in time and the baseline fluorescence. A data sanity test discarded ROIs with fluorescence signals too low and/or presenting artifactual fluorescence traces, i.e., sudden variation of the baseline fluorescence (as in unhealthy or dying neurons, or healthy neurons that drifted in and out of focus). To infer the Ca^{2+} related fluorescence events associated with neuronal activity, we calculated the statistical significance of single-neuron calcium dynamics in an adaptive and unsupervised manner [Romano et al., 2017, Pérez-Schuster et al., 2016]. We considered that any event in the fluorescence time series data belongs to either a neuronal activity process or an underlying noisy baseline. To discriminate, with a desired degree of confidence, between these two sources, we built a data-driven model of the noise [Romano et al., 2017]. Moreover, we took into account the biophysical constraints of the fluorescent calcium indicator (H2B-GCaMP6f fluorescence time constant 2.88 sec) [Kawashima et al., 2016]. Then, we applied a Bayesian odds ratio estimation framework. This method labels as significant with at least 95% confidence the fluorescence data points whose dynamics meet two conditions: i) it cannot be explained by the underlying fluorescence noise; ii) they are compatible with the H2B-GCaMP6f time constant. We obtained significantly and non-significantly active portions of the $\Delta F/F$ traces. A more detailed explanation of the calculation significance can be found in Romano et al., 2017.

The pipeline presented above is the one that was followed for each Ca^{2+} imaging experiment. The details of analyses carried out specifically for each experiment are explained in the corresponding sections of the upcoming chapters.

2.3 Behavioral experiments and stimulation

2.3.1 Motor behaviour quantification (Tail deflection)

Using the binarized images of the larvae acquired using the high-speed camera, we first fitted an ellipse. Then, we split the image into two segments to fit an ellipse on each of them according to its minor axis. Afterward, we calculated the center of the curvature as the intersection of the minor axis of the two last ellipses. Finally, the tail deflection was defined as the inverse of the averaged distance from the center of curvature to the pixels of the binarized image (1/R) multiplied by the length of the larvae at rest (L0/R). More information can be found in [Jouary et al., 2016]. The probability to have tail deflection associated with motor behavior was quantified between the 10 first secs. after the onset of all RGCs synchronous events and a similar time windows selected at random time points, excluding 30 secs. Before and after RGCs synchronous events. Larvae with motor behavior probabilities less than 0.01 were not taken into account for data analysis.

2.3.2 Mild electric stimulation

Individual larvae were placed as was described in the two-photon Ca^{2+} imaging section *see* 2.2.1, and we added to the recording chamber a custom-printed electrode holder. In the holder, we introduced a pair of silver electrodes (0.381 mm, diameter, A-M systems) separated by 4 cm. The larva was placed equidistant and parallel to both electrodes. For the stimulus, we used a 22.5 V pulse of a duration of 100 msec using the SD9 stimulator (A-M systems). An arduino board was used to synchronize the two-photon Ca^{2+} imaging, behavior video recordings, and the mild electric stimuli.

2.3.3 Optogenitic stimulation

For optogenetic stimulation of the LC, we placed the larvae in the recording chamber as previously explained *see* 2.2.1. A 100 µm optic fiber (AFS105/125Y 0.22 NA, Thorlabs), was mounted on a manipulator (FX-117, Electron Microscopy Sciences) and directed towards the LC from the side of the larva. The LC was identified according to its red fluorescence. The optic fiber was coupled to a blue LED (488 nm, Thor Labs). The stimulation consisted of a 1-sec pulse of 1 mW/cm2. For control, the same optic fiber was displaced to a nearby brain region. *For an schematic representation fee figure* 2.1C. An arduino board was used to synchronize the two-photon Ca^{2+} imaging, behavior acquisition, and optogenetic stimuli.

2.3.4 Two-photon ablation of LC

For the ablations we used a two-photon laser tuned at 920 nm with a power of 450 mW after the objective (Spectra-Physics Mai Tai DeepSee), to scan each optical plane containing neurons of the LC for 1-3 min (the duration gradually increased as we scanned more ventral layers). For the LC ablations, the optical planes were separated by 6 µm. To identify the LC, we performed the ablations in transgenic larvae expressing a red fluorescence protein under the control of a noradrenergic neurons promoter (dbh:nfsb-mCherry). *For an schematic representation fee figure* 2.1B. In control experiments, similar numbers of neurons nearby LC were ablated with the same protocol [Pérez-Schuster et al., 2016].

Labeling apoptotic neurons with acridine

To confirm neuronal death following the laser ablations of LC, we used the apoptosis marker acridine orange. For this purpose, we submerged the larvae in a 3% acridine in E3 embryo medium, for 30 min in the dark. Then, the larvae were rinsed twice with fresh embryo medium. After 5 min the larvae were immobilized in low-melting agarose, placed in the recording chamber, and imaged using a two-photon microscope tuned at 970 nm [Pérez-Schuster et al., 2016].

Retrograde Labeling and Two-photon ablation of reticulospinal neurons

To label the reticulospinal neurons, retrograde labeling was performed by injecting a Dextran Texas Red dye (10,000MW, Invitrogen) into the spinal cord. One day before imaging, 6 dpf, huc:H2B-GCaMP6f larvae were embedded in 2% low-melting agarose placed on their side. A solution of 25 mg/ml Dextran Texas Red in Ringer solution was pressure-injected using Glass capillaries (1.0 mm outer diameter, 0.5 mm inner diameter, without filament, FHC, USA) into the caudal spinal cord at the level of the anus using a pneumatic pico pump, 3× 100 ms pulses (PV 820, World Precision Instrument). To enable the precise positioning of the capillar, this was mounted on a micromanipulator (Model FX-117, Electron Microscopy Sciences). The dye penetrated the spinal cord via the damaged axons. Fluorescent-labeled reticulospinal neurons were imaged using two-photon scanning microscopy [Candelier et al., 2015]. Reticulospinal neurons were ablated using the same protocol described for LC.

2.3.5 Visual stimulation

Larvae were embedded in low-melting agarose and placed on an elevated stage within a custom-made cylindrical chamber filled with E3 embryo medium which offers an unob-

structed view of the entire field of view. Visual stimuli were projected on a screen placed around the wall of the chamber, using a pico-projector (refresh rate: 60 Hz, P4X, AAXA, USA). Larvae were carefully aligned to the projector using a custom-made program, Visual stimuli were presented to the left eye only. The stimulation field covered approximately 180° x 60° (azimuth x height) of the larva's visual field. To avoid interference of the projected light with the GCaMP emission signal, we only used the red LED (620 nm) of the projector and a long-pass filter (BLP01-561, Semrock, USA) placed in the front of the projector. The minimal luminance of the projected stimuli (background) was 8 lux, and the luminance of the red stimuli was 800 lux. The contrast was calculated as 0.98 (Michelson contrast, commonly used for periodic functions: (ImaxImin)/(Imax+Imin) = 792/808 = 0.98). All stimuli were generated using Matlab (The MathWorks, Inc) and the Psychophysics Toolbox Version 3 extension. A geometrical deformation was imposed on the stimuli to take into account the curvature of the chamber, so as to not affect the spatial frequency of the stimulus.

To study how the RGCs synchronization affects neurons' response to visual stimuli in the OT, we presented two types of visual stimuli: light spots of 13°, 23°, and 44° projected at the center of the larva's field of view (45° azimuth and 0 ° elevation), and a 10° x 60° light bars moving in rostro-caudal and caudo-rostral directions. Each stimulus lasted 1 sec and was presented individually at three-time points according to the RGCs synchronization dynamics: 10 sec before the onset of the RGCs synchronization, 10.5 sec after (when the RGCs reached their highest activity peak), and 20 sec after (at the end of the RGCs Ca^{2+} synchronous event). The RGCs synchronous events were triggered by a mild electric shock (55 times separated by 70 sec). The order of the different types of presented stimuli was shuffled to prevent habituation. These experiments were performed using transgenic larvae expressing GCaMP under a pan-neuronal promoter, tg(huc:H2B-GCaMP6f) and transgenic larvae expressing GCaMP under a glia promoter, Tg(her4.1:GCaMP6m) as a RGCs activity control. *For an schematic representation fee figure* 2.2.

Calculation of direction selectivity

We quantified the direction selectivity of a neuron according to a direction selectivity index. For this analysis, we just considered neurons with significant Ca^{2+} traces within a 2.5 sec time window from the stimulus onset, in response to at least one-third of the presented stimuli. Then, we calculated the difference of their average neuronal responses to the light bars moving in opposite directions (Rostro-caudal and caudo-rostral) divided by their sum (Rostro-caudal - caudo-rostral)/(Rostro-caudal+caudo-rostral). Thus, a direction selectivity index around zero will correspond to a non-directional selective neu-

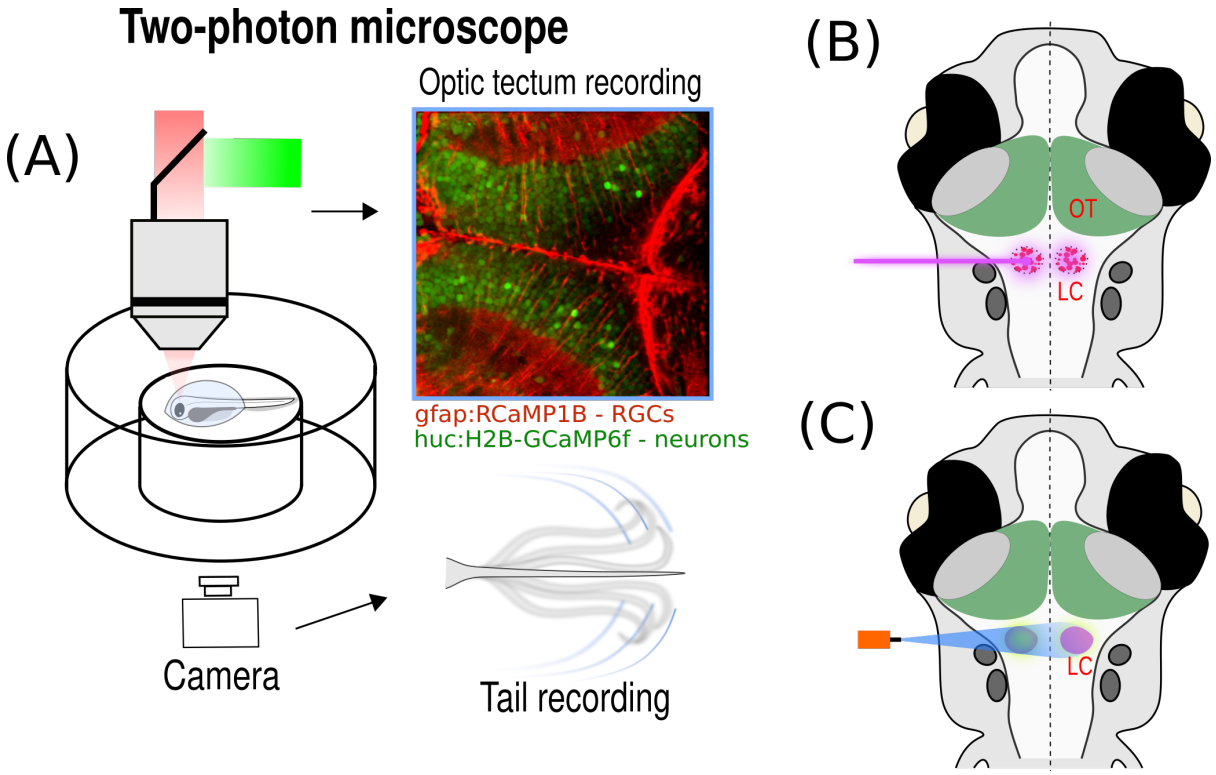

Figure 2.2: **Visual stimulation experimental design. (A)** Schematic of the visual stimulation paradigm. Visual stimuli were projected on a screen on the right visual hemifield using a pico-projector. Light spots of 13°, 23°, and 44° and bars moving in the rostro-caudal or caudo-rostral directions were presented to the larva's right eye. Tectal neurons were recorded using a two-photon microscope, imaged area (red square). **(B)** top: Schematic of the stimulation paradigm. The grey curve represents a hypothetical RGC Ca^{2+} synchronization event induced by a mild electric shock (dashed line, time zero) that can induce an escape behavior. Red bars: the 3-time points in which visual stimuli were presented (before, during, and after the RGC synchronous event). Each stimulus lasted 1 sec and was presented in random order. Botton: left, Schematic representation of RGCs Ca^{2+} activity in the 3 evaluated points (before, during, and after the RGC synchronous event). Right, Schematic of the zebrafish head showing the imaged area (red square).

ron, while those around 1 or -1 will indicate a rostro-caudal or caudo-rostral directionally selective neuron, respectively.

Auditory stimulation

To monitor the neuronal activity induced by auditory stimuli, we placed the larvae in a 3D-printed recording chamber with a waterproof speaker embedded in its wall (Visaton K28 WP). We presented two broadband auditory stimuli (300-400 Hz and 800-1000 Hz) lasting 1 sec. To study how RGC synchronization could modulate the neuronal response to auditory stimulation in the OT, we presented to the larva the two types of auditory stimuli 10 sec before an induced RGC synchronization and 10 sec and 20 sec after the synchronization. Each stimulus was presented at random 20 times at each of the time

points concerning the RGC synchronization. The RGC synchronous events were triggered every 70 sec.

2.4 cell labeling experiment

Immunofluorescence

Larvae were fixed for 2 hours in 4% paraformaldehyde (PFA) in PBS at 4°C and washed in PBST (PBS/0.5% Triton). The larvae tissue was then blocked with blocking buffer (10% fetal bovine serum diluted in 1% DMSO and PBST) for 1 hour at room temperature (RT). After blocking, the samples were incubated in primary antibody mouse anti-β2-AR (Cat. No. sc-271322, E-3, Santa Cruz Biotechnology, Santa Cruz, CA) 1:100 dilution, in blocking buffer overnight at 4°C. After 3 washes in PBST and another incubation in the blocking buffer for 1 hour at RT, secondary goat anti-mouse Alexa Fluor 488 IgG (catalog A-11001, RRID AB 2534069, Thermo Fisher Scientific, Waltham, MA) was added and left overnight at 4°C. The secondary antibody was then washed 3 times with PBST. Larvae were kept in PBST until confocal imaging.

Kaede photoconversion

The offspring of tg(dbh:Gal4) and tg(uas:Kaede) crossed lines were raised in darkness to prevent pre-conversion of neurons. A unilateral group of dbh green positive cell bodies in the LC of 6 dpf larvae was exposed to 405 nm for 10 seconds. Photoconversion of dbh cell bodies from green to red was confirmed right after exposure. Photoconverted larvae were then placed in freshwater in the dark for 24 hours and then imaged under a confocal microscope.

Confocal imaging of morphology and immunostaining

Immunostained, tg(her4.1:mCherry; dbh:Gal4/uas:EGFP-caax) and Kaede photoconverted larvae were mounted in low-melting agarose (1.5%) and imaged using Zeiss LSM710 upright confocal microscope equipped with a DPSS 561 nm and 488 nm lasers (Zeiss, Oberkochen, Germany) with NA 1, 20X objective (resolution of 1024x1024). All images were processed using ImageJ (National Institutes of Health, Bethesda, MD). In this study we used the tg(dbh:Gal4) and tg(UAS:ChR2-mCherry) crossed together with tg(her4.1:CGaMP6m) to produce the tg(her4.1:GCaMP6m/dbh:Gal4/UAS:ChR2-mCherry) line.

2.5 Statistics

For two-group comparisons, we used t-student if the data were normally distributed. If this was not the case, we used the two-sided rank-sum test. For comparison among multiple groups when data distributions were normal, we used the ANOVA test. Otherwise, we used the Kruskal-Wallis test followed by the multicomparation test. For comparison between histograms, we used the Kolmogorov–Smirnov test. p values lower than 0.05 were considered to be statistically significant. All results are represented as mean $\pm$ SEM.

All the developed software for data analysis and visual stimulation was coded in MATLAB R2020b. The codes will be made available upon request.

3

Results

Recent studies show that brain computations and complex behaviours are controlled by neuro-astrocyte network interactions. To study these interactions in visual processing, I used two-photon microscopy to image transgenic zebrafish larvae expressing GECIs under the control of a glia promoter (her4), to study Ca^{2+} dynamics of radial glia cells (RGCs) in the optic tectum (OT). I found that the Ca^{2+} activity of individual RGCs synchronizes just after the end of an escape behaviour. This synchronous activity is mediated by the locus coeruleus (LC), the main brain's source of Norepinephrine (NE). Tectal RGCs synchronization occurs in a specific layer of the OT and specifically modulates the direction selectivity of tectal neurons and their long-distance functional correlations. These results shed light on the relevant role of tectal–RGCs interaction in the modulation of neuronal visual processing.

In following pages is enclosed the article *"Radial glia synchronous activity modulates visual responses and functional connectivity in the zebrafish optic tectum"* that will be submitted in *Neuron*, detailing the results obtained and the discussion.

Radial glia synchronous activity modulates visual responses and functional connectivity in the zebrafish optic tectum

Abstract

Uribe-Arias Alejandro[1], R. Rozenblat[2]*, A. Kulkarni[1]*, D. Zada[2] *, S. Charpy[1], E. Marachlian[1], L. Appelbaum[2], G. Sumbre[1]

1. Institut de Biologie de l'ENS (IBENS), Département de biologie, École normale supérieure, CNRS, INSERM, Université PSL, 75005 Paris, France

2. Bar-Ilan University, The Faculty of Life Sciences and The Multidisciplinary Brain Research Center, Ramat-Gan, Israel

Abstract (150)

Recent studies suggest that several brain computations and motor behaviors are mediated by the interaction between neuronal and astrocyte networks. To explore these interactions in the visual system, we used two-photon Ca^{2+} imaging of zebrafish larvae expressing GCaMP in both neurons and radial glia cells (RGCs). We found that RGCs synchronize their Ca^{2+} transients immediately after the end of an escape behavior. Using optogenetics and ablations, we found that RGC synchronous Ca^{2+} events are mediated by the locus coeruleus. RGC synchronization was specific to the ventral planes of the optic tectum and modulated the direction selectivity of tectal neurons and their long-distance functional correlations. This mechanism may support freezing behavior following a switch to an alerted state and improve visual detection. Overall, these results show that a switch to an arousal state modulates visual responses through the interaction between neuronal and glia circuits.

Introduction

Astrocytes play an important role in supporting neurons (e.g., neurotransmitter clearance, ion buffering, blood flow regulation and metabolite delivery) (Araque and Durkee, 2019; Perea and Araque, 2010) . Although they do not display largeintracellular voltage changes as in neurons, they show large Ca^{2+} transients in response to neuronal activity, sensory stimulation and locomotion (Lines et al., 2020; Nimmerjahn et al., 2009; Schummers et al., 2008; Srinivasan et al., 2015). These Ca^{2+} transients can trigger the release of several gliotransmitters such as glutamate, ATP, and D-serine, which are capable of modulating neuronal synaptic transmission (Araque et al., 2014; Savtchouk and Volterra, 2018) and

synaptic plasticity (De Pittà and Brunel, 2016). Likewise, astrocytes are involved in dentritic spine maturation in the hippocampus by regulating the vesicular release of D-serine (Sultan et al., 2015).

Recent studies show that hippocampal astrocytes induce synaptic potentiation, enhancing memory acquisition and improving cognitive behavior in mice (Adamsky et al., 2018; Kol et al., 2020). In the central medial amygdala of mice, chemogenetic activation of astrocytes modulates fear responses by the regulation of specific synapses (Martin-Fernandez et al., 2017). In the neocortex of mice, astrocytes show an increase in Ca^{2+} events prior to transitions from slow-wave sleep to wakefulness (Bojarskaite et al., 2020). Moreover, astrocytes trigger synchronized transitions to up states in nearby cortical neurons in mice (Poskanzer and Yuste, 2011) and mediate the transition between working and resting states (Kjaerby et al., 2017). These global state shifts have been associated with the brain-wide release of norepinephrine (NE), which is also associated with arousal and alertness states (Bekar et al., 2008; Paukert et al., 2014; Srinivasan et al., 2015; Wahis et al., 2021). Furthermore, motor behavior gates astrocyte Ca^{2+} transients in response to visual stimulation (Paukert et al., 2014). These studies and several others (Araque and Durkee, 2019; Kofuji and Araque, 2021; Semyanov, 2019) suggest that astrocytes play an important role in brain computations.

In zebrafish, radial glial cells (RGCs) have been proposed to have an analogous function to that of mammalian astrocytes despite their absence of star-shaped (Chen et al., 2020; Jurisch-Yaksi et al., 2020). In contrast to mammals, RGCs in zebrafish do not degenerate; they have elaborated processes and express proteins considered to be specific markers of astrocytes (e.g., aquaporin-4, markers of tight junctions, glutamine synthetase and glutamate transporters) (Chen et al., 2020; Jurisch-Yaksi et al., 2020; Lyons and Talbot, 2014). Recent studies show that RGCs in the hindbrain of zebrafish larvae function as integrators of futileswim responses to visual flow when deprived of visual feedback. This integration enables larvae to switch to a quiescent behavioral state (Mu et al., 2019). Moreover, in the zebrafish forebrain, RGC activity is anti-correlated with bursts of neuronal activity, suggesting that RGCs may regulate neuronal activity. During induced epilepsy, perturbations of these glia-neuron interactions lead to the emergence of epileptic seizures (Verdugo et al., 2019). However, the functional role of RGCs in the visual system is unknown.

To address this open question, we used two-photon microscopy to image transgenic zebrafish larvae expressing GCaMP-7a or GCaMP6m under the control of a glial promoter (her4.1 or GFAP), to study RGC Ca^{2+} dynamics in the optic tectum (OT). In zebrafish, the OT, homologous to the mammalian superior colliculus, is involved in the detection of visual features and the generation of goal-directed motor behaviors (e.g., prey capture) (Bollmann, 2019). We found that the Ca^{2+} activity of individual RGCs synchronizes a few seconds after the end of an escape behavior. This synchronous Ca^{2+} activity is

mediated by the locus coeruleus (LC), the brain's main source of NE. Tectal RGC synchronization only occurs on the ventral planes of the OT and specifically modulates the direction selectivity of tectal neurons and their long-distance functional correlations.

This RGC-mediated modulation of visual circuits is associated with behavioral passivity and may serve to adapt the visual system to the new contextual and behavioral constraints during brain-state transitions (e.g., arousal).

RESULTS

Tectal RGCs synchronize their Ca^{2+} transients following an escape behavior

To study the functional role of radial glia cells (RGCs) in visual processing, we first characterized the spontaneous Ca^{2+} activity of RGCs in the optic tectum (OT). For this purpose, we used two-photon scanning microscopy to image 6-7 days post-fertilization (dpf) zebrafish larvae expressing the genetically encoded Ca^{2+} indicator GCaMP-7a or GCaMP6m under a glial promoter (gfap or her4) (Figure 1A). We found that individual RGCs sporadically displayed synchronous Ca^{2+} transients across the entire imaged RGC population (10 ± 2 times per hour, Figure 2C, n = 11 larvae). The spontaneous increase in Ca^{2+} propagated from the tectal neuropil along the RGC projections to the RGC somata located on the borders of the tectal ventricle (Figure 1A). Using a high-speed video camera in combination with the two-photon microscope, we observed that RGC synchronous events followed tail movements (delay between onset of movement and that of RGC synchronous event: 3.13 ± 0.60 s, Figure 1B and 1D). Moreover, we found that the RGC synchronous events emerged mainly after large tail deflections (Jouary et al., 2016), rather than following small tail deflections (routine turns, forward scoots, j-turns, etc.) (Budick and O'Malley, 2000). The mean amplitude of the RGC Ca^{2+} transients associated with escape behaviors was significantly larger than that associated with small tail deflections (large deflection, 0.98 ± 0.16; small deflection, 0.24 ± 0.03 $\Delta F/F$; $p < 0.001$, two-sided rank-sum test, n = 11 larvae, Figure 1E, 1F and Figure S1A-D). Furthermore, we found that for the first 10 sec after the onset of an RGC synchronous Ca^{2+} event, the probability of observing an additional motor behavior significantly decreased with respect to the probability of observing a motor behavior in the absence of a RGC synchronous Ca^{2+} event (P(spontaneous behavior during RGC synchronization per 10 sec) = 0.04 ± 0.02, P(spontaneous behavior per 10 sec) = 0.33 ± 0.07, p = 0.003, two-sided rank-sum test, n = 8 larvae, Figure S1E).

Analysis of the pairwise correlations between the Ca^{2+} transients of the tectal RGCs showed significant correlations with respect to a null model (RGCs; 0.38 ± 0.04; null model, $4.3 \times 10^{-4} \pm 7.8 \times 10^{-4}$; p

< 0.001, two-sided rank-sum test, n = 11 larvae, Figure 1G). Clustering analysis using k-means (Figure 1H) and principal component analysis (PCA) showed that these correlations are organized as a single cluster. PCA showed that much of the variability can be explained by a single component (PC1: 41.08 % ± 4.97, Figure 1I). This suggests that in the current paradigm the RGCs mainly function as a single unit. This result was supported by quantifying the robustness of RGC activity with respect to escape behaviors, which showed that most RGCs were active during all synchronous Ca^{2+} events (robustness: 0.70 ± 0.09, Figure S2A), and that the probability of a single RGC being part of a synchronous Ca^{2+} event does not depend on the position of the RGC in the OT circuit (Figure S2B and S2C).

RGCs are found throughout the entire volume of the OT (Figure 2A). However, two-photon Ca^{2+} imaging of RGC activity at different optical planes of the OT revealed that RGC synchronous Ca^{2+} events are specific to the ventral region (90-100 µm from the dorsal surface, Figure 2B-E). Tectal regions within 60-80 µm of the dorsal surface showed a significantly smaller number of RGC synchronous Ca^{2+} events (60 µm, 0.56 ± 0.38; 70 µm, 0.50 ± 019 ; 80 µm, 2.00 ± 0.41; 90 µm, 9.60 ± 1.43; 100 µm, 10.67 ± 1.71; p < 0.001, Kruskal–Wallis test and multi-comparison test, Figure 2C and 2D), and lower pairwise correlations (60 µm, 0.03 ± 0.01; 70 µm, 0.04 ± 0.04; 80 µm, 0.06 ± 0.01; 90 µm, 0.37 ± 0.07; 100 µm, 0.30 ± 0.05, p < 0.001, Kruskal–Wallis test and multi-comparison test, Figure 2E). Overall, these results suggest that RGCs in the ventral regions of the OT synchronize their Ca^{2+} transients, acting as a single unit following escape motor behaviors.

Muscle proprioception does not play a role in RGC Ca^{2+} synchronization

Given that tectal RGC synchronizations occur a few seconds after an escape movement, it is possible that muscular tail propioception is involved in this phenomenon. To test this hypothesis, we performed two-photon Ca^{2+} imaging of tectal RGCs in paralyzed larvae (300 µM pancuronium bromide). Under these conditions, RGCs still displayed spontaneous Ca^{2+} synchronous events (Fig. 3A). To test whether these spontaneous RGC synchronous Ca^{2+} events were associated with escape or burst behaviors, we stimulated the paralyzed larvae using mild electric shocks that in control larvae induce escape or burst behaviors. We found that tectal RGCs of paralyzed larvae displayed robust synchronous Ca^{2+} events right after mild electric shocks. The mean amplitude of the RGC synchronous Ca^{2+} events in paralyzed larvae was not significantly different from that in control larvae (0.98 ± 0.16; paralyzed, 0.83 ± 0.15 ΔF/F, p = 0.85; two-sided rank-sum test, Fig. 3C). This suggests that RGC synchronization does not depend on muscular proprioception. Therefore, RGC synchronization may be triggered by an efferent copy from a motor center or mediated by a parallel process to the generation of the tail motor behavior.

Tectal RGC synchronization is mediated by the locus coeruleus

In vertebrates, the locus coeruleus (LC) is the main source of norepinephrine (NE) projecting widely across the brain (Benarroch, 2018). Given that RGCs in the zebrafish hindbrain respond to NE (Mu et al., 2019), we investigated the role of the LC in tectal RGC synchronization. For this purpose, we first imaged larvae expressing EGFP under an LC promoter (dbh:egfp) and a red fluorescence protein in RGCs (Her4:mCherry). We observed that LC projections innervate the OT neuropil (Figure 4A). To learn whether these projections represent direct innervation of LC into the neuropil of the OT, we used zebrafish larvae expressing the photoconvertible fluorescence protein Kaede under a LC promoter (dbh:Kaede). Photoconversion of neurons in the LC of the right hemisphere revealed that LC projects directly to the ipsilateral neuropil of the OT (Figure 4B). Immunostaining of Her4:mCherry larvae for the β2-adrenoreceptor showed a punctate pattern (receptors) co-localizing with RGC processes in the neuropil of the OT (Figure 4C). We therefore performed two-photon Ca^{2+} imaging of LC neurons while simultaneously monitoring tail movements using double transgenic larvae expressing pan-neuronal GCaMP6f (HuC:GCaMP6f) and a red fluorescent protein under a LC-specific promoter (dbh:mCherry) (Figure 5A). We observed that neurons in LC displayed large synchronous Ca^{2+} transients following spontaneous and induced escape behaviors (Figure 5B). Peak activity of LC neurons preceded that of RGC synchronization in the optic tectum (LC neurons, 2.61 ± 0.50 s; RGCs, 10.70 ± 0.71 s; $p < 0.001$, Figure 5G). Laser ablation of the LC (demonstrated by tissue labeling with acrydine, see Methods) suppressed the Ca^{2+} synchronization events of RGCs in the OT (control, 0.89 ± 0.17; LC ablation, 0.12 ± 0.03 $\Delta F/F$, $p > 0.001$; Figure 5C, 5D and 5G). We then performed optogenetic stimulation of LC while monitoring tectal RGC Ca^{2+} dynamics. For this purpose, we used double transgenic larvae expressing ChR2 under an LC specific promoter (dbh:gal4; UAS:ChR2-mCherry, Figure 5E), and GCaMP6m under a glial promoter (Her4:GCaMP6m). Using an optical fiber placed on the side of rhombomere 1 coupled to a 455 nm LED (see Methods), we stimulated the LC using 1 s light pulses while monitoring RGC Ca^{2+} activity in the optic tectum (Figure 5G). The optogenetic LC stimulation induced similar RGC synchronous Ca^{2+} events in the OT as in control larvae following an escape or burst behavior (control: 0.89 ± 0.17; LC stimulation: 0.88 ± 0.11 $\Delta F/F$ $p= 0.98$, Figure 5F and 5G). To test whether the escape behaviors preceding the RGC synchronous Ca^{2+} events are mediated by the LC, we monitored the tail movements in LC-ablated larvae. We observed that LC ablations did not affect the spontaneous nor the induced tail movements (Figure 5H). Likewise, LC optogenetic stimulation did not induce any type of tail movement (Figure 5H). Laser ablations of the reticular spinal nucleus and laser transections at the initiation point of the spinal cord did not affect the LC activity nor RGC synchronous Ca^{2+} events in the OT (Figure S3).Overall, these results suggest that LC activity is necessary and sufficient for tectal RGC synchronization. This synchronization is mediated by direct NE ipsilateral projections from LC to the OT neuropil. However, the escape behaviors and tectal RGC synchronization seem to be two independent parallel processes with a common input rather than having a causal relationship.

RGC synchronization modulates the directional selectivity of tectal neurons

To learn about the functional role of RGCs in visual processing, we first asked whether RGCs in the optic tectum show Ca^{2+} events in response to visual stimuli. For this purpose, in the right hemifield of the larva, we presented visual stimuli consisting of light spots of 13°, 23°, and 44° and bars moving in the rostro-caudal or caudo-rostral directions (Figure S4A), while monitoring RGC Ca^{2+} dynamics in the ventral layers of the optic tectum. We found that RGCs did not respond to any of the presented visual stimuli (Figure S4C-D). We then studied whether RGC synchronous Ca^{2+} events can modulate the neuronal visual response in the OT. We therefore presented the same light spots and moving bars before the RGC Ca^{2+} transients, at their peak, and at the end of decay (Figure S4A-B). We found that the mean amplitude and the percentage of neurons that responded to the visual stimuli were not significantly different before, during and after the RGC synchronous Ca^{2+} events (mean amplitude: before, 0.89 ± 0.27; during, 0.82 ± 0.23; after, 0.78 ± 0.24 ΔF/F; p = 0.46; percentage of neurons: before, 9.12 ± 1.33; during, 8.23 ± 0.98; after, 7.33 ± 1.06 ΔF/F.sec; p = 0.39, Kruskal–Wallis test, and multi-comparison test, Figure 6A and Figure S4D). When we analyzed the neuronal responses to the light spots of different sizes for the 3 different conditions (before, duringand after the RGC synchronous Ca^{2+} events), we did not observe any significant changes (light spots of 13°, before, 0.67 ± 0.14; during, 0.81 ± 0.16; after, 0.78 ± 0.17 ΔF/F per sec, p = 0.70; light spots of 23°, before, 0.65 ± 0.18; during, 0.81 ± 0.13; after, 0.69 ± 0.13 ΔF/F per sec, p = 0.43; light spots of 44°, before, 0.64 ± 0.16; during, 0.77 ± 0,16; after, 0.67 ± 0.16 ΔF/F per sec, p= 0.85. Kruskal–Wallis test, and multi-comparison test, Figure 6B). However, when we analyzed the neural responses to moving bars, we found that its amplitude was significantly smaller during the RGC synchronization periods. The decrease in the response was significant only for bars moving in the rostro-caudal direction (rostro-caudal, p = 0.03; caudo-rostral, p = 0.13, Kruskal–Wallis test, and multi-comparison test, Figure 6B). We therefore calculated the directional selectivity index of all recorded tectal neurons before, during and at the end of RGC synchronous Ca^{2+} events. We observed that this index was significantly smaller during and at the end of RGC synchronous Ca^{2+} events (before-during, $p = 6.8 \times 10^{-3}$; before-after, $p = 3.6 \times 10^{-3}$; during-after, p = 0.98;Kolmogorov-Smirnov test,, Figure 6C and D). In a more dorsal tectal area in which the RGCs synchronization was not observed, there repetitive activation of RGCs did not modulate the the directional selectivity index of tectal neuron (before-during, p = 0.70 before-after, p = 0.66 ; during-after, p = 0.98. Kolmogorov-Smirnov test). The latter suggests that tectal RGCs can modulate the directional selectivity of tectal neurons. This modulation was larger for direction-selective neurons responding to a rostro-caudal direction.

Previous studies showed that in the OT of zebrafish larvae, auditory stimuli modulate the visual response rather than representing specific properties of the stimuli (Thompson et al., 2016). We there-

fore tested the hypothesis that RGC synchronous Ca^{2+} events gate auditory representation in the OT. We found that auditory neuronal responses were not significantly different before, during and at the end of RGC synchronous Ca^{2+} events (Figure S5). Overall, these results suggest that RGC synchronization specifically modulates the directional selectivity of tectal neurons without affecting their size tuning curves or auditory processing.

RGC synchronous events modulate the functional correlations between tectal neurons

To further understand the interactions between RGCs and tectal neurons, we analyzed the pair-wise correlations between the spontaneous Ca^{2+} transients of tectal RGCs and those of tectal neurons. For this purpose, we used double transgenic larvae expressing GCaMP6f in neurons (Huc:H2B-GCaMP6f) and RCaMP1b in RGCs (gfap:GAL4; uas:RCaMP1b, Figure 7B). We observed no significant pair-wise correlations between the spontaneous Ca^{2+} transients of RGCs and those of tectal neurons (with respect to a null model, Figure 7A and C). However, a very small group of neurons sparsely distributed across the tectal circuit displayed low but significant correlations with individual RGCs (15 ± 2 neurons, Figure S7), suggesting that RGCs are functionally connected through excitatory synapses to only a minimal number of tectal neurons. We then asked whether RGC synchronous events can affect the functional connectivity between tectal neurons. For this purpose, we calculated the pair-wise correlations between the spontaneous Ca^{2+} transients of tectal neurons, under control conditions or during periods of repetitive activation of RGCs, induced by mild electric shocks to elicit escape responses. Per se, the mild electric shocks did not induce Ca^{2+} transients in tectal neurons (Figure S6). The RGC synchronous Ca^{2+} events did not affect the overall pair-wise correlations between tectal neurons (spontaneous activity, $1.59 \times 10^{-2} \pm 0.20 \times 10^{-2}$; RGC synchronization; $1.37 \times 10^{-2} \pm 0.16 \times 10^{-2}$; student t-test; $p > 0.05$). However, when we analyzed the relationship of the pair-wise correlations between neurons and the Euclidean distance between them, we found significant differences for correlations between neurons that were distant. This suggests that RGCs can modulate long-range functional connectivity between neurons ($p > 0.05$ from 5 µm to 168 µm. At 182 µm: spontaneous activity, $6.8 \times 10^{-3} \pm 4.10 \times 10^{-3}$; RGC synchronization; $0.9 \times 10^{-3} \pm 1.2 \times 10^{-3}$; $p = 0.03$. At 208 µm: spontaneous activity, $1.8 \times 10^{-3} \pm \pm 8.7 \times 10^{-3}$. RGC synchronization: $-6.6 \times 10^{-3} \pm 4.9 \times 10^{-3}$; $p = 0.049$. All two-sided rank-sum tests, Figure 7D).

Furthermore, to test the hypothesis that RGC synchronization inhibits tectal neurons to regulate their potential hyper-activation, we analyzed spontaneous neuronal Ca^{2+} dynamics after laser ablation of the LC (LC ablation prevents RGC synchronous Ca^{2+} events, Figure 5C and 5D). We did not find any significant increase in the spontaneous activity of tectal neurons with respect to control larvae during periods of induced escape behaviors (control, 0.079 ± 0.03; LC ablation, 0.070 ± 0.02 ΔF/F; $p = 0.77$, two-sided rank-sum test, Figure 7E). These results show that RGC synchronous Ca^{2+} events do not in-

hibit the tectal neurons but rather prune the functional correlations between distant tectal neurons, a mechanism that may modulate visual processing.

Discussion

An increasing number of studies support the hypothesis that brain computations do not depend exclusively on neuronal activity, but rather on the coordinated interactions between astrocytes and neurons (Araque and Durkee, 2019; Kofuji and Araque, 2021; Semyanov, 2019). Here, we studied the neural-glia interaction in the visual system of the zebrafish larvae. Although zebrafish lack astrocyte-like cells, their RGCs play an analogous role to that of mammalian astrocytes (Chen et al., 2020; Jurisch-Yaksi et al., 2020). Specifically, we studied the interactions between neurons and RGCs in the zebrafish OT. We found that RGCs in the ventral regions of the OT synchronize their Ca^{2+} transients, acting as a single unit following an escape motor behavior. This synchronization does not depend on muscular proprioception or motor centers in the spinal cord or the reticulo-spinal circuit, but rather on the activation of the LC via direct NE ipsilateral projections to the OT neuropil.

We found that LC optogenetic activation did not trigger any escape behavior, but it was sufficient to induce the synchronous activity of the tectal RGCs. This suggests that the association between the RGC synchronization and the escape behaviors is not causal but rather the result of parallel processes triggered by a common source. Using immunohistochemistry, we observed co-localization of LC ipsilateral projections and β2-adrenoreceptors expression in the neuropil of the OT. In mammals (Bazargani and Attwell, 2017; Oe et al., 2020) and zebrafish (Mu et al., 2019; Orts-Del'Immagine et al., 2022), NE induces Ca^{2+} transients in astrocytes, and its release is associated with alertness, attention, wakefulness, and fight-or-flight responses. We thus suggest that the RGC synchronization is induced by a switch into an alertness state, that in parallel triggers an escape behavior. In this scenario, the LC will trigger the switch to an arousal state, while the slow Ca^{2+} dynamics of RGCs will mediate the time course of the arousal state.

In contrast to previous studies that showed that astrocytes in primary visual cortex respond to visual stimuli during motor behavior (Paukert et al., 2014), RGCs in the ventral region of the optic tectum of the zebrafish larvae did not respond to visual stimuli. However, when RGCs synchronize their Ca^{2+} events, they strongly modulate the directional selectivity of tectal neurons without affecting their size tuning curves or gating auditory processing. RGC synchronous events occur only in ventral regions of the OT, which represent the lower part of the visual field (the riverbed in natural conditions) (Nevin et al., 2010). Thus, it is possible that the RGC neuronal modulation reduces the optomotor response (OMR) without strongly affecting other types of visual responses (OMR is induced by relative movement with respect to the riverbed when the larva is not moving). This mechanism may support freezing behavior following a switch to an alerted state. This hypothesis is supported by our results that follow-

ing an RGC synchronous Ca^{2+} event, larvae enter a period of behavioral passivity (the probability of observing a motor behavior decreases, Figure S1E).

We also observed that the RGC synchronous events modulate the functional connectivity between tectal neurons by pruning correlations between distant neurons. The OT circuit is organized according to assemblies of highly correlated neurons showing attractor-like dynamics that may improve visual detection of vital stimuli (Romano et al., 2015). Modulation of the long-distance functional connections may improve the detection of vital visual objects by creating more compact neuronal assemblies. In addition, a previous study showed that the brain of zebrafish displays scale-invariant neuronal avalanches (sequential activation of a group of neurons generating cascade-like events). This is suggestive of brain dynamics operating at a critical state, a regime between phases of order and disorder in which several brain functions could be optimized. In zebrafish, criticality improves visual decoding (Ponce-Alvarez et al., 2018). Therefore, modulation of tectal functional connectivity may temporally deviate the brain from a critical regime to a more ordered one affecting brain processing. This would indicate that RGC synchronous activation enables the brain to auto-regulate its own dynamics towards and away from a critical regime to adapt the computational brain capabilities to the current context or brain state.

Overall, our results suggest the following scenario: a switch to an arousal state induces the activity of the LC. LC NE projections to the tectum generate synchronous Ca^{2+} events among the ventral population of RGCs. The RGC synchronous events modulate the directional selectivity of tectal neurons and prune their functional correlations to adapt the larva's visual system to cope with the environmental context associated with an arousal state.

Alternatively, it is possible that the NE released by the LC in the tectal neuropil is sensed by β2-adrenoreceptors in both RGCs and neurons. In this case, the observed adaptations of the visual system during the arousal states are underpinned by the tight interactions between tectal RGCs and the NE-secreting neurons of the LC.

In zebrafish, RGCs display different functional roles. For example, RGCs in the hindbrain integrate errors in visual feedback during visuo-motor behaviors to trigger futility. However, in contrast to our results, this phenomenon is not mediated by LC, but rather triggered by the noradrenergic cluster of the medulla oblongata (NE-MO) (Mu et al., 2019). This finding indicates that the LC-mediated tectal RGC Ca^{2+} synchronous events and the NE-MO-mediated hindbrain RGC activations are two different phe-

nomena occurring through two independent pathways, involving two processes with different biological relevance (futility vs. switch to an arousal state). In a zebrafish epilepsy model, RGCs in the telencephalon are involved in the transition from the preictal period to seizures after the release of glutamate (Verdugo et al., 2019)(Diaz verdugo, 2019). In the rostral spinal cord, acousto-vestibular stimuli induce RGC Ca^{2+} waves traveling bi-directionally to the hindbrain and the caudal spinal cord (Orts-Del'Immagine et al., 2022). Here, we observed an additional functional role of RGCs that can modulate brain computations and functional connectivity to cope with different brain behavioral states. This study adds to the emerging evidence that brain computations and behavioral states depend on the coordinated interactions between astrocytes and neurons.

References

Adamsky, A., Kol, A., Kreisel, T., Doron, A., Ozeri-Engelhard, N., Melcer, T., et al. (2018). Astrocytic Activation Generates De Novo Neuronal Potentiation and Memory Enhancement. *Cell* 174, 59-71.e14. doi:10.1016/J.CELL.2018.05.002.

Araque, A., Carmignoto, G., Haydon, P. G., Oliet, S. H. R., Robitaille, R., and Volterra, A. (2014). Gliotransmitters travel in time and space. *Neuron* 81, 728–739. doi:10.1016/j.neuron.2014.02.007.

Araque, A., and Durkee, C. A. (2019). Diversity and Specificity of Astrocyte-Neuron Communication. *Neuroscience*, 73–78. doi:10.1016/j.neuroscience.2018.11.010.DIVERSITY.

Bazargani, N., and Attwell, D. (2017). Amines, Astrocytes, and Arousal. *Neuron* 94, 228–231. doi:10.1016/j.neuron.2017.03.035.

Bekar, L. K., He, W., and Nedergaard, M. (2008). Locus coeruleus alpha-adrenergic-mediated activation of cortical astrocytes in vivo. *Cereb. Cortex* 18, 2789–2795. doi:10.1093/CERCOR/BHN040.

Benarroch, E. E. (2018). Locus coeruleus. *Cell Tissue Res.* 373, 221–232. doi:10.1007/S00441-017-2649-1.

Bojarskaite, L., Bjørnstad, D. M., Pettersen, K. H., Cunen, C., Hermansen, G. H., Åbjørsbråten, K. S., et al. (2020). Astrocytic Ca2+ signaling is reduced during sleep and is involved in the regulation of slow wave sleep. *Nat. Commun. 2020 111* 11, 1–16. doi:10.1038/s41467-020-17062-2.

Bollmann, J. H. (2019). The Zebrafish Visual System: From Circuits to Behavior. *Annu. Rev. Vis. Sci.* 5, 269–293. doi:10.1146/annurev-vision-091718-014723.

Budick, S., and O'Malley, D. (2000). Locomotor repertoire of the larval zebrafish: swimming, turning and prey capture. *J. Exp. Biol.* 203, 2565–2579. doi:10.1242/jeb.01529.

Chen, J., Poskanzer, K. E., Freeman, M. R., and Monk, K. R. (2020). Live-imaging of astrocyte morphogenesis and function in zebrafish neural circuits. *Nat. Neurosci.* 23, 1297–1306. doi:10.1038/s41593-020-0703-x.

De Pittà, M., and Brunel, N. (2016). Modulation of Synaptic Plasticity by Glutamatergic Gliotransmission: A Modeling Study. *Neural Plast.* 2016. doi:10.1155/2016/7607924.

Jouary, A., Haudrechy, M., Candelier, R., and Sumbre, G. (2016). A 2D virtual reality system for visual goal-driven navigation in zebrafish larvae. *Sci. Rep.* 6, 34015. doi:10.1038/srep34015.

Jurisch-Yaksi, N., Yaksi, E., and Kizil, C. (2020). Radial glia in the zebrafish brain: Functional, structural, and physiological comparison with the mammalian glia. *Glia*, glia.23849. doi:10.1002/glia.23849.

Kjaerby, C., Rasmussen, R., Andersen, M., and Nedergaard, M. (2017). Does Global Astrocytic Calcium Signaling Participate in Awake Brain State Transitions and Neuronal Circuit Function? *Neurochem. Res.* 42, 1810–1822. doi:10.1007/s11064-017-2195-y.

Kofuji, P., and Araque, A. (2021). Astrocytes and Behavior. *Annu. Rev. Neurosci.* 44, 49–67. doi:10.1146/ANNUREV-NEURO-101920-112225.

Kol, A., Adamsky, A., Groysman, M., Kreisel, T., London, M., and Goshen, I. (2020). Astrocytes contribute to remote memory formation by modulating hippocampal–cortical communication during learning. *Nat. Neurosci. 2020 2310* 23, 1229–1239. doi:10.1038/s41593-020-0679-6.

Lines, J., Martin, E. D., Kofuji, P., Aguilar, J., and Araque, A. (2020). Astrocytes modulate sensory-evoked neuronal network activity. *Nat. Commun. 2020 111* 11, 1–12. doi:10.1038/s41467-020-17536-3.

Lyons, D. A., and Talbot, W. S. (2014). Glial cell development and function in zebrafish. *Cold Spring Harb. Perspect. Biol.* 7. doi:10.1101/CSHPERSPECT.A020586.

Martin-Fernandez, M., Jamison, S., Robin, L. M., Zhao, Z., Martin, E. D., Aguilar, J., et al. (2017). Synapse-specific astrocyte gating of amygdala-related behavior. *Nat. Neurosci. 2017 2011* 20, 1540–1548. doi:10.1038/nn.4649.

Mu, Y., Bennett, D. V., Rubinov, M., Narayan, S., Yang, C.-T., Tanimoto, M., et al. (2019). Glia Accumulate Evidence that Actions Are Futile and Suppress Unsuccessful Behavior. *Cell* 178, 27-43.e19. doi:10.1016/j.cell.2019.05.050.

Nevin, L. M., Robles, E., Baier, H., and Scott, E. K. (2010). Focusing on optic tectum circuitry through the lens of genetics. *BMC Biol.* 8, 126. doi:10.1186/1741-7007-8-126.

Nimmerjahn, A., Mukamel, E. A., and Schnitzer, M. J. (2009). Motor behavior activates Bergmann glial networks. *Neuron* 62, 400–12. doi:10.1016/j.neuron.2009.03.019.

Oe, Y., Wang, X., Patriarchi, T., Konno, A., Ozawa, K., Yahagi, K., et al. (2020). Distinct temporal integration of noradrenaline signaling by astrocytic second messengers during vigilance. *Nat. Commun. 2020 111* 11, 1–15. doi:10.1038/s41467-020-14378-x.

Orts-Del'Immagine, A., Dhanasekar, M., Lejeune, F. X., Roussel, J., and Wyart, C. (2022). A norepinephrine-dependent glial calcium wave travels in the spinal cord upon acoustovestibular stimuli. *Glia* 70, 491–507. doi:10.1002/GLIA.24118.

Paukert, M., Agarwal, A., Cha, J., Doze, V. A., Kang, J. U., and Bergles, D. E. (2014). Norepinephrine controls astroglial responsiveness to local circuit activity. *Neuron* 82, 1263–70. doi:10.1016/j.neuron.2014.04.038.

Perea, G., and Araque, A. (2010). GLIA modulates synaptic transmission. *Brain Res. Rev.* 63, 93–102. doi:10.1016/j.brainresrev.2009.10.005.

Ponce-Alvarez, A., Jouary, A., Privat, M., Deco, G., and Sumbre, G. (2018). Whole-Brain Neuronal Activity Displays Crackling Noise Dynamics. *Neuron* 100, 1446-1459.e6. doi:10.1016/j.neuron.2018.10.045.

Poskanzer, K. E., and Yuste, R. (2011). Astrocytic regulation of cortical UP states. *Proc. Natl. Acad. Sci. U. S. A.* 108, 18453–18458. doi:10.1073/PNAS.1112378108/-/DCSUPPLEMENTAL/PNAS.201112378SI.PDF.

Romano, S. A., Pietri, T., Pérez-Schuster, V., Jouary, A., Haudrechy, M., and Sumbre, G. (2015). Spontaneous neuronal network dynamics reveal circuit's functional adaptations for behavior. *Neuron* 85, 1070–85. doi:10.1016/j.neuron.2015.01.027.

Savtchouk, I., and Volterra, A. (2018). Gliotransmission: Beyond black-and-white. *J. Neurosci.* 38, 14–25. doi:10.1523/JNEUROSCI.0017-17.2017.

Schummers, J., Yu, H., and Sur, M. (2008). Tuned responses of astrocytes and their influence on hemodynamic signals in the visual cortex. *Science* 320, 1638–43. doi:10.1126/science.1156120.

Semyanov, A. (2019). Spatiotemporal pattern of calcium activity in astrocytic network. *Cell Calcium* 78, 15–25. doi:10.1016/j.ceca.2018.12.007.

Srinivasan, R., Huang, B. S., Venugopal, S., Johnston, A. D., Chai, H., Zeng, H., et al. (2015). Ca(2+) signaling in astrocytes from Ip3r2(-/-) mice in brain slices and during startle responses in vivo. *Nat. Neurosci.* 18, 708–717. doi:10.1038/NN.4001.

Sultan, S., Li, L., Moss, J., Petrelli, F., Cassé, F., Gebara, E., et al. (2015). Synaptic Integration of Adult-Born Hippocampal Neurons Is Locally Controlled by Astrocytes. *Neuron* 88, 957–972. doi:10.1016/j.neuron.2015.10.037.

Thompson, A. W. W., Vanwalleghem, G. C. C., Heap, L. A. A., and Scott, E. K. K. (2016). Functional profiles of visual-, auditory-, and water flow-responsive neurons in the Zebrafish Tectum. *Curr. Biol.* 26, 743–754. doi:10.1016/j.cub.2016.01.041.

Verdugo, C. D., Myren-Svelstad, S., Aydin, E., Hoeymissen, E. Van, Deneubourg, C., Vanderhaeghe, S., et al. (2019). Glia-neuron interactions underlie state transitions to generalized seizures. *Nat. Commun.* 10. doi:10.1038/S41467-019-11739-Z.

Wahis, J., Holt, M. G., Tang, W., Pankratov, Y., Zorec, R., Wahis, J., et al. (2021). Astrocytes, Noradrenaline, α1-Adrenoreceptors, and Neuromodulation: Evidence and Unanswered Questions. *Front. Cell. Neurosci.* 15, 42. doi:10.3389/fncel.2021.645691.

FIGURE LEGENDS

Fig 1. Tectal RGCs synchronize their Ca^{2+} transients following an escape behavior.

A) Left: Schematic of the zebrafish head showing the imaged area (red square). Shaded green: optic tectum. Right: A temporal series of an optical section of the optic tectum of a zebrafish larva expressing GCaMP in radial glia, imaged using a two-photon microscope (red square on the left). Note the changes in fluorescence across the radial glia. Time zero indicates the onset of an escape behavior. Yellow dashed line, brain midline; cb, cerebellum; np, neuropil; pvz, periventricular zone. Gray scale bar: normalized florescence. Scale bar: 80 μm. B) Top: Raster of RGC spontaneous activity. Gray scale bar: ΔF/F, middle: number of active RGCs, bottom: tail deflection (L0/R). Note the synchronous spontaneous Ca^{2+} events across all RGCs. L0, length of the fish at rest; R, distance to the center of the tail curvature. C) Zoom of the area in B, indicated by the magenta dashed lines. D) Histogram of the delay between the onset of the spontaneous escape behaviors and the onset of the RGC synchronous Ca^{2+} events (mean: 3.13 ± 0.6 s). E) Top: Rasters of RGC activity around 14 representative spontaneous tail movements, Gray scale bar: ΔF/F. Middle: number of active RGCs. Bottom: tail deflection (L0/R). The first 7 subplots show representative escape behaviors; the 7 last subplots display low-deflection swimming bouts. F) Mean amplitude of the RGC Ca^{2+} transients following a spontaneous tail movement (dashed line, time zero), for large-deflection (orange) and low-deflection tail movements (magenta). Large deflection, 0.98 ± 0.16; low-deflection; 0.24 ± 0.03 ΔF/F, $p = 2.2 \times 10^{-4}$; two-sided rank-sum test, n = 11 larvae. G) Average probability density distribution of RGC pairwise correlations (magenta) and the corresponding null model (orange). Mean, RGCs, 0.38 ± 0.04; null model, $4.3 \times 10^{-4} \pm 7.8 \times 10^{-4}$; $p = 8 \times 10^{-5}$, two-sided rank-sum test; n = 11). H) Example of a pairwise correlation matrix between the Ca^{2+} transients of RGCs. Note that RGCs form a single main cluster. Color scale bar: correlation value. I) The eigenvector values of the different principal components (PC) representing the RGC ΔF/F Ca^{2+} activity. Note that most of the variance can be explained by a single component (PC1), suggesting that the synchronous events involve all RGCs.

Fig 2. Tectal RGC synchronization is specific to the ventral area of the optic tectum.

A) Optical sections of the optic tectum showing the morphology of RGCs expressing GCaMP, imaged at different depths using two-photon microscopy. Zero μm, dorsal skin. Yellow dashed line, the midline; cb, cerebellum; np, neuropil; pvz, periventricular zone. Scale bar: 100 μm. B) Top: Representative raster of RGC activity in a dorsal region of the optic tectum (60 μm). Gray scale bar: ΔF/F. Middle: number of active RGCs, bottom: tail deflection (L0/R). Red line, time of mild electric shocks. C) Mean

of the number of RGC synchronous Ca^{2+} events per hour at five different depths of the OT. (Mean: 60 µm, 0.56 ± 0.38; 70 µm, 0.50 ± 0.19; 80 µm, 2.00 ± 0.41; 90 µm, 9.60 ± 1.43; 100 µm, 10.67 ± 1.71; p = 5.85 x 10^{-5}, Kruskal–Wallis test and multi-comparison test). D) Mean amplitude of the ΔF/F of RGCs following a mild electric shock, at different tectal depths. Note that at depths of 90 and 100 µm, the amplitude of the synchronous Ca^{2+} events was significantly higher than for the dorsal tectal regions (Mean: 60 µm, 0.15 ± 0.03; 70 µm, 0.12 ± 0.02; 80 µm, 0.13 ± 0.04; 90 µm, 1.02 ± 0.21; 100 µm, 0.94 ± 0.28; p = 7.8 x10^{-4}, ΔF/F; Kruskal–Wallis test and multi-comparison test). E) The probability density of the pairwise correlations between RGCs, at the different imaged depths of the optic tectum. The medians of the distributions for the depths of 90 and 100 µm were significantly higher than the rest (median: 60 µm, 0.03 ± 0.01; 70 µm, 0.04 ± 0.04; 80 µm, 0.06 ± 0.01; 90 µm, 0.37 ± 0.07; 100 µm, 0.30 ± 0.05; p = 4.69 x 10^{-6} ; Kruskal–Wallis test and multi-comparison test). 60 µm, green, n = 9 larvae; 70 µm, blue, n = 8 larvae; 80 µm, black, n = 4 larvae; 90 µm, violet, n = 5 larvae; 100 µm, orange, n = 6 larvae. From the dorsal skin above the optic tectum.

Fig 3. Muscle proprioception does not play a role in tectal radial glia Ca^{2+} synchronization.

A) Top: Raster of RGC spontaneous Ca^{2+} activity. Middle: Number of Ca^{2+} events across RGCs. Bottom: Tail deflection (L0/R). Gray scale bar: ΔF/F. B) As in A, but mild electric shocks were presented every 180 s to induce escape behaviors. Red line: time of the mild electric shock. C) The mean Ca^{2+} activity of RGCs induced by mild electric shocks (time zero) in paralyzed (magenta) and non-paralyzed larvae (orange). Mean amplitude of the two distributions were not significantly different (non-paralyzed, 0.98 ± 0.16; paralyzed, 0.83 ± 0.15, ΔF/F; p = 0.85; two-sided rank-sum test, n = 11 control, n = 5 paralyzed). Larvae were paralyzed using pancuronium bromide (300 µM).

Figure 4. Locus coeruleus neuronal projections and β2-adrenoceptors co-localize with RGC processes in the optic tectum.

A) Optical section of the OT of a larva expressing mCherry under an RGC promoter (her4.1:mCherry, magenta) and EGFP under a LC promoter (dbh:Gal4/uas:EGFP-caax, green). (I) RGCs. (II) LC neurons and their projections to the optic tectum. (III) Superposition of (I) and (II). Note the co-localization between RGCs and LC terminals in the tectal neuropil. B) (I-IV) Optical section of a larva expressing GFP under a LC promoter (dbh:gfp). (V-VIII) The same optical section as in (I-IV) expressing Kaede after photoconversion of LC neurons in the right hemisphere. The blue arrowheads indicate the photoconversion of Kaede in LC. (IX-XII) Superposition of (I-IV) and (V-VIII). Note the LC projects mainly to the ipsilateral tectum. C) (I) Optical section of the OT of a larva expressing mCherry under an RGC promoter (her4.1:mCherry). (II) The same optical section as in (I) immunostained for β2-adrenorecep-

tor. Note the punctate pattern. (III) Superposition of (I) and (II). (IV) Zoom of the dashed square area in (III). Note the colocalization of the β2-adrenoreceptor puncta with the processes of RGCs. np: tectal neuropil, pvz: periventricular zone, cb: cerebellum. White dashed curves: borders of pvz with np and cb. Yellow dashed line: brain midline. Yellow circle, LC. Scale bars: 50 μm.

Fig 5. The tectal RGC synchronization is mediated by the locus coeruleus.

A) Left: Schematic of the head of a zebrafish larva. Red circles, locus coeruleus (LC), shaded green, optic tectum. Red square, area imaged on the right. Right: Optical section containing the LC (red neurons). Green, neurons expressing GCaMP. Red, neurons expressing mCherry under an LC specific promoter (dbh). White dashed line: brain midline. Scale bar: 80 μm. B) Top: Raster of the LC. Gray scale bar: ΔF/F. Middle: Number of active LC neurons. Bottom: tail deflection (L0/R). Red line: time of mild electric shocks. C) Left: Optical section containing the LC (neurons in red) before laser ablation. Green, RGCs expressing GcaMP7. Red, neurons expressing mCherry under an LC specific promoter (dbh). Right: Staining of the same optical section after ablation with acridine orange to label apoptotic cells. Dashed line: brain midline. D) Top: Raster of the activity of RGCs in the optic tectum following LC ablation, while presenting mild electric shocks. Gray scale bar: ΔF/F. Middle: Number of active LC neurons. Bottom: Tail deflection (L0/R). Red line: time of mild electric shocks. Note the absence of RGC synchronization. E) Left: Schematic of the head of the zebrafish larva. Red circles, LC, shaded green, optic tectum. Red square, area imaged on the right. Blue, position of the beam of light for optogenetic stimulation (100 μm fiber optic). Right: Optical section containing the LC neurons expressing ChR-2 (red). Green, RGCs expressing GCaMP. Red, neurons expressing ChR2-mCherry under an LC-specific promoter (dbh). White dashed line: brain midline. Magenta dashed circle: LC area. F) Top: Raster of the activity of RGCs in the optic tectum following LC optogenetic stimulation. Gray scalebar: ΔF/F. Middle: Number of active RGCs. Bottom: tail deflection (L0/R). Red line: time of LC optogenetic stimulation. Note the RGC synchronization following LC stimulation. G) Mean ΔF/F of RGCs following an escape behavior (control, magenta, n = 10), after ablation of the LC (LC ablation, orange, n = 4) and after optogenetic stimulation of LC (LC stim., green, n = 7). The mean ΔF/F of LC neurons following an escape behavior (LC activity, blue). Note that the mean amplitude of ΔF/F of RGCs in control and LC stimulation conditions were not significantly different. However, these were significantly different from LC ablation (control, 0.89 ± 0.17; LC stimulation, 0.88 ± 0.11; LC ablation, 0.12 ± 0.03, ΔF/F; $p = 8.7 \times 10^{-3}$; Kruskal–Wallis test, and multi-comparison test). The colored arrowheads depict the peak ΔF/F. Note that LC neurons preceded RGC tectal synchronization (LC neurons, 2.61 ± 0.50 s; RGCs after LC optogenetic stimulation, 9.61 RGCs ± 0.30 s; RGCs after escape behavior, 10.70 ± 0.71 s. $p = 1.8 \times 10^{-5}$; Kruskal–Wallis test, and multicomparison test). H) Mean rectified tail deflection aligned to the onset of a spontaneous tail movement (time zero). Magenta, control conditions; orange, after LC ablation; green, LC optogenetic stimulation. Note that the integral of the deflection was not

significantly different between control and LC ablation conditions, but these were significantly different from the direct stimulation of LC (control, 0.36 ± 0.05; LC ablation, 0.39 ± 0.09; LC stimulation 0.08 ± 0.05 L0.sec/R; p = 0.01; Kruskal–Wallis test, and multicomparison test). Scale bar: 80 μm. Dashed line: onset of induced escape behavior.

Figure 6. RGC synchronization modulates the directional selectivity of tectal neurons.

A) Top: Mean ΔF/F of tectal neuron responses to visual stimulation before (orange), during (magenta), and after (green) an RGC synchronization event. Bottom: As in top but for the percentage of responsive neurons. Shaded red area: time of the visual stimulus. The 3 curves do not show any significant difference. Top: before, 0.89 ± 0.27; during, 0.82 ± 0.23; after, 0.78 ± 0.24 ΔF/F.sec; p = 0.46, Kruskal–Wallis test, and multi-comparison test. Bottom: Before, 9.12 ± 1.32; during, 8.23 ± 0.984; after, 7.33 ± 1.06 ΔF/F.sec; p = 0.39, Kruskal–Wallis test, and multi-comparison test. B) Top: Mean ΔF/F of tectal neuron responses to visual stimuli consisting of light spots of 13^{o}(orange), 23^{o} (green), and 44^{o}(magenta). Light spots of 13^{o}; before, 0.67 ± 0.14; during, 0.81 ± 0.16; after, 0.78 ± 0.17 ΔF/F.sec; p = 0.70. Light spots of 23^{o} before, 0.65 ± 0.18; during, 0.81 ± 0.13; after, 0.69 ± 0.13 ΔF/F.sec; p= 0.43. Light spots of 44^{o}; before, 0.64 ± 0.16; during, 0.77 ± 0.16; after, 0.67 ± 0.16 ΔF/F.sec; p = 0.85. Kruskal–Wallis test and multi-comparison test). Bottom: As on top for moving bars moving in a rostro-caudal (orange) or caudo-rostral (magenta) direction. Rostro-caudal: before, 1.54 ± 0.42; during, 0.99 ± 0.32; after, 0.90 ± 0.25 ΔF/F.sec; p = 0.03. Caudo-rostral, before, 1.47 ± 0.35; during, 1.10 ± 0.25; after, 0.94 ± 0.29 ΔF/F.sec; p = 0.13, Kruskal–Wallis test, and multi-comparison test. C) Three examples of the ΔF/F of individual neuron response to the rostro-caudal (orange) and caudo-rostral (magenta) moving bars before, during and after the induction of RGC synchronization. Note the clear reduction in a specific direction selectivity during and right after the RGC synchronization event. D) Distributions of the direction selectivity of tectal neurons before (top), during (middle) and after (bottom) the induction of RGC synchronization. Note that high direction selective values are reduced during and right after RGC synchronization (Kolmogorov-Smirnov test; before-during, p= 6.8 x 10^{-3}; before-after, p = 3.6 x 10^{-3}; during-after, p = 0.98).

Figure 7. RGC synchronous events modulate the functional correlations between tectal neurons.

A) First: Raster of the spontaneous activity of RGCs. Second: Raster of spontaneous activity of tectal neurons; gray scale bar: ΔF/F. Third: number of active RGCs. Fourth: number of active neurons. B) Optical section of the optic tectum of a zebrafish larva expressing GCaMP under a neuronal promoter (HuC:GCaMP6f, green) and RCaMP under the control of a glia promoter (GFAP:RCaMP, red). White dashed line: brain midline. cb, cerebellum; np, neuropil; prv, periventricular zone. Scale bar: 80 μm. C)

Probability density of the mean pairwise correlations between RGCs and neurons in the optic tectum (orange) and its respective null model (magenta). RGCs, 0.01 ± 4 x 10^{-3}; null model, 4 x10^{-3} ± 3 x 10^{-3} ΔF/F.sec, p = 0.053; two-sided rank-sum test, n = 7 larvae. D) The relationship between the mean pairwise correlations of the tectal neurons and their physical distance during spontaneous activity recordings (magenta, control) and during induced RGC synchronization. Note that RGC synchronization decreases the pairwise correlations at long distances (182 μm, spontaneous activity, 6.8 x 10^{-3} ± 4.10 x 10^{-3}; RGC synchronization; 0.9 x 10^{-3} ± 1.2 x 10^{-3}; p = 0.03. 208 μm, spontaneous activity, 1.8 x 10^{-3} ± 9 x 10^{-3} ± 8.7 x 10^{-3}. RGC synchronization: -6.6 x 10^{-3} ± 4.9 x 10^{-3}; p = 0.049, two-sided rank-sum test, n = 7 larvae. Kolmogorov-Smirnov test was applied to evaluate if the distributions are different, p = 0.0054). E) Mean ΔF/F of tectal neurons following an escape behavior (time zero). Orange: following LC ablation. Magenta: control conditions. Mean amplitude of two distributions were not significantly different (control, 0.079 ± 0.03; LC ablation, 0.070 ± 0.02 ΔF/F; p = 0.77, two-sided rank-sum test, n = 4 larvae).

Supplemental Figures

Sup Fig 1: RGC synchronization events are associated with high-deflection tail movements.

A) Example of mean ΔF/F activity of an RGC spontaneous activity. Red: RGC synchronous Ca^{2+} events. B) Example of tail deflection during spontaneous swimming. Red: Times in which tectal RGCs displayed synchronous events in A. Note their association with high deflection tail movements (escape behaviors). C) t-SNE analysis visualization of the larva's tail deflection (L0/R). Red: tail movements associated with RGC synchronization events. Note the different clusters representing different types of tail movements. Only one discrete cluster is associated with tectal RGC synchronization. D) Probability density of the tail deflection associated with RGC synchronous events (orange) and control (magenta). The median of the tail deflection associated with RGC synchronous events was significantly higher (synchronous, 0.04 ± 1.7 x 10^{-3}; control, 0.02 ± 3.2 x 10^{-3}, p = 6.39 x 10^{-4}; two-sided rank-sum test, n = 11 larvae). E) Top: A representative raster showing spontaneous tail movements. Color scale bar: tail deflection; dashed line: onset of RGC synchronous Ca^{2+} event. Bottom: The averaged tail deflection across trials of spontaneous tail movements aligned according to the onset of RGC synchronous Ca^{2+} events. Note that the averaged tail deflection during the first 10 s after the onset of RGC synchronous Ca^{2+} events is significantly smaller than during the 10 s time windows before the RGC synchronization. After RGC synchronization: 10 s windows, 0.18 x 10^{-3} ± 0.04 x 10^{-3}. Before RGC synchronization: 10 s windows, 1.2 x 10^{-3} ± 0.58 x 10^{-3}, p= 0.009; two-sided rank-sum test, n = 6 larvae). Vertical dashed bars: onset of RCG synchronous Ca^{2+} events.

Sup Fig 2: During synchronous Ca^{2+} events, tectal RGCs behave as one assembly.

A) Probability of RGC robustness (probability of an individual RGC being active in a synchronous event). Note that ~85% of the RGCs are active in at least half the synchronous events. B) Left: Schematic of the zebrafish head showing the imaged area (red square). Shaded green: optic tectum. Right: Optical section of the optic tectum of a zebrafish larva expressing GCaMP in radial glia, imaged using a two-photon microscope (red square on the left). White line, example of the tectal rostro-caudal axis. Yellow dashed line, brain midline; cb, cerebellum; np, neuropil; pvz, periventricular zone. Gray scale bar: normalized florescence. Scale bar: 80 µm. C) The relationship between RGC robustness and position across the rostro-caudal axis of the optic tectum. RGCs were projected on a curve connecting, for each hemisphere, the rostral and the caudal borders of the tectum, passing through the middle of the periventricular zone (See B). The positions of the RGCs were normalized according to this rostro-caudal axis (rostral border: -1, caudal border: 1). Note that the probability of a RGC being active is homogeneously distributed across the entire axis (n = 6 larvae).

Sup Fig 3. Ablation of the reticulospinal circuit does not prevent locus coeruleus (LC) and the tectal RGC synchronization.

A) Top: Example of raster of the activity of tectal RGCs before and after ablation of the reticulospinal circuit. Gray scale bar: ΔF/F, bottom: number of active RGCs. B) Top: Raster of the activity of LC neurons before and after ablation of the reticulospinal circuit. Gray scale bar: ΔF/F. Bottom: Number of active LC neurons. Red line, mild electric shock. Note the spontaneous and induced RGCs synchronous Ca^{2+} events and the neural activation of the LC neurons after the ablation. C) Right: Optical section of the reticulospinal circuit of a larva before (left) and after (right) laser ablation. Green: expression of GCaMP in RGCs (GFAP promoter). Magenta: Reticulospinal nucleus (retrograde labeling using Dextran Texas Red). Note the dispersion of the dye following ablation, indicating that the membranes of the labeled neurons were damaged. Scale bar: 80 µm.

Sup Fig 4: Experimental paradigm to study the effect of RGC synchronization on the visual response of tectal neurons.

A) Schematic of the visual stimulation paradigm. Visual stimuli were projected on a screen on the right visual hemifield using a pico-projector. Light spots of 13°, 23° and 44° and bars moving in the rostro-caudal or caudo-rostral directions were presented to the larva's right eye. B) Schematic of the stimulation paradigm. The grey curve represents a hypothetical RGC Ca^{2+} synchronization event induced by a mild electric shock (dashed line, time zero) that can induce an escape behavior. Red bars: the 3 time points in which visual stimuli were presented (before, during, and after the RGC synchronous event). Each stimulus lasted 1 sec and was presented at random order. C-D) RGCs do not respond to visual

stimulation. C) Mean ΔF/F of RGC responses to visual stimuli consisting of light spots of 13°, 23° and 44° presented at the center of the visual right hemifield. D) Mean ΔF/F of RGC responses to visual stimuli consisting of bars moving in a rostro-caudal or caudo-rostral direction (n = 5 larvae). E) Top: Mean ΔF/F of tectal neuron responses to visual stimulation. Bottom: the percentage of responsive neurons. Shaded red area: time of the visual stimulus; dashed line, induced behavior.

Sup Fig 5: RGCs synchronization does not modulate the auditory neuronal response in the optic tectum.

A) Top: Raster of tectal neurons during a period of spontaneous activity, auditory stimulation, and mild electric shocks to induce tectal RGC synchronization. Gray scale bar: Δ F/F. Bottom: Number of active neurons. Red dashed line, 200-400 Hz or 800-1000 Hz band auditory stimuli; black dashed line, mild electric shock. B) Mean ΔF/F of neuronal responses to 200-400 Hz (orange) or 800-1000 Hz (magenta) stimuli, before, during, and after an induced RGC synchronization event. The 2 curves do not show any significant difference (200-400 Hz, before, 0.81 ± 0.32; during, 0.85 ± 0.36; after, 0.79 ± 0.30 ΔF/F.sec, p = 0.77; 800-1000 Hz, before, 0.77 ± 0.28; during, 0.82 ± 0.30; after, 0.81 ± 0.30 ΔF/F.sec, p = 0.77. Kruskal–Wallis test following by a multiple comparison test (n = 6 larvae). Shaded red area: presentation of auditory stimuli.

Sup Fig 6: Tectal neurons show minimal activity associated with spontaneous or induced escape behavior.

A) Top: Mean ΔF/F of the response of tectal neurons in association with spontaneous escape behaviour (magenta) and a mild electric shock (orange). Botton: As on top but for the percentage of responsive neurons. Note the mild increase in activity and the number of active neurons following the onset of behavior. Neither the ΔF/F nor the number of active neurons were significantly different between the spontaneous and induced behaviors (spontaneous, 2.11 ± 0.37; induced, 2.05 ± 0.30, p = 0.99; two-sided rank-sum test, n = 5 larvae). Dashed line: onset of the spontaneous or induced behavior.

Sup Fig 7. A handful of tectal neurons show activity correlations with RGCs.

A) Four examples of rasters of tectal neurons (top) significantly correlated with individual RGCs (bottom, ΔF/F). Gray scale bar: ΔF/F. B) Optical sections depicting the correlated neurons (circles colored according to their correlation values with the RGC) with the individual RGCs from (A); green, region of interest. Magenta arrowheads: examples of neurons correlated with all RGCs. Color scale bar: RGC-neuron correlation. Note that some of these neurons are correlated with the same RGCs but some are correlated with just one cell.

Figure 1

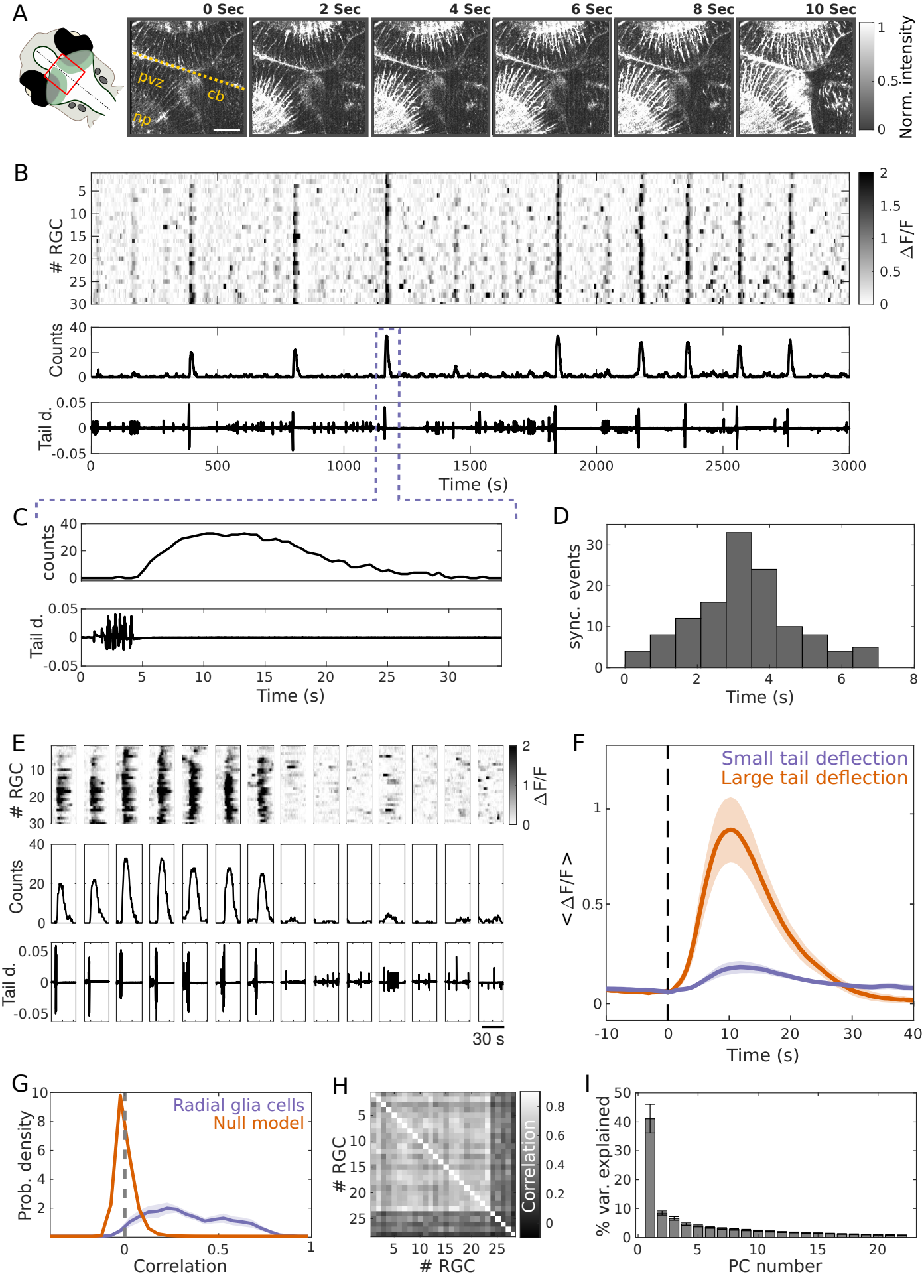
A
0 Sec
2 Sec
4 Sec
6 Sec
8 Sec
10 Sec
pvz
cb
hb
Norm. intensity
B
RGC
ΔF/F
Counts
Tail d.
Time (s)
C
counts
Tail d.
Time (s)
D
sync. events
Time (s)
E
RGC
ΔF/F
Counts
Tail d.
30 s
F
Small tail deflection
Large tail deflection
< ΔF/F >
Time (s)
G
Radial glia cells
Null model
Prob. density
Correlation
H
RGC
Correlation
I
% var. explained
PC number

Figure 2

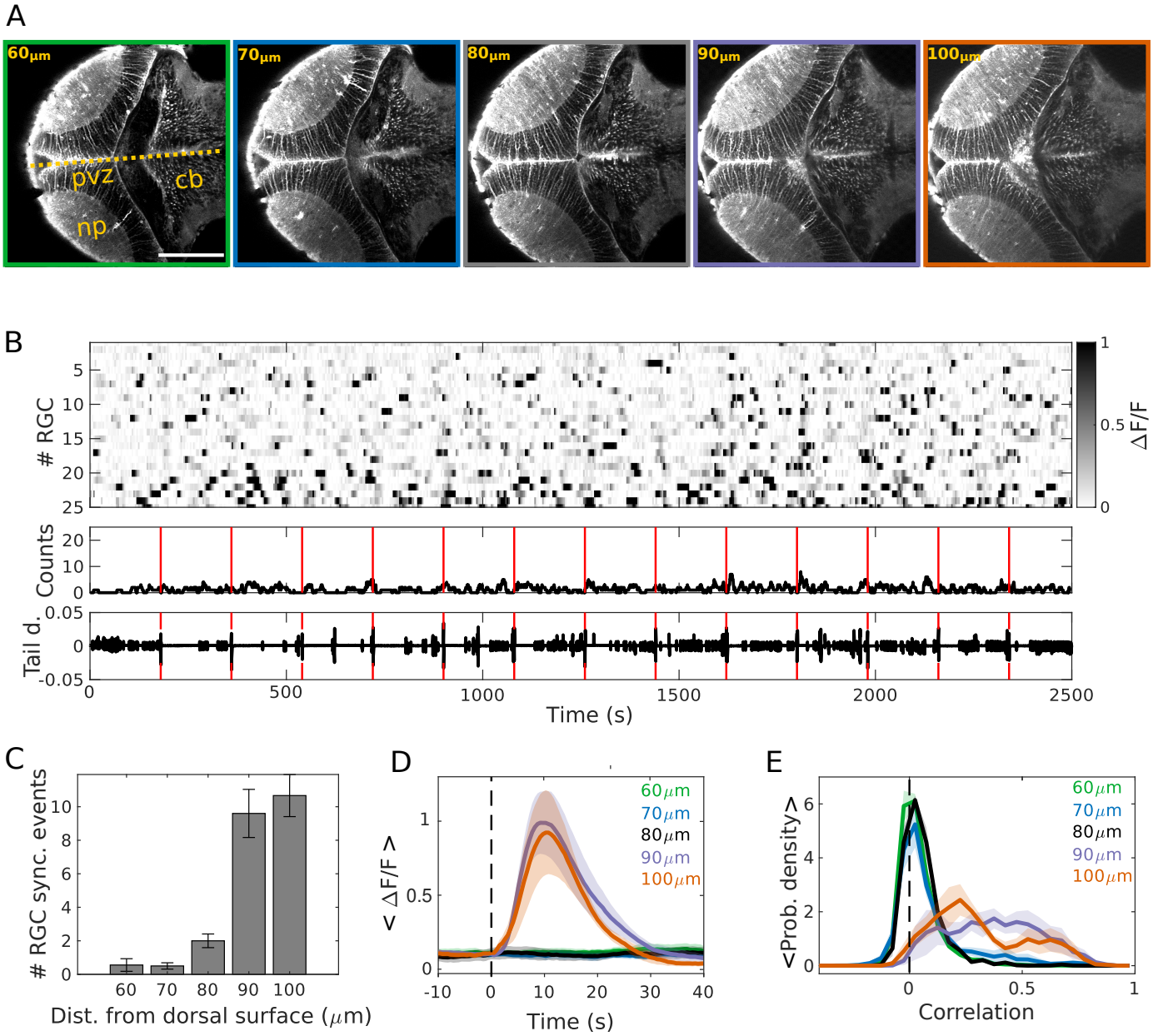
A
60µm
70µm
80µm
90µm
100µm
pvz
cb
np
B
RGC
ΔF/F
Counts
Tail d.
Time (s)
C
RGC sync. events
Dist. from dorsal surface (µm)
D
< ΔF/F >
60µm
70µm
80µm
90µm
100µm
Time (s)
E
<Prob. density>
Correlation

Figure 3

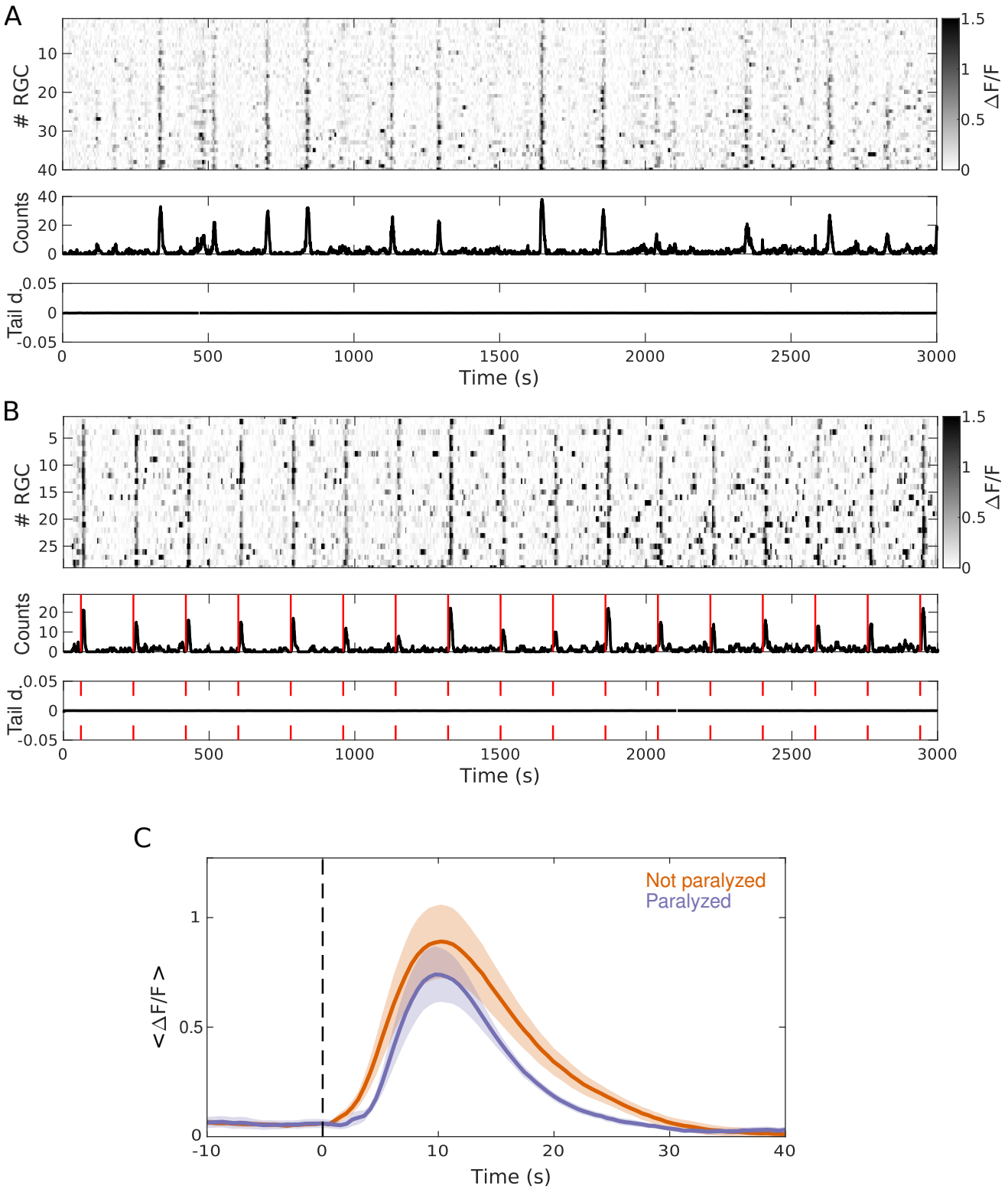
A
RGC
Counts
Tail d.
ΔF/F
Time (s)
B
RGC
Counts
Tail d.
ΔF/F
Time (s)
C
Not paralyzed
Paralyzed
< ΔF/F >
Time (s)

Figure 4

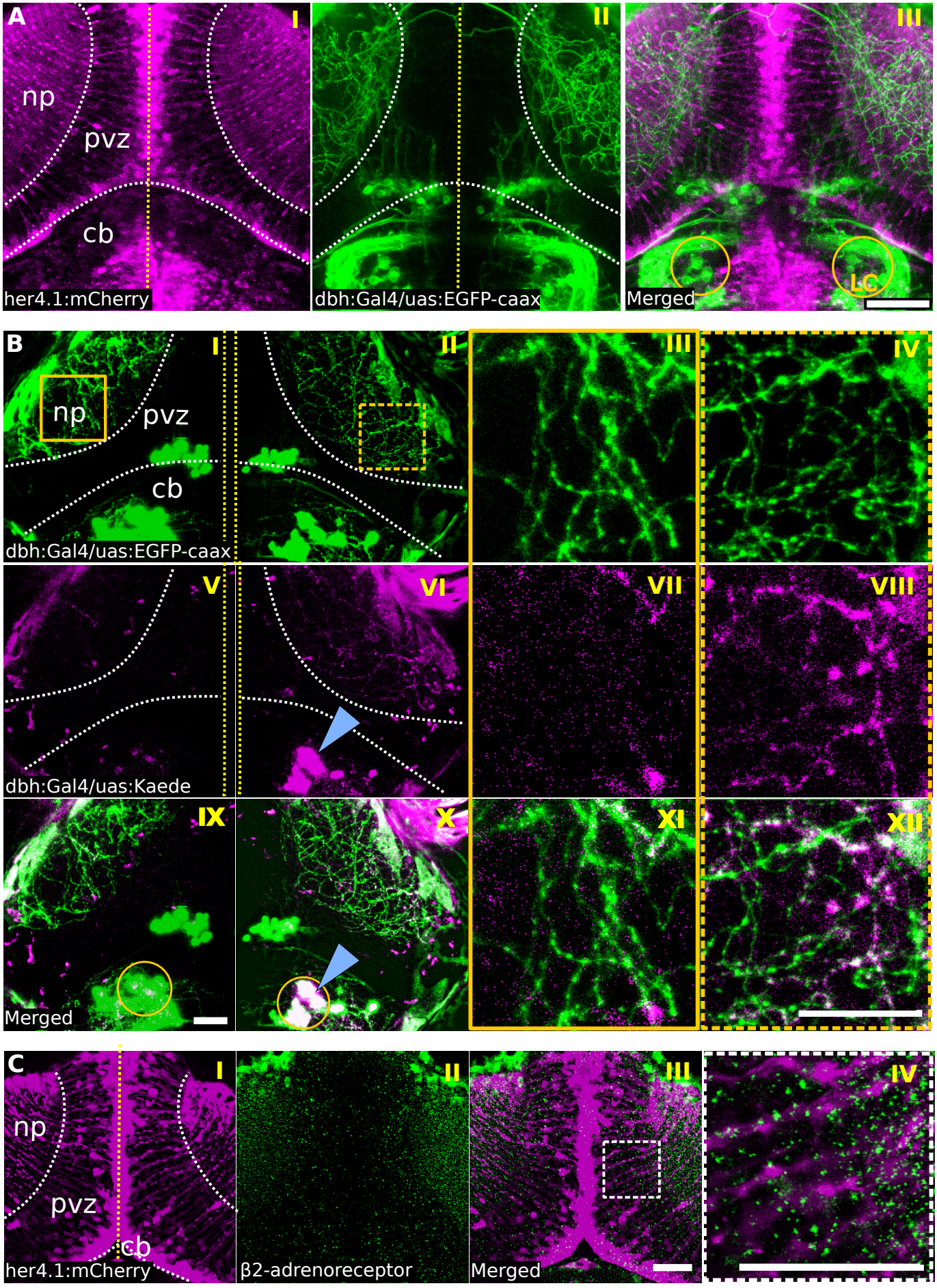
A
I
II
III
np
pvz
cb
her4.1:mCherry
dbh:Gal4/uas:EGFP-caax
Merged
LC
B
I
II
III
IV
np
pvz
cb
dbh:Gal4/uas:EGFP-caax
V
VI
VII
VIII
dbh:Gal4/uas:Kaede
IX
X
XI
XII
Merged
C
I
II
III
IV
np
pvz
cb
her4.1:mCherry
β2-adrenoreceptor
Merged

Figure 5

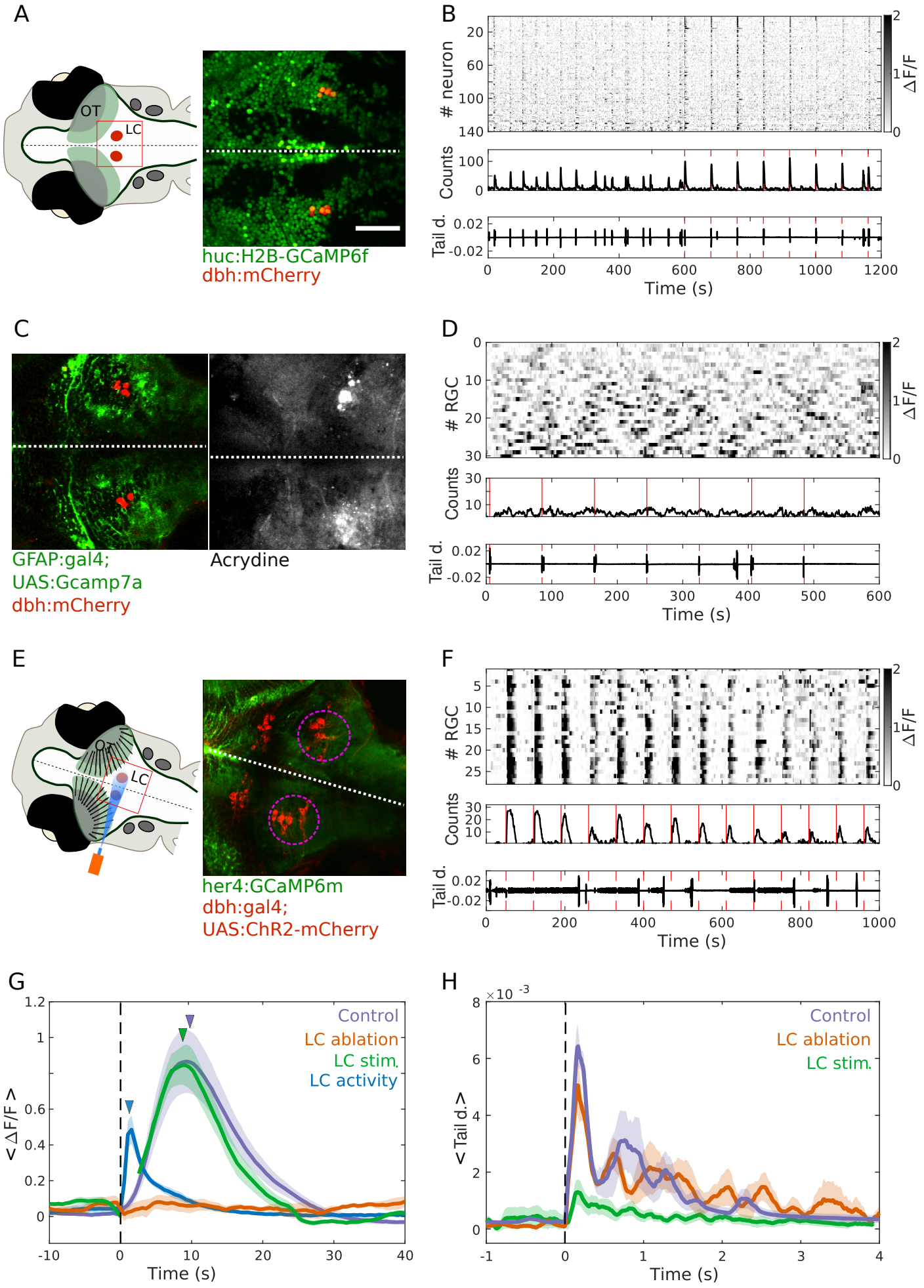
A
OT
LC
huc:H2B-GCaMP6f
dbh:mCherry
B
neuron
ΔF/F
Counts
Tail d.
Time (s)
C
GFAP:gal4;
UAS:Gcamp7a
dbh:mCherry
Acrydine
D
RGC
ΔF/F
Counts
Tail d.
Time (s)
E
OT
LC
her4:GCaMP6m
dbh:gal4;
UAS:ChR2-mCherry
F
RGC
ΔF/F
Counts
Tail d.
Time (s)
G
Control
LC ablation
LC stim.
LC activity
< ΔF/F >
Time (s)
H
Control
LC ablation
LC stim.
< Tail d. >
Time (s)

Figure 6

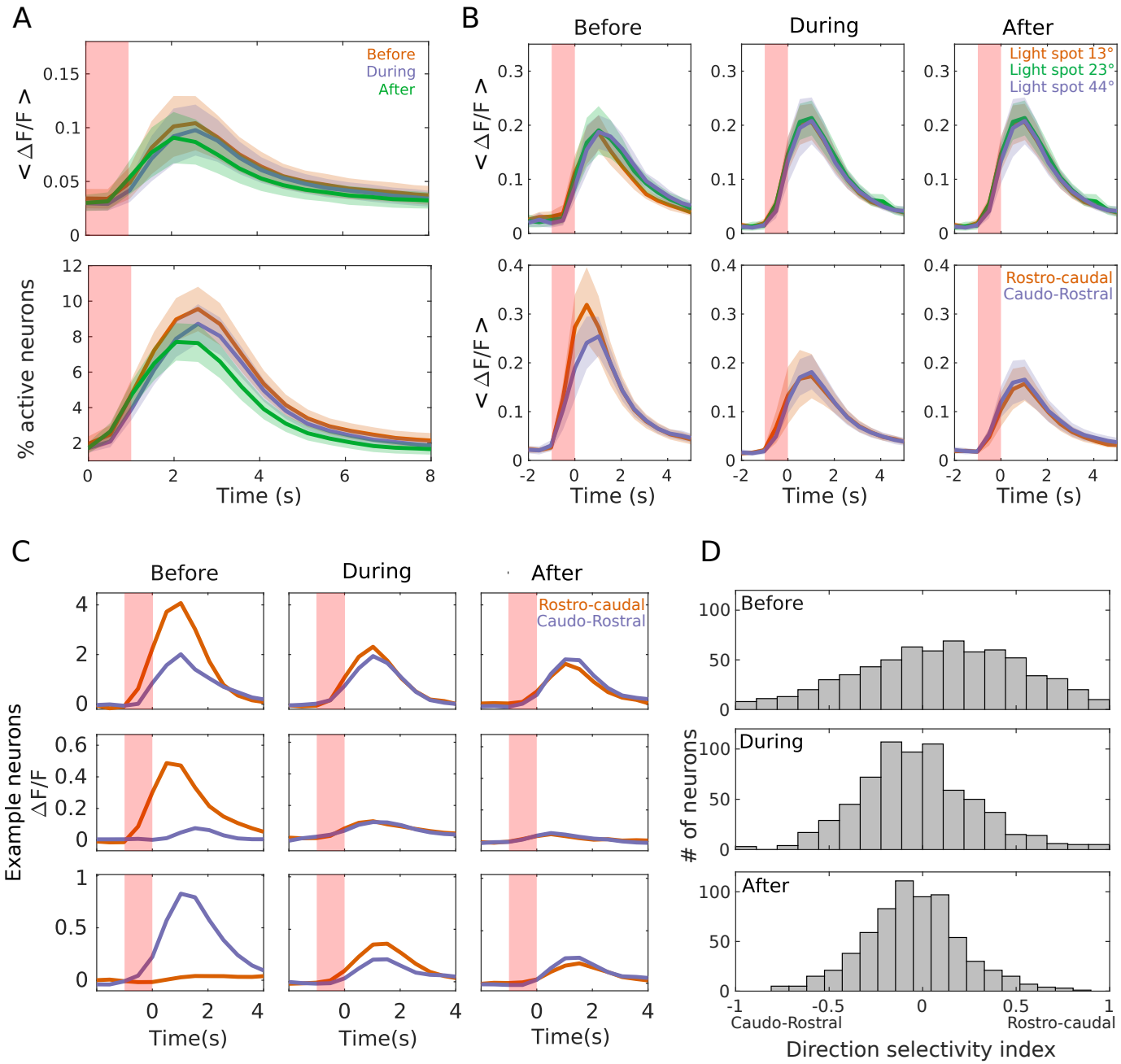
A
Before
During
After
< ΔF/F >
% active neurons
Time (s)
B
Before
During
After
Light spot 13°
Light spot 23°
Light spot 44°
Rostro-caudal
Caudo-Rostral
C
Example neurons ΔF/F
Time(s)
D
# of neurons
Direction selectivity index
Caudo-Rostral
Rostro-caudal

Figure 7

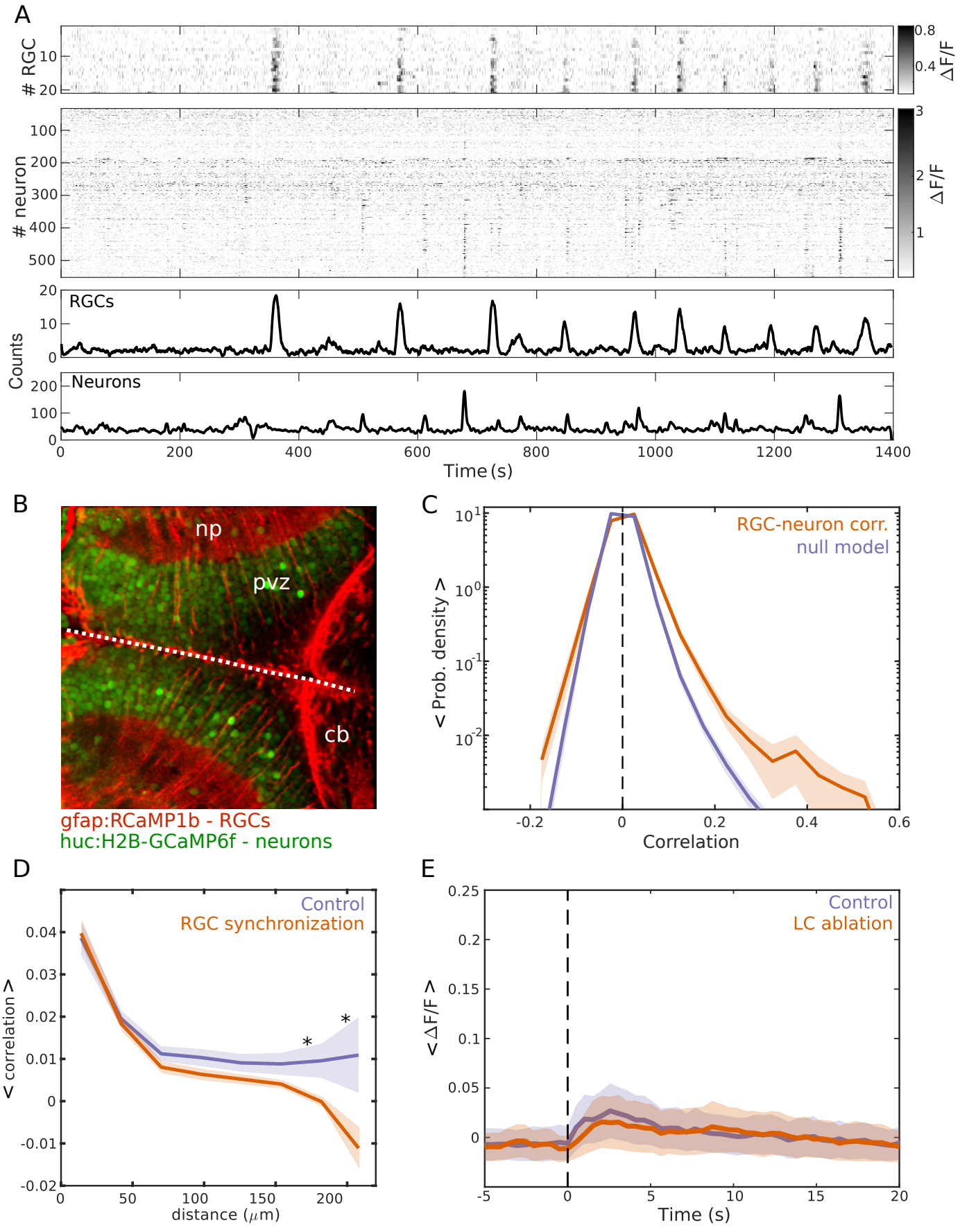
A
RGC
neuron
ΔF/F
RGCs
Neurons
Counts
Time (s)
B
np
pvz
cb
gfap:RCaMP1b - RGCs
huc:H2B-GCaMP6f - neurons
C
RGC-neuron corr.
null model
< Prob. density >
Correlation
D
Control
RGC synchronization
< correlation >
distance (μm)
E
Control
LC ablation
< ΔF/F >
Time (s)

Figure S1

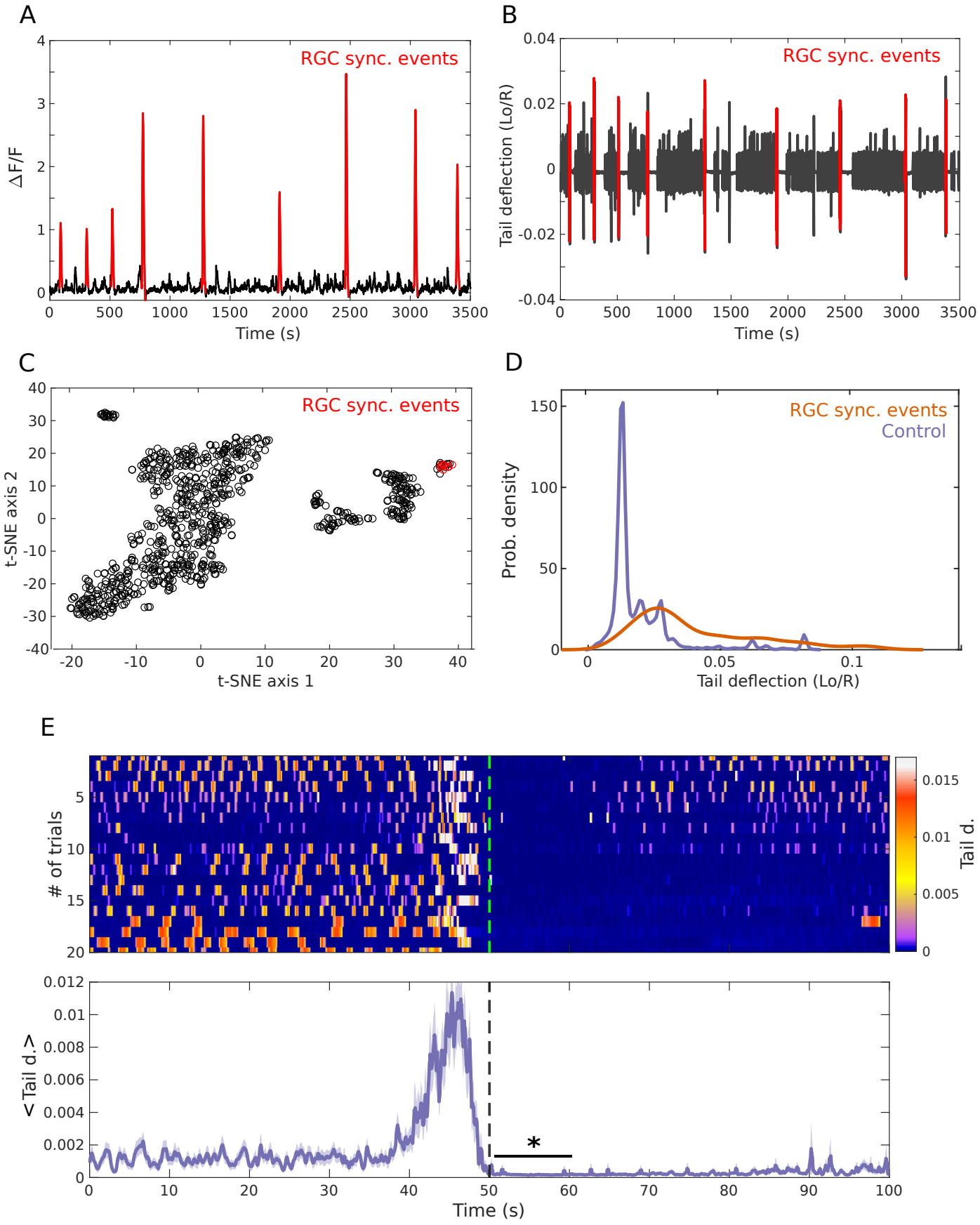
A
RGC sync. events
ΔF/F
Time (s)
B
RGC sync. events
Tail deflection (Lo/R)
Time (s)
C
RGC sync. events
t-SNE axis 2
t-SNE axis 1
D
RGC sync. events
Control
Prob. density
Tail deflection (Lo/R)
E
# of trials
Tail d.
< Tail d. >
*
Time (s)

Figure S2

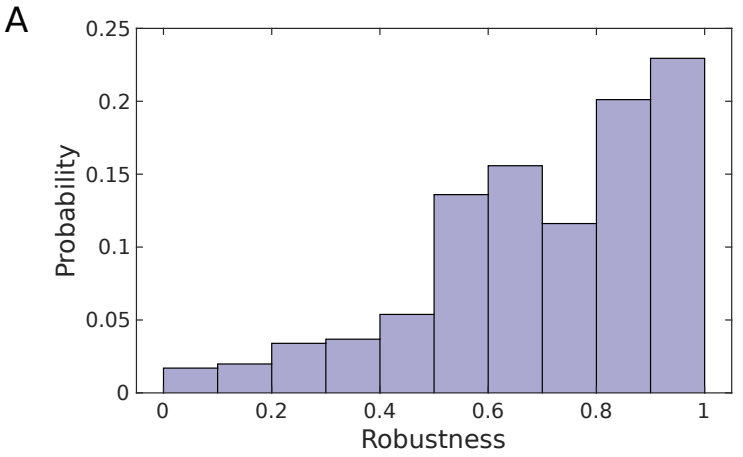
A
0.25
0.2
0.15
0.1
0.05
0
Probability
0
0.2
0.4
0.6
0.8
1
Robustness

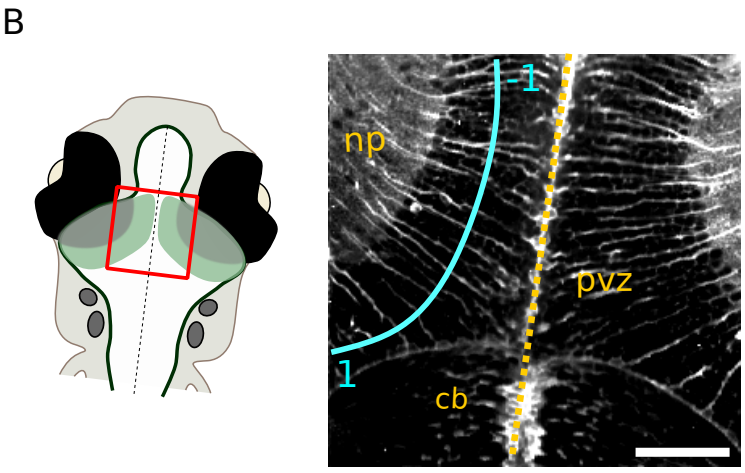
B
-1
np
pvz
1
cb

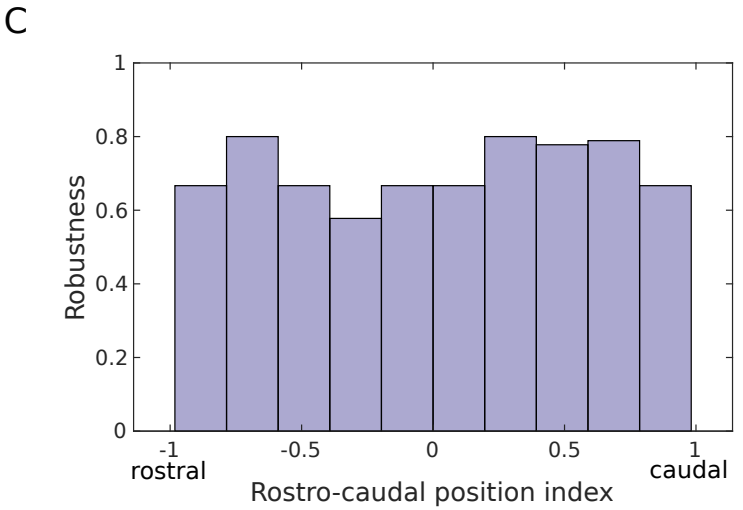
C
1
0.8
0.6
0.4
0.2
0
Robustness
-1
rostral
-0.5
0
0.5
1
caudal
Rostro-caudal position index

Figure S3

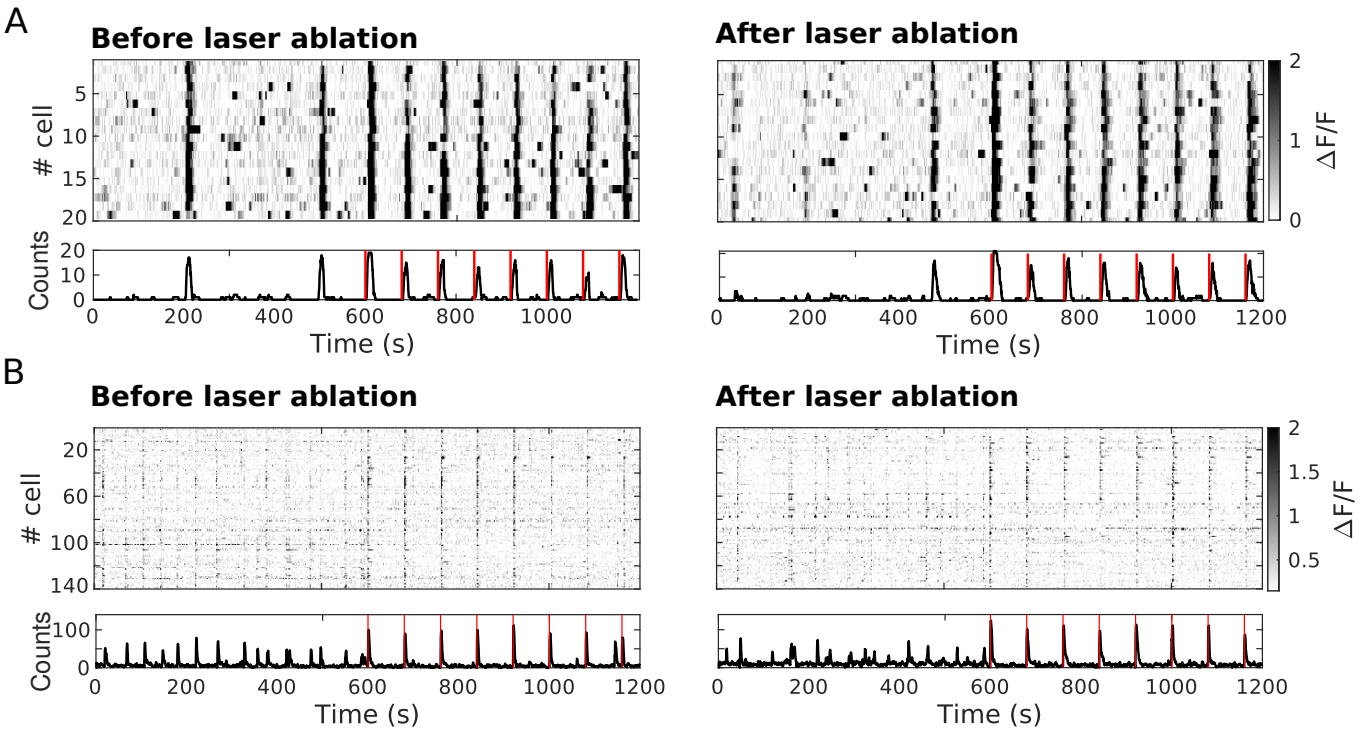
A
Before laser ablation
After laser ablation
cell
Counts
Time (s)
ΔF/F
B
Before laser ablation
After laser ablation
cell
Counts
Time (s)
ΔF/F

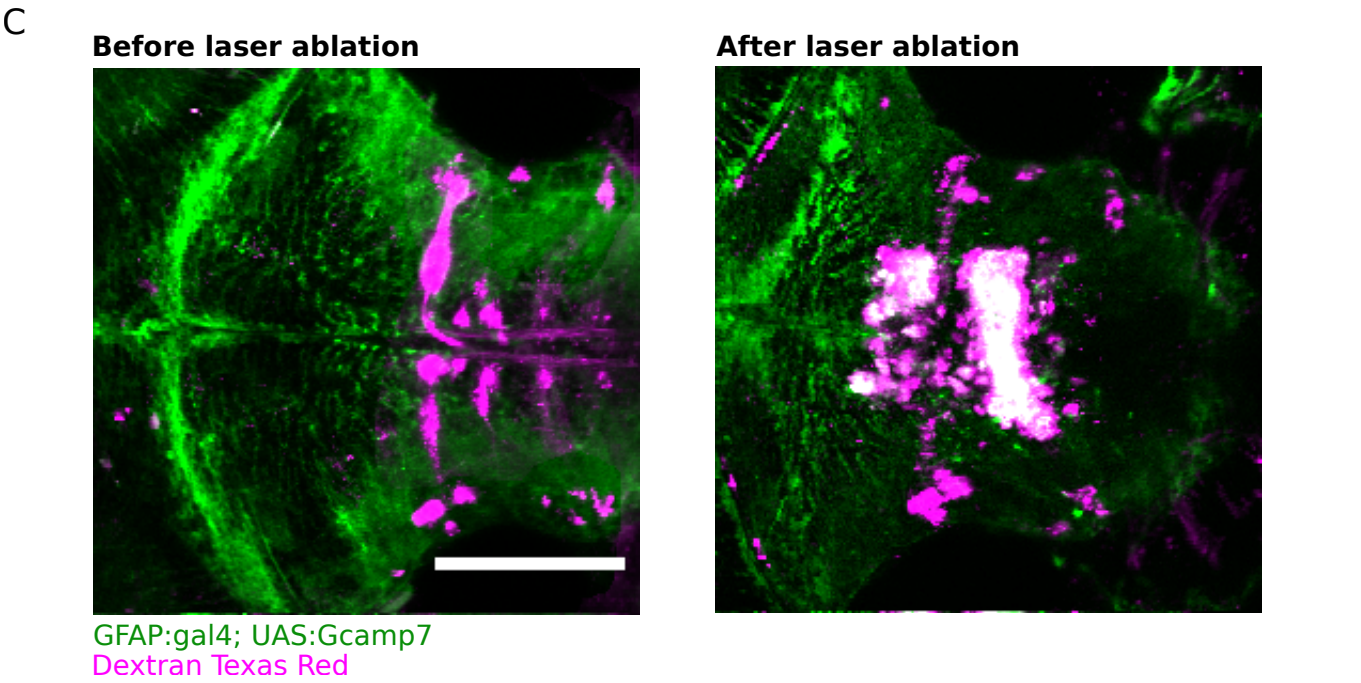
C
Before laser ablation
After laser ablation
GFAP:gal4; UAS:Gcamp7
Dextran Texas Red

Figure S4

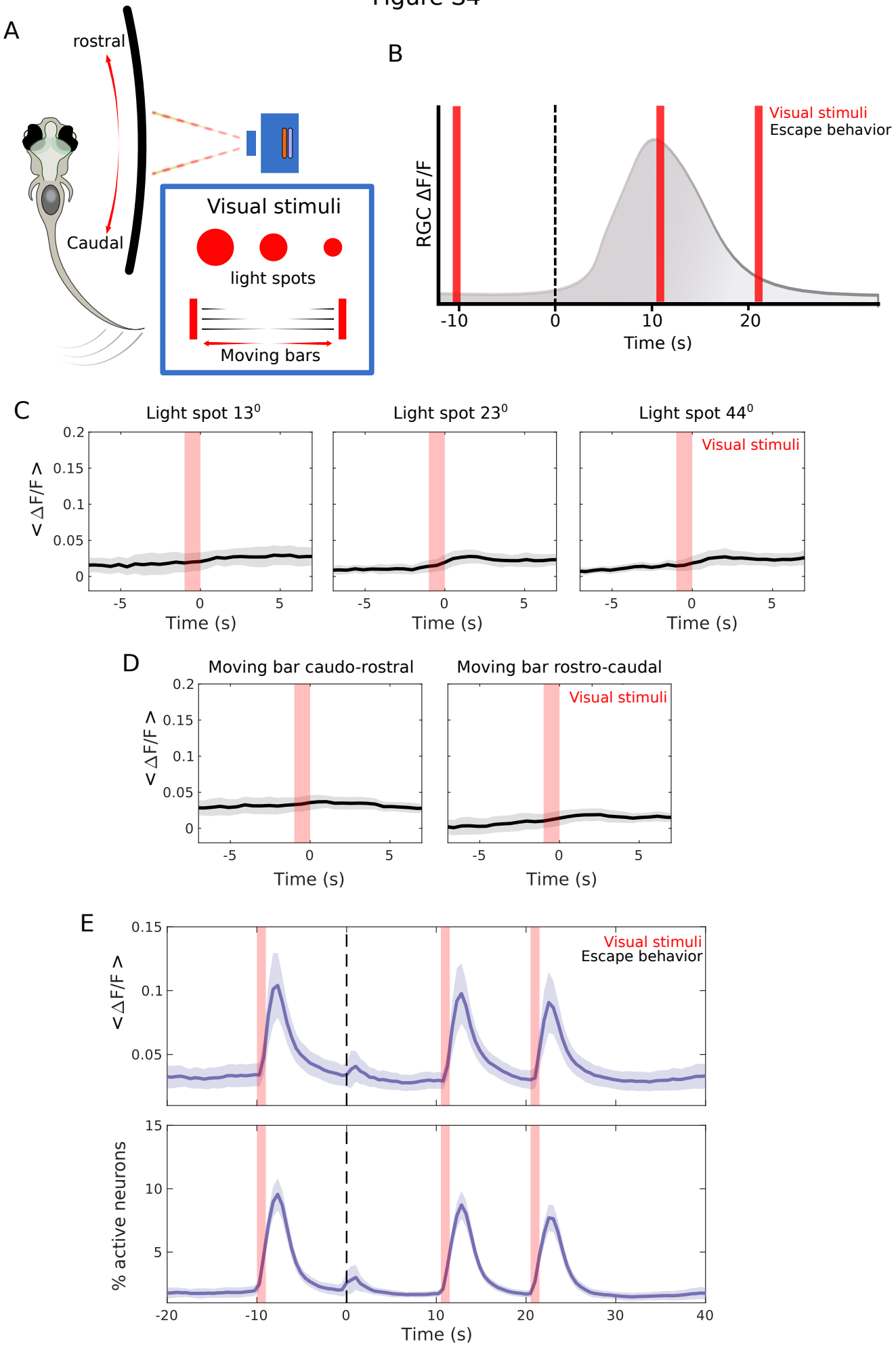
A
rostral
Caudal
Visual stimuli
light spots
Moving bars
B
Visual stimuli
Escape behavior
RGC ΔF/F
-10
0
10
20
Time (s)
C
Light spot 13⁰
Light spot 23⁰
Light spot 44⁰
Visual stimuli
< ΔF/F >
0.2
0.15
0.1
0.05
0
-5
0
5
Time (s)
D
Moving bar caudo-rostral
Moving bar rostro-caudal
Visual stimuli
< ΔF/F >
Time (s)
E
Visual stimuli
Escape behavior
< ΔF/F >
% active neurons
15
10
5
-20
-10
0
10
20
30
40
Time (s)

Figure S5

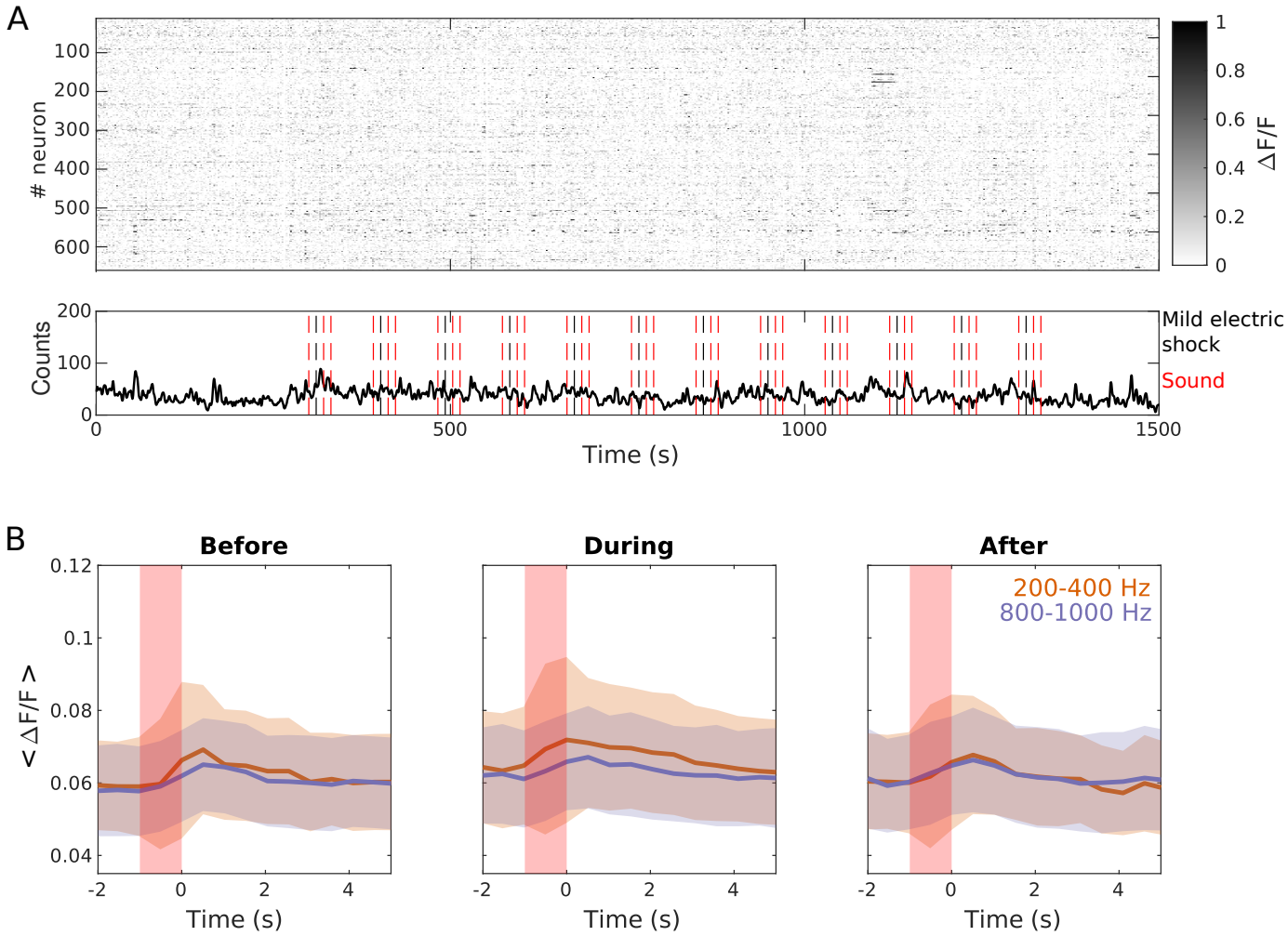
A
neuron
100
200
300
400
500
600
1
0.8
0.6
0.4
0.2
0
ΔF/F
Counts
200
100
0
0
500
1000
1500
Time (s)
Mild electric shock
Sound
B
Before
During
After
< ΔF/F >
0.12
0.1
0.08
0.06
0.04
-2
0
2
4
Time (s)
200-400 Hz
800-1000 Hz

Figure S6

A

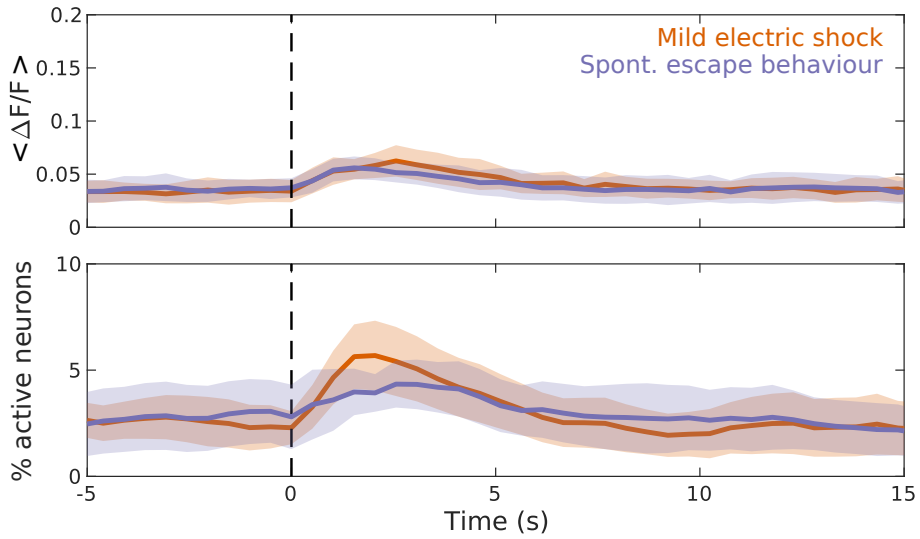
Mild electric shock
Spont. escape behaviour
<ΔF/F>
% active neurons
Time (s)
0.2
0.15
0.1
0.05
0
10
5
0
-5
0
5
10
15

Figure S7

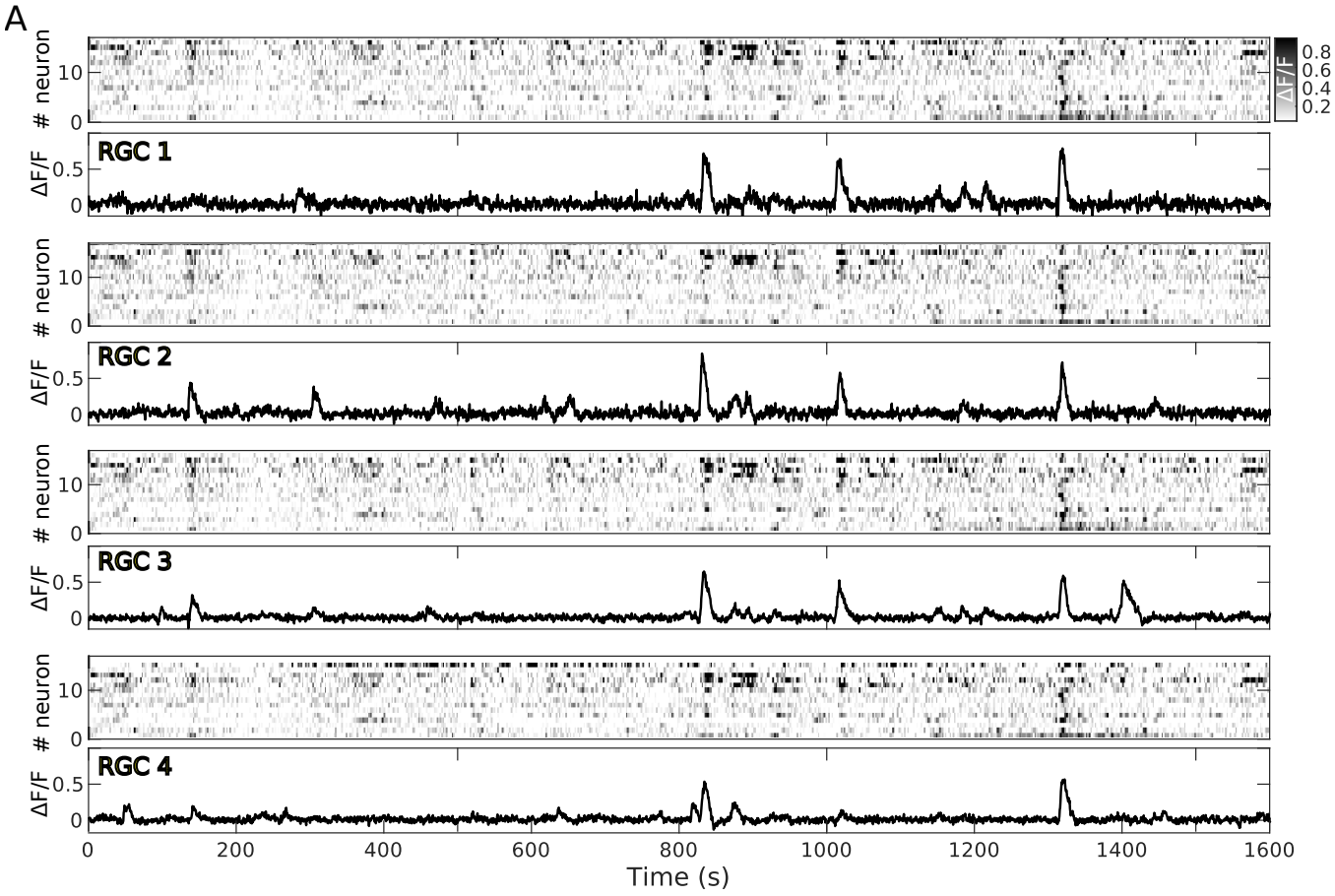
A
neuron
ΔF/F
RGC 1
RGC 2
RGC 3
RGC 4
0.8
0.6
0.4
0.2
0
200
400
600
800
1000
1200
1400
1600
Time (s)

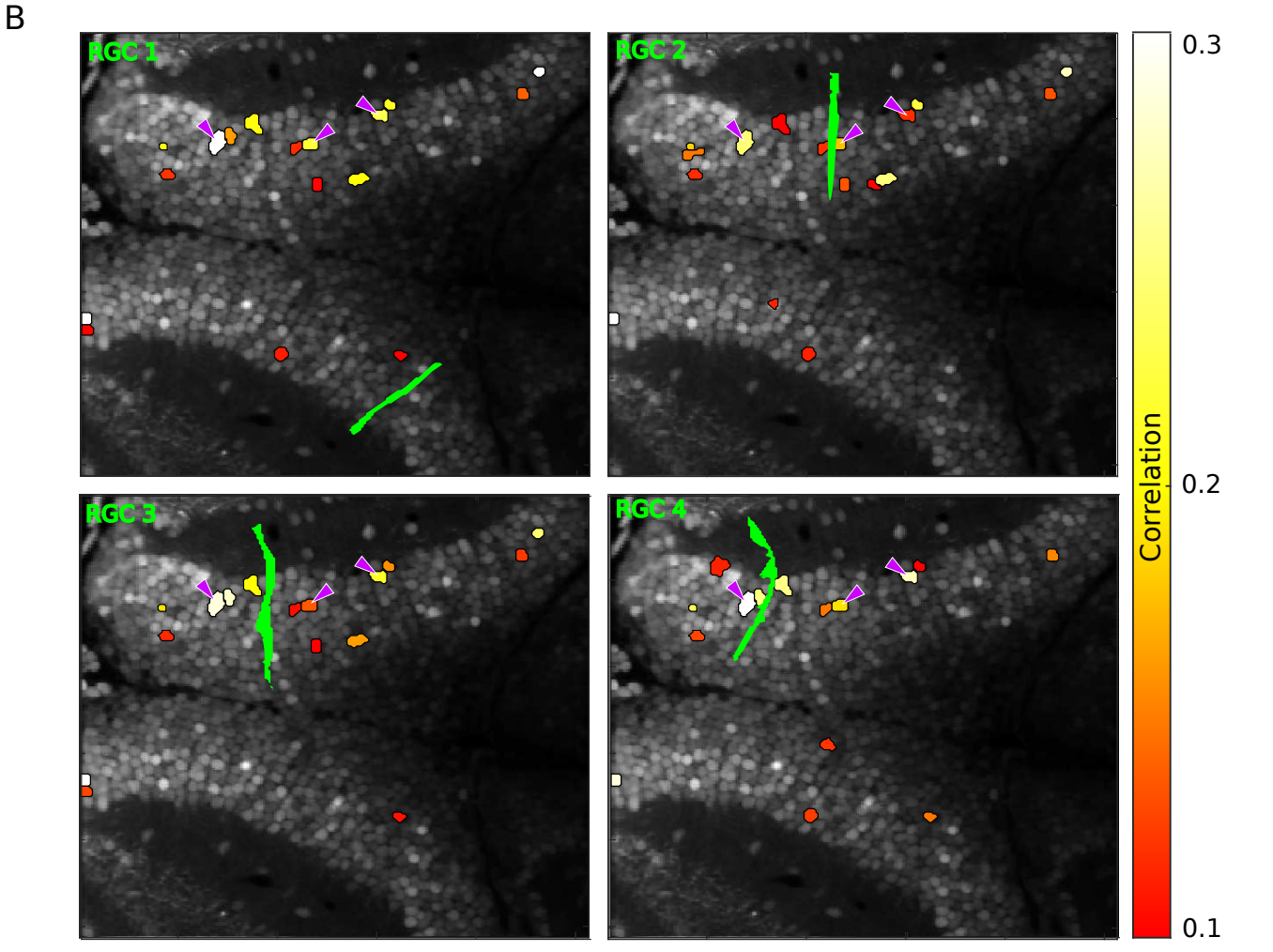
B
RGC 1
RGC 2
RGC 3
RGC 4
Correlation
0.3
0.2
0.1

4

Discussion

Since the description of the tripartite synapse and the reciprocate communication between astrocytes and neurons, it is known that astrocytes are involved in several brain functions once considered specific to neurons. Recent evidence *in vivo* highlighted these astrocytes contributions. For example, in rodents, the chemogenetic activation of Ca^{2+} signaling in hippocampal astrocytes facilitates NMDA dependent LTP and enhanced memory allocation in fear conditioning and spatial learning [Adamsky et al., 2018]. Later work confirmed this finding showing that the optogenetic activation of hippocampal astrocytes increases synaptic plasticity and enhances episodic-like memory [Mederos and Perea, 2019]. On the another hand, abnormal Ca^{2+} signaling in astrocytes perturbs memory consolidation [Pinto-Duarte et al., 2019]. Recent evidence indicates that astrocyte signaling plays a fundamental role in sensory responses. Astrocyte Ca^{2+} imaging in the olfactory bulb of mice revealed an odor map associated with odor discrimination and detection [Ung et al., 2020]. Furthermore, it has been found in thalamic astrocytes that the GABA gliotransmission which results in the tonic inhibition in thalamocortical neurons is associated with the discrimination performance in the touch-based novel object recognition essay [Kwak et al., 2020].

In my thesis project, I studied the role of glia in visual processing through a comprehensive *in vivo* approach using the visual system of an intact, non-anesthetized, non-paralyzed vertebrate. I used two-photon microscopy, transgenic zebrafish larvae expressing GECIs in neurons and RGCs, optogenetics, and motor behavior. This approach en-

abled monitoring with near-single-cell resolution, the neuronal and radial glia dynamics in the zebrafish main's visual center the optic tectum (OT).

Despite the different morphology between zebrafish RGCs and mammalian astrocytes, RGCs have been proposed to have an analogous function to that of the mammalian astrocytes [Chen et al., 2020, Jurisch-Yaksi et al., 2020]. I monitored the Ca^{2+} dynamics in RGCs and in neurons to study the functional interaction between both in the zebrafish OT. I found that individual RGCs displayed synchronous Ca^{2+} transients across the RGCs population only in the ventral layers of the OT. These synchronous events were followed specifically by escape behaviors and not by other types of tail movements.

Remarkably, we found that this Ca^{2+} propagation does not depend on muscular proprioception neither on motor centers located in the spinal cord or the reticulo-spinal circuit. Despite these results we found a clear association between RGCs synchronization with escape behaviour. These results suggest that the association between the RGCs synchronization and the escape behaviors was not causal but rather depicted two parallel process probably triggered by a change to an arousal state. Given the role of the LC-NE system in arousal states and the fact that astrocytes respond to NE [Bazargani and Attwell, 2017, Oe et al., 2020], I hypothesized that the RGCs synchronization can be the consequence of a change in an internal state that triggers escape behaviors and the LC in parallel. To test this hypothesis, I studied the relationship between LC activity and that of the RGCs in the OT. I observed that LC projections innervate mainly ipsilaterally the OT neuropil and β2-adrenoreceptors are co-localized with the processes of the RGCs to the tectal neuropil. Furthermore, LC optogenetic stimulation induced RGC synchronous Ca^{2+} events without triggering any type of tail movement, and LC ablation suppressed the Ca^{2+} synchronization without affecting tail behavior. These results suggest that LC activity is necessary and sufficient to trigger tectal RGCs synchronization. These results coincide with preview studies which report that NE induces Ca^{2+} transients in astrocytes in mammals [Bazargani and Attwell, 2017, Oe et al., 2020] and zebrafish [Mu et al., 2019, Orts-Del'Immagine et al., 2022]. Despite the clear correlation between the escape behaviors and tectal RGCs synchronization, this is not a causal relationship. Thus, these two phenomena may be triggered by a common input.*for a schematic representation see figure* 4.1 Additional experiments are underway to address this open question *see section* 4.1.2.

Overall, these findings suggest that a switch into an alertness state induces RGCs synchronization through the LC activation and in parallel also triggers escape responses. In this scenario, the slow Ca^{2+} dynamics of RGCs will mediate the time course of the arousal state. This is supported by recent evidence. For example, aversive stimuli such footshocks or air-puff startle trigger astrocytes responses via LC discharge of NE [Bekar et al., 2008, Ding et al., 2013, Oe et al., 2020]. In addition, in the mouse visual cortex,

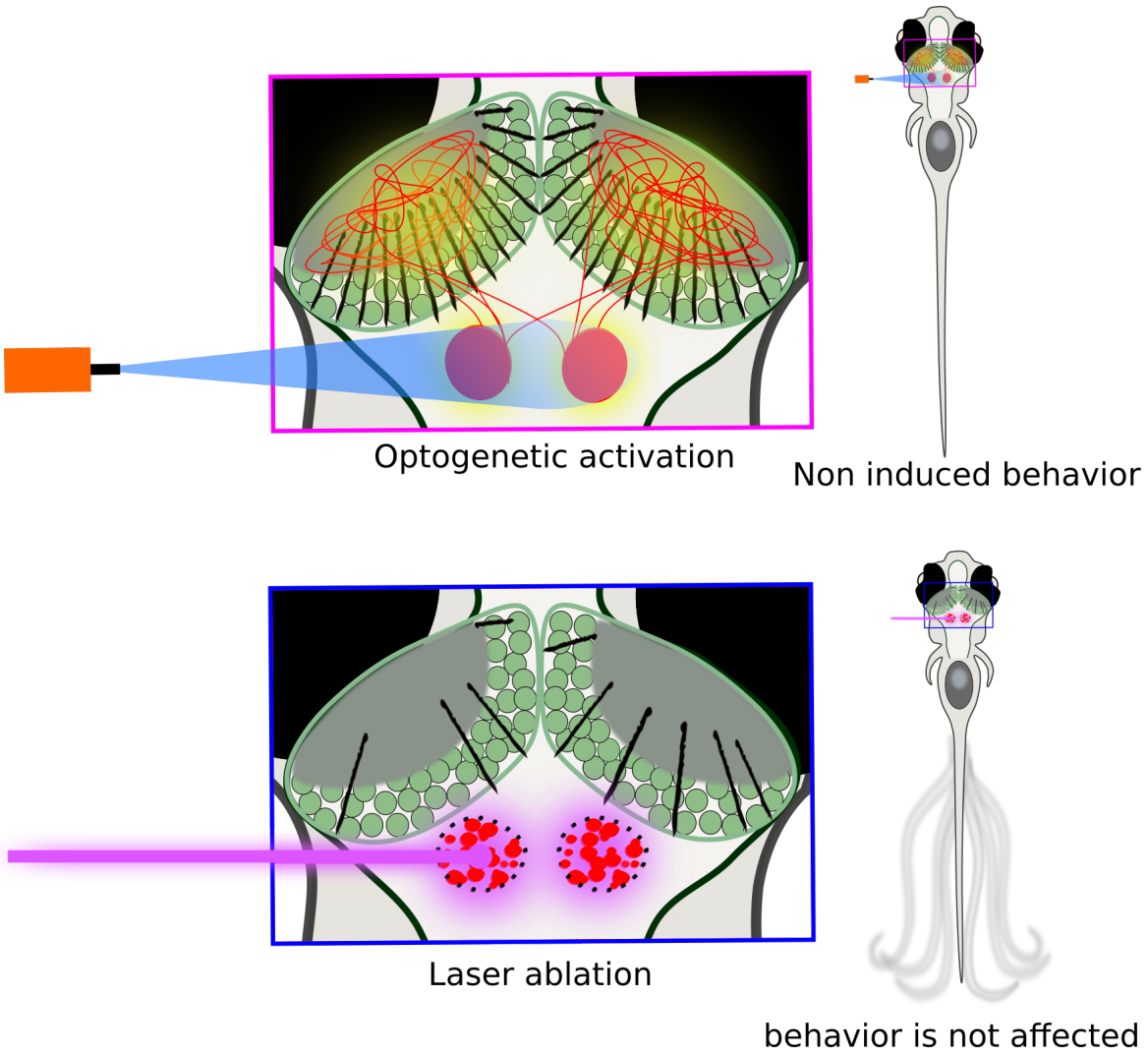

Figure 4.1: **Escape behaviors and tectal RGCs synchronization do not have a causal relationships.** TOP: LC optogenetic stimulation induced RGC synchronous Ca^{2+} events without triggering any type of tail movement, Botton: LC ablation suppressed the Ca^{2+} synchronization without affecting tail behavior. Despite the clear correlation between the escape behaviors and tectal RGCs synchronization, this is not a causal relationship. Thus, these two phenomena may be triggered by a common input.

enforced locomotion paired with simultaneous visual stimulation induce Ca^{2+} transients in cortical astrocytes depending on LC activation [Paukert et al., 2014, Slezak et al., 2019]. The amplitudes of astrocytic responses are correlated with changes in arousal state [Slezak et al., 2019] see section 1.5.

In contrast to findings in rodents showing that astrocytes in the primary visual cortex increase their Ca^{2+} concentration following visual stimulation [Paukert et al., 2014, Slezak et al., 2019, Sonoda et al., 2018], RGCs in the OT, the main visual processing center in zebrafish, did not respond to different types of visual stimuli. However, I found that RGCs synchronization modulates the neuronal responses to moving bars stimuli decreasing their direction selectivity. Notably, the neural response to light spots was not affected

during the RGCs synchronization. Consequently, It is likely that RGCs neuronal modulation can reduce the optomotor response (OMR) without strongly affecting other types of visual responses (OMR is induced by relative movement of the fish with respect to the riverbed when the larva is not moving). In support of this hypothesis, I found that during the duration of the RGCs synchronizations, the probability of observing tail motor movements with respect to similar periods before the onset of the RGCs synchronization, was significantly reduced. This mechanism may support freezing behavior following a switch to an alerted state. Notably, this selective modulation coincide with some observations in humans that report that freezing is associated with better discrimination of coarse cues at the expense of detailed visual information [Lojowska et al., 2015].

We found that RGCs synchronization elicited by spontaneous escape behaviours or mild electric shocks did not significantly increase the activity of tectal neurons. Moreover, laser ablation of the LC to prevent RGC synchronizations did not affect the spontaneous activity of tectal neurons. These results and the fact that tectal neurons and RGCs are not functionally correlated suggest that RGCs synchronization does not inhibit neither excite the tectal neurons. Nevertheless, we observed that RGC synchronizations significantly reduced the pair-wise correlations only between distant neurons, while correlations between near-by neurons remained unchanged. Thus, our observation suggest that RGC synchronous events modulate the functional connectivity between tectal neurons. The OT circuit is organized in functional assemblies of highly correlated neurons showing attractor-like dynamics (all-or-none activations and winner-takes-all dynamics). This mechanism has been proposed to improve the visual discrimination of vital cues in noisy environments [Romano et al., 2015]. Thus, modulation of the long-distance functional connectivity may improve the detection of vital visual objects by creating more compact neuronal assemblies.

In addition, a previous study showed that the brain of zebrafish displays scale-invariant neuronal avalanches (sequential activation of a group of neurons generating cascade-like events). This is suggestive of brain dynamics operating at a critical state, a regime between phases of order and disorder in which several brain functions could be optimized. In zebrafish, criticality improves visual decoding [Ponce-Alvarez et al., 2018]. Therefore, modulation of tectal functional connectivity may temporally deviate the brain from a critical regime to a more ordered one affecting brain processing. This would indicate that RGC synchronous activations enable the brain to auto-regulate its own dynamics towards and away from a critical regime to adapt the computational brain capabilities to the current context or brain state.

Overall, our results suggest the following scenario: a switch to an arousal state induces the activity of the LC. LC NE projections to the tectum generate synchronous Ca^{2+} events among the ventral population of RGCs. The RGCs synchronous events modulate

the directional selectivity of tectal neurons and prune their functional correlations to adapt the larva's visual system to cope with the environmental context associated with an arousal state. Although some evidence suggest that NE-effect in the bran is most likely mediated by astrocytes [Pankratov and Lalo, 2015], and that the immunochemistry labeling of β2-adrenoreceptors show a tight co-localization with the RGC projections rather than the tectal neurons, it is possible that the NE released by the LC in the tectal neuropil is sensed by β2-adrenoreceptors in both RGCs and neurons. In this case, the observed adaptations of the visual system during the arousal states may be related to the tight interactions between tectal RGCs and the NE-secreting neurons of the LC. Thus, LC-NE modulation via RGCs or tectal neurons may not be mutually exclusive, but are likely to work in conjunction to coordinate the sensorial computations during transition of behavioral states. *for a schematic representation see figure* 4.2

In zebrafish, RGCs display different functional roles. RGCs in the hindbrain function as error integrators of futile swim responses to visual flow when is deprived of visual feedback. However, in contrast to our results, this phenomenon is not mediated by LC, but rather triggered by NE neurons located in the medulla oblongata (NE-MO) [Mu et al., 2019]. This finding indicates that the LC-mediated tectal RGCs synchronous Ca^{2+} events and the medulla oblongata-mediated hindbrain RGC activations are two different phenomena occurring through two independent pathways, involving two processes with different biological relevance (futility vs switch to an arousal state). In a zebrafish model of epilepsy, the impairment in the glia-neuron functional connectivity in the forebrain induces epileptic seizures following an excessive release of glutamate that lead the transition from the preictal period to seizures [Verdugo et al., 2019]. A third study in zebrafish RGCs showed that in the rostral spinal cord, Ca^{2+} waves are propagated bidirectionally to the hindbrain and to the caudal spinal cord after an acousto-vestibular stimuli [Orts-Del'Immagine et al., 2022]. The results of my PhD project report an additional functional role of RGCs in brain computations and functional connectivity to adapt the brain to the with different behavioral states. This study adds to the emerging evidence that brain computations and behavioral states depend on the coordinated interactions between astrocytes and neurons.

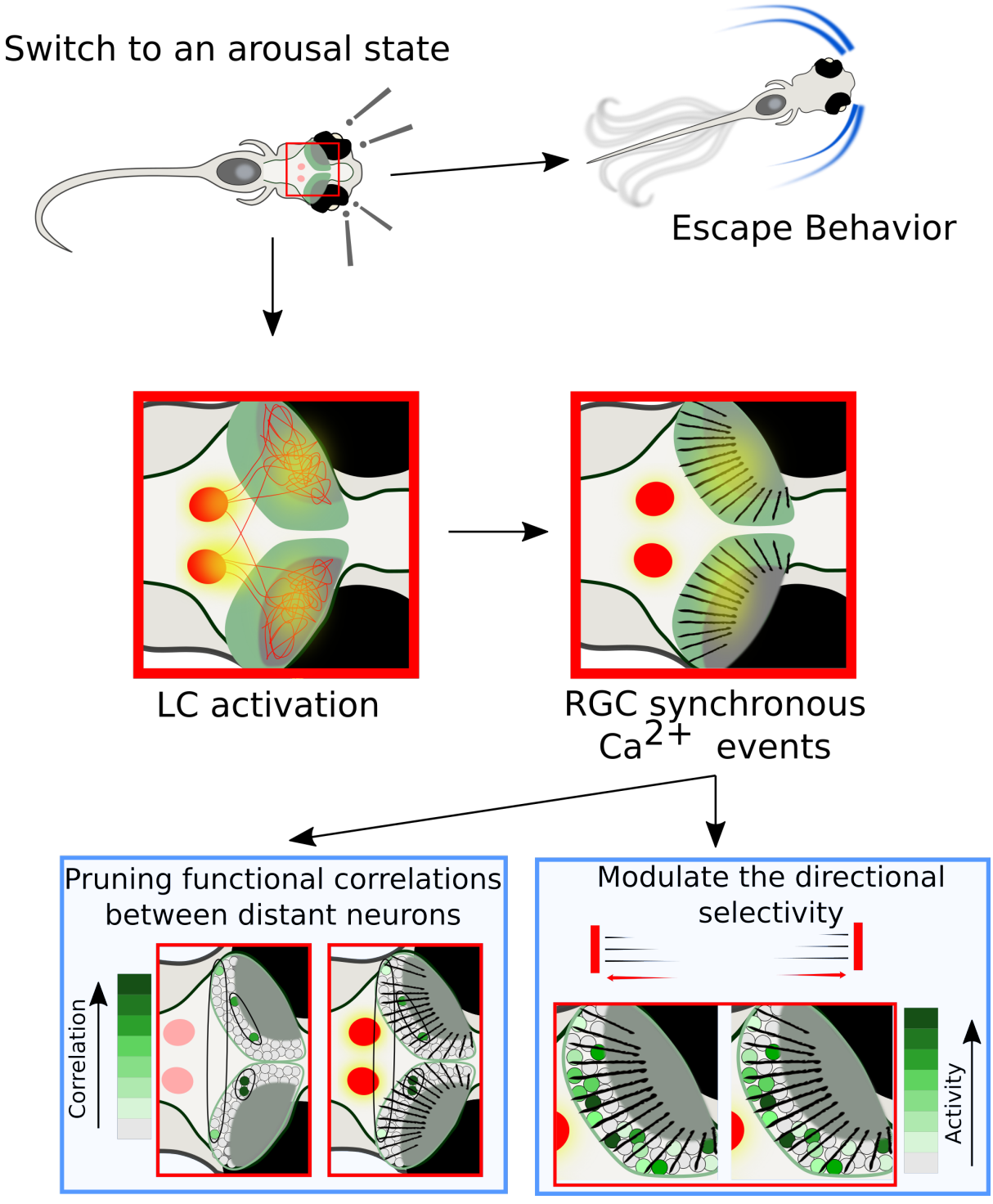

Figure 4.2: **Graphical abstract.** a switch to an arousa state induces an escape response and in parallel the activity of the LC. LC-NE projections to the tectum generate synchronous Ca^{2+} events of RGCs. These RGC synchronous events modulate the directional selectivity of tectal neurons and prune their functional correlations. Shaded green: OT; Shaded gray: OT neuropile. Red lines, LC projections to the OT neuropile. Red scare zoom from the schematic representation of the zebrafish larvae. Hypothetical green scale bar: bottom left, correlation; bottom right, neuronal activity.

4.1 Limitations and perspecives

4.1.1 Is the LC-NE system effect directly driven by RGCs Ca^{2+} activity?

We found a reduction in the neuronal directional selectivity and in the functional connectivity among distant neurons during the RGC synchronizations in the OT. Nevertheless, it is possible that the observed neural modulations are mediated by the direct effect of the LC discharge of NE, or the coordinated modulation via both cells. To address this open question I intend to perform the following experiments :

Optogetenetic activation and ablation of tectal RGCs

I will perform optogenetical activation of RGCs using trasgenic zebrafish larvae expressing CoChR or ChR2 under a glial promoter (gfap or her4). Then, I will evaluate the visual responses to moving bars and light spots of the tectal neurons in the OT, and test whether direct RGC activation without the implication of the LC is sufficient to reproduce the modulations of the direction-selective neurons and the pruning of the distant pair-wise correlations among neurons. This experiment will allow me to discard a potential NE direct effect on the tectal neurons.

Alternatively, I will induced the the specific ablation of RGCs using transgenic zebrafish larvae expressing nfsB under control of a glial promoter (gfap). This bacterial gene (nfsB) encodes a nitroreductase (NTR) enzyme to catalyze the reduction of the innocuous prodrug metrodinazole. Therefore, producing a cytotoxic product that induces cell death. Base on this technique, I will inject the optic tectum of the transgenic larvae with metrodinazole to induce cell death in RGCs. Afterwards, I will observe the neuronal response to visual stimulation and their functional connectivity following the activation of the LC.

4.1.2 Common input(S) to trigger the escape behaviors and RGCs synchronization

I found that LC-mediated RGCs Ca^2 synchronization and the escape behaviors do not have a causal relationship. Instead, they seem to be two independent parallel processes with a common input. To search for this shared source, I will use transgenic zebrafish larvae expressing GCaMP in all neurons in combination with light-sheet microscopy to monitor whole-brain dynamics with single-neuron resolution, while simultaneously recording tail movements. Then, I will study the neural spontaneous activity before the activation

of the LC following an escape behavior capable of predicting both. Using this experimental paradigm, I expect to described a mechanism capable of spontaneously trigger the LC-mediated RGCs synchronization and escape behaviors.

4.1.3 Have the different activity patterns of the LC a differential influence in RGCs function?

LC neurons exhibit phasic and tonic firing activity patterns in response to external stimuli or internal states respectively. [Devilbiss and Waterhouse, 2011], *see section* 1.5. Although, it is known that this differential activity influences the NE release features, their influence in astroglia functions remains to be elucidated. To evaluate this question, I will drive different patterns of activation in the LC using the selective photostimulation with ChR2 expressing lines. For this purpose, I will use a digital micro-mirror device that enables projecting on the tissue being recorded, patterns of light (e.g. 450nm) corresponding to the anatomy of neurons I would like to stimulate. I will then evaluate the stimulation influence on brain computations.

Bibliography

[Abbracchio and Ceruti, 2006] Abbracchio, M. P. and Ceruti, S. (2006). Roles of p2 receptors in glial cells: focus on astrocytes. *Purinergic signalling*, 2:595–604.

[Adamsky et al., 2018] Adamsky, A., Kol, A., Kreisel, T., Doron, A., Ozeri-Engelhard, N., Melcer, T., Refaeli, R., Horn, H., Regev, L., Groysman, M., London, M., and Goshen, I. (2018). Astrocytic activation generates de novo neuronal potentiation and memory enhancement. *Cell*, 174:59–71.e14.

[Admati et al., 2020] Admati, I., Wasserman-Bartov, T., Tovin, A., Rozenblat, R., Blitz, E., Zada, D., Lerer-Goldshtein, T., and Appelbaum, L. (2020). Neural alterations and hyperactivity of the hypothalamic–pituitary–thyroid axis in oatp1c1 deficiency. *https://home.liebertpub.com/thy*, 30:161–174.

[Agarwal et al., 2017] Agarwal, A., Wu, P. H., Hughes, E. G., Fukaya, M., Tischfield, M. A., Langseth, A. J., Wirtz, D., and Bergles, D. E. (2017). Transient opening of the mitochondrial permeability transition pore induces microdomain calcium transients in astrocyte processes. *Neuron*, 93:587–605.e7.

[Agulhon et al., 2010] Agulhon, C., Fiacco, T. A., and McCarthy, K. D. (2010). Hippocampal short- and long-term plasticity are not modulated by astrocyte ca2+ signaling. *Science (New York, N.Y.)*, 327:1250–1254.

[Agulhon et al., 2008] Agulhon, C., Petravicz, J., McMullen, A. B., Sweger, E. J., Minton, S. K., Taves, S. R., Casper, K. B., Fiacco, T. A., and McCarthy, K. D. (2008). What is the role of astrocyte calcium in neurophysiology? *Neuron*, 59:932–946.

[Ahrens and Engert, 2015] Ahrens, M. B. and Engert, F. (2015). Large-scale imaging in small brains. *Current Opinion in Neurobiology*, 32:78–86.

[Angulo et al., 2004] Angulo, M. C., Kozlov, A. S., Charpak, S., and Audinat, E. (2004). Glutamate released from glial cells synchronizes neuronal activity in the hippocampus. *The Journal of neuroscience : the official journal of the Society for Neuroscience*, 24:6920–6927.

[Araque et al., 2014] Araque, A., Carmignoto, G., Haydon, P. G., Oliet, S. H., Robitaille, R., and Volterra, A. (2014). Gliotransmitters travel in time and space. *Neuron*, 81:728–739.

[Araque et al., 2000] Araque, A., Li, N., Doyle, R. T., and Haydon, P. G. (2000). Snare protein-dependent glutamate release from astrocytes. *The Journal of neuroscience : the official journal of the Society for Neuroscience*, 20:666–673.

[Araque et al., 2002] Araque, A., Martín, E. D., Perea, G., Arellano, J. I., and Buño, W. (2002). Synaptically released acetylcholine evokes ca2+ elevations in astrocytes in hippocampal slices. *The Journal of neuroscience : the official journal of the Society for Neuroscience*, 22:2443–2450.

[Araque et al., 1999] Araque, A., Parpura, V., Sanzgiri, R. P., and Haydon, P. G. (1999). Tripartite synapses: glia, the unacknowledged partner. *Trends in Neurosciences*, 22:208–215.

[Araque et al., 1998] Araque, A., Sanzgiri, R. P., Parpura, V., and Haydon, P. G. (1998). Calcium elevation in astrocytes causes an nmda receptor-dependent increase in the frequency of miniature synaptic currents in cultured hippocampal neurons. *The Journal of neuroscience : the official journal of the Society for Neuroscience*, 18:6822–6829.

[Arizono et al., 2020] Arizono, M., Inavalli, V. V., Panatier, A., Pfeiffer, T., Angibaud, J., Levet, F., Veer, M. J. T. T., Stobart, J., Bellocchio, L., Mikoshiba, K., Marsicano, G., Weber, B., Oliet, S. H. R., and Nägerl, U. V. (2020). Structural basis of astrocytic ca2+ signals at tripartite synapses. *Nature Communications 2020 11:1*, 11:1–15.

[Azevedo et al., 2009] Azevedo, F. A. C., Carvalho, L. R. B., Grinberg, L. T., Farfel, J. M., Ferretti, R. E. L., Leite, R. E. P., Filho, W. J., Lent, R., and Herculano-Houzel, S. (2009). Equal numbers of neuronal and nonneuronal cells make the human brain an isometrically scaled-up primate brain. *The Journal of comparative neurology*, 513:532–541.

[Barker and Baier, 2015] Barker, A. J. and Baier, H. (2015). Sensorimotor decision making in the zebrafish tectum. *Current Biology*, 25:2804–2814.

[Bazargani and Attwell, 2017] Bazargani, N. and Attwell, D. (2017). Amines, astrocytes, and arousal. *Neuron*, 94:228–231.

[Becker and Becker, 2014] Becker, T. and Becker, C. G. (2014). Axonal regeneration in zebrafish. *Current opinion in neurobiology*, 27:186–191.

[Bekar et al., 2008] Bekar, L. K., He, W., and Nedergaard, M. (2008). Locus coeruleus α-adrenergic–mediated activation of cortical astrocytes in vivo. *Cerebral Cortex (New York, NY)*, 18:2789.

[Bene et al., 2010] Bene, F. D., Wyart, C., Robles, E., Tran, A., Looger, L., Scott, E. K., Isacoff, E. Y., and Baier, H. (2010). Filtering of visual information in the tectum by an identified neural circuit. *Science*, 330:669–673.

[Bergeron et al., 2012] Bergeron, S. A., Hannan, M. C., Codore, H., Fero, K., Li, G., Moak, Z., Yokogawa, T., and Burgess, H. A. (2012). Brain selective transgene expression in zebrafish using an nrse derived motif. *Frontiers in Neural Circuits*, 0:110.

[Bernardinelli et al., 2011] Bernardinelli, Y., Salmon, C., Jones, E. V., Farmer, W. T., Stellwagen, D., and Murai, K. K. (2011). Astrocytes display complex and localized calcium responses to single-neuron stimulation in the hippocampus. *The Journal of Neuroscience*, 31:8905.

[Bezzi et al., 2004] Bezzi, P., Gundersen, V., Galbete, J. L., Seifert, G., Steinhäuser, C., Pilati, E., and Volterra, A. (2004). Astrocytes contain a vesicular compartment that is competent for regulated exocytosis of glutamate. *Nature neuroscience*, 7:613–620.

[Bianco et al., 2011] Bianco, I. H., Kampff, A. R., and Engert, F. (2011). Prey capture behavior evoked by simple visual stimuli in larval zebrafish. *Frontiers in Systems Neuroscience*, 5:101.

[Boddum et al., 2016] Boddum, K., Jensen, T. P., Magloire, V., Kristiansen, U., Rusakov, D. A., Pavlov, I., and Walker, M. C. (2016). Astrocytic gaba transporter activity modulates excitatory neurotransmission. *Nature Communications*, 7:1–10.

[Bojarskaite et al.,] Bojarskaite, L., Bjørnstad, D. M., Pettersen, K. H., Cunen, C., Hermansen, G. H., Åbjørsbråten, K. S., Sprengel, R., Vervaeke, K., Tang, W., Enger, R., and Nagelhus, E. A. Ca 2+ signaling in astrocytes is sleep-wake state specific and modulates sleep.

[Borla et al., 2002] Borla, M. A., Palecek, B., Budick, S., and O'Malley, D. M. (2002). Prey capture by larval zebrafish: evidence for fine axial motor control. *Brain, behavior and evolution*, 60:207–229.

[Bradl and Lassmann, 2010] Bradl, M. and Lassmann, H. (2010). Oligodendrocytes: biology and pathology. *Acta Neuropathologica*, 119:37.

[Breton-Provencher et al., 2021] Breton-Provencher, V., Drummond, G. T., and Sur, M. (2021). Locus coeruleus norepinephrine in learned behavior: Anatomical modularity and spatiotemporal integration in targets. *Frontiers in neural circuits*, 15.

[Budick and O'Malley, 2000] Budick, S. A. and O'Malley, D. M. (2000). Locomotor repertoire of the larval zebrafish: swimming, turning and prey capture. *The Journal of experimental biology*, 203:2565–2579.

[Bushong et al., 2002] Bushong, E. A., Martone, M. E., Jones, Y. Z., and Ellisman, M. H. (2002). Protoplasmic astrocytes in ca1 stratum radiatum occupy separate anatomical domains. *The Journal of neuroscience : the official journal of the Society for Neuroscience*, 22:183–192.

[Buss and Drapeau, 2001] Buss, R. R. and Drapeau, P. (2001). Synaptic drive to motoneurons during fictive swimming in the developing zebrafish. *Journal of neurophysiology*, 86:197–210.

[Candelier et al., 2015] Candelier, R., Murmu, M. S., Romano, S. A., Jouary, A., Debrégeas, G., and Sumbre, G. (2015). A microfluidic device to study neuronal and motor responses to acute chemical stimuli in zebrafish. *Scientific reports*, 5.

[Carter et al., 2010] Carter, M. E., Yizhar, O., Chikahisa, S., Nguyen, H., Adamantidis, A., Nishino, S., Deisseroth, K., and Lecea, L. D. (2010). Tuning arousal with optogenetic modulation of locus coeruleus neurons. *Nature Neuroscience 2010 13:12*, 13:1526–1533.

[Chen et al., 2020] Chen, J., Poskanzer, K. E., Freeman, M. R., and Monk, K. R. (2020). Live-imaging of astrocyte morphogenesis and function in zebrafish neural circuits. *Nature neuroscience*, 23:1297–1306.

[Chen et al., 2013] Chen, T.-W., Wardill, T. J., Sun, Y., Pulver, S. R., Renninger, S. L., Baohan, A., Schreiter, E. R., Kerr, R. A., Orger, M. B., Jayaraman, V., Looger, L. L., Svoboda, K., and Kim, D. S. (2013). Ultrasensitive fluorescent proteins for imaging neuronal activity. *Nature*, 499:295–300.

[Colwill and Creton, 2011] Colwill, R. M. and Creton, R. (2011). Imaging escape and avoidance behavior in zebrafish larvae. *Reviews in the Neurosciences*, 22:63–73.

[Cornell-Bell et al., 1990] Cornell-Bell, A. H., Finkbeiner, S. M., Cooper, M. S., and Smith, S. J. (1990). Glutamate induces calcium waves in cultured astrocytes: long-range glial signaling. *Science (New York, N.Y.)*, 247:470–473.

[Curreli et al., 2022] Curreli, S., Bonato, J., Romanzi, S., Panzeri, S., and Fellin, T. (2022). Complementary encoding of spatial information in hippocampal astrocytes. *PLoS Biology*, 20.

[Dallérac et al., 2018] Dallérac, G., Zapata, J., and Rouach, N. (2018). Versatile control of synaptic circuits by astrocytes: where, when and how? *Nature Reviews Neuroscience 2018 19:12*, 19:729–743.

[Davalos et al., 2020] Davalos, D., Akassoglou, K., and Cardona, A. E. (2020). Microglia. *Patterning and Cell Type Specification in the Developing CNS and PNS*, pages 995–1020.

[DeMarco et al., 2020] DeMarco, E., Xu, N., Baier, H., and Robles, E. (2020). Neuron types in the zebrafish optic tectum labeled by an id2b transgene. *Journal of Comparative Neurology*, 528:1173–1188.

[Devilbiss and Waterhouse, 2011] Devilbiss, D. M. and Waterhouse, B. D. (2011). Phasic and tonic patterns of locus coeruleus output differentially modulate sensory network function in the awake rat. *Journal of Neurophysiology*, 105:69.

[Dimou and Gallo, 2015] Dimou, L. and Gallo, V. (2015). Ng2-glia and their functions in the central nervous system. *Glia*, 63:1429.

[Ding et al., 2013] Ding, F., O'Donnell, J., Thrane, A. S., Zeppenfeld, D., Kang, H., Xie, L., Wang, F., and Nedergaard, M. (2013). α1-adrenergic receptors mediate coordinated ca2+ signaling of cortical astrocytes in awake, behaving mice. *Cell calcium*, 54:387–394.

[Doengi et al., 2009] Doengi, M., Hirnet, D., Coulon, P., Pape, H. C., Deitmer, J. W., and Lohr, C. (2009). Gaba uptake-dependent ca(2+) signaling in developing olfactory bulb astrocytes. *Proceedings of the National Academy of Sciences of the United States of America*, 106:17570–17575.

[Dunn et al., 2016] Dunn, T. W., Mu, Y., Narayan, S., Randlett, O., Naumann, E. A., Yang, C. T., Schier, A. F., Freeman, J., Engert, F., and Ahrens, M. B. (2016). Brain-wide mapping of neural activity controlling zebrafish exploratory locomotion. *eLife*, 5:1–29.

[Durkee and Araque, 2019] Durkee, C. A. and Araque, A. (2019). Diversity and specificity of astrocyte-neuron communication. *Neuroscience*, 396:73.

[Easter and Nicola, 1997] Easter, S. S. and Nicola, G. N. (1997). The development of eye movements in the zebrafish (danio rerio). *Developmental psychobiology*, 31:267–276.

[Easter and Nicola, 1996] Easter, S. S. J. and Nicola, G. N. (1996). The development of vision in the zebrafish. *Developmental biology*, 180:646–663.

[Eder and Bading, 2007] Eder, A. and Bading, H. (2007). Calcium signals can freely cross the nuclear envelope in hippocampal neurons: Somatic calcium increases generate nuclear calcium transients. *BMC Neuroscience*, 8:1–11.

[Ehmsen et al., 2013] Ehmsen, J. T., Ma, T. M., Sason, H., Rosenberg, D., Ogo, T., Furuya, S., Snyder, S. H., and Wolosker, H. (2013). D-serine in glia and neurons derives from 3-phosphoglycerate dehydrogenase. *The Journal of neuroscience : the official journal of the Society for Neuroscience*, 33:12464–12469.

[Fiacco and McCarthy, 2004] Fiacco, T. A. and McCarthy, K. D. (2004). Intracellular astrocyte calcium waves in situ increase the frequency of spontaneous ampa receptor currents in ca1 pyramidal neurons. *The Journal of neuroscience : the official journal of the Society for Neuroscience*, 24:722–732.

[Fischer and Reh, 2003] Fischer, A. J. and Reh, T. A. (2003). Potential of müller glia to become neurogenic retinal progenitor cells. *Glia*, 43:70–76.

[Florian et al., 2011] Florian, C., Vecsey, C. G., Halassa, M. M., Haydon, P. G., and Abel, T. (2011). Astrocyte-derived adenosine and a1 receptor activity contribute to sleep loss-induced deficits in hippocampal synaptic plasticity and memory in mice. *The Journal of neuroscience : the official journal of the Society for Neuroscience*, 31:6956–6962.

[Friedrich et al., 2010] Friedrich, R. W., Jacobson, G. A., and Zhu, P. (2010). Circuit neuroscience in zebrafish. *Current Biology*, 20:R371–R381.

[Förster et al., 2020] Förster, D., Helmbrecht, T. O., Mearns, D. S., Jordan, L., Mokayes, N., and Baier, H. (2020). Retinotectal circuitry of larval zebrafish is adapted to detection and pursuit of prey. *eLife*, 9:1–26.

[Gabriel et al., 2012] Gabriel, J. P., Trivedi, C. A., Maurer, C. M., Ryu, S., and Bollmann, J. H. (2012). Layer-specific targeting of direction-selective neurons in the zebrafish optic tectum. *Neuron*, 76:1147–1160.

[Gahtan, 2005] Gahtan, E. (2005). Visual prey capture in larval zebrafish is controlled by identified reticulospinal neurons downstream of the tectum. *The Journal of neuroscience : the official journal of the Society for Neuroscience*, 25:9294–9303.

[Giaume et al., 2010] Giaume, C., Koulakoff, A., Roux, L., Holcman, D., and Rouach, N. (2010). Astroglial networks: a step further in neuroglial and gliovascular interactions. *Nature Reviews Neuroscience 2010 11:2*, 11:87–99.

[Gordon et al., 2005] Gordon, G. R., Baimoukhametova, D. V., Hewitt, S. A., Rajapaksha, W. R. J., Fisher, T. E., and Bains, J. S. (2005). Norepinephrine triggers release of glial atp to increase postsynaptic efficacy. *Nature Neuroscience 2005 8:8*, 8:1078–1086.

[Grama and Engert, 2012] Grama, A. and Engert, F. (2012). Direction selectivity in the larval zebrafish tectum is mediated by asymmetric inhibition. *Frontiers in Neural Circuits*, 6:1–9.

[Grupp et al., 2010] Grupp, L., Wolburg, H., and Mack, A. F. (2010). Astroglial structures in the zebrafish brain. *The Journal of comparative neurology*, 518:4277–4287.

[Guerra-Gomes et al., 2018] Guerra-Gomes, S., Sousa, N., Pinto, L., and Oliveira, J. F. (2018). Functional roles of astrocyte calcium elevations: From synapses to behavior. *Frontiers in Cellular Neuroscience*, 11:427.

[Hamilton, 1822] Hamilton, F. (1822). *An account of the fishes found in the river Ganges and its branches.* Printed for A. Constable and company;.

[Hamilton and Attwell, 2010] Hamilton, N. B. and Attwell, D. (2010). Do astrocytes really exocytose neurotransmitters? *Nature reviews. Neuroscience*, 11:227–238.

[Han et al., 2013] Han, X., Chen, M., Wang, F., Windrem, M., Wang, S., Shanz, S., Xu, Q., Oberheim, N. A., Bekar, L., Betstadt, S., Silva, A. J., Takano, T., Goldman, S. A., and Nedergaard, M. (2013). Forebrain engraftment by human glial progenitor cells enhances synaptic plasticity and learning in adult mice. *Cell stem cell*, 12:342–353.

[Hardingham et al., 2001] Hardingham, G. E., Arnold, F. J. L., and Bading, H. (2001). Nuclear calcium signaling controls creb-mediated gene expression triggered by synaptic activity. *Nature Neuroscience*, 4:261–267.

[Harper and Lawrence, 2010] Harper, C. and Lawrence, C. (2010). *The Laboratory Zebrafish*. CRC Press.

[Hayat et al., 2020] Hayat, H., Regev, N., Matosevich, N., Sales, A., Paredes-Rodriguez, E., Krom, A. J., Bergman, L., Li, Y., Lavigne, M., Kremer, E. J., Yizhar, O., Pickering, A. E., and Nir, Y. (2020). Locus coeruleus norepinephrine activity mediates sensory-evoked awakenings from sleep. *Science Advances*, 6.

[Helmbrecht et al., 2018] Helmbrecht, T. O., Maschio, M. D., Donovan, J. C., Koutsouli, S., and Baier, H. (2018). Topography of a visuomotor transformation. *Neuron*, 100:1429—-1445.e4.

[Henneberger et al., 2010] Henneberger, C., Papouin, T., Oliet, S. H. R., and Rusakov, D. A. (2010). Long term potentiation depends on release of d-serine from astrocytes. *Nature*, 463:232.

[Howe et al., 2013] Howe, K., Clark, M. D., Torroja, C. F., Torrance, J., Berthelot, C., Muffato, M., Collins, J. E., Humphray, S., McLaren, K., Matthews, L., McLaren, S.,

Sealy, I., Caccamo, M., Churcher, C., Scott, C., Barrett, J. C., Koch, R., Rauch, G.-J., White, S., Chow, W., Kilian, B., Quintais, L. T., Guerra-Assunção, J. A., Zhou, Y., Gu, Y., Yen, J., hinnerk Vogel, J., Eyre, T., Redmond, S., Banerjee, R., Chi, J., Fu, B., Langley, E., Maguire, S. F., Laird, G. K., Lloyd, D., Kenyon, E., Donaldson, S., Sehra, H., Almeida-King, J., Loveland, J., Trevanion, S., Jones, M., Quail, M., Willey, D., Hunt, A., Burton, J., Sims, S., McLay, K., Plumb, B., Davis, J., Clee, C., Oliver, K., Clark, R., Riddle, C., Elliott, D., Threadgold, G., Harden, G., Ware, D., Begum, S., Mortimore, B., Kerry, G., Heath, P., Phillimore, B., Tracey, A., Corby, N., Dunn, M., Johnson, C., Wood, J., Clark, S., Pelan, S., Griffiths, G., Smith, M., Glithero, R., Howden, P., Barker, N., Lloyd, C., Stevens, C., Harley, J., Holt, K., Panagiotidis, G., Lovell, J., Beasley, H., Henderson, C., Gordon, D., Auger, K., Wright, D., Collins, J., Raisen, C., Dyer, L., Leung, K., Robertson, L., Ambridge, K., Leongamornlert, D., McGuire, S., Gilderthorp, R., Griffiths, C., Manthravadi, D., Nichol, S., Barker, G., Whitehead, S., Kay, M., Brown, J., Murnane, C., Gray, E., Humphries, M., Sycamore, N., Barker, D., Saunders, D., Wallis, J., Babbage, A., Hammond, S., Mashreghi-Mohammadi, M., Barr, L., Martin, S., Wray, P., Ellington, A., Matthews, N., Ellwood, M., Woodmansey, R., Clark, G., Cooper, J. D., Tromans, A., Grafham, D., Skuce, C., Pandian, R., Andrews, R., Harrison, E., Kimberley, A., Garnett, J., Fosker, N., Hall, R., Garner, P., Kelly, D., Bird, C., Palmer, S., Gehring, I., Berger, A., Dooley, C. M., Ersan-Ürün, Z., Eser, C., Geiger, H., Geisler, M., Karotki, L., Kirn, A., Konantz, J., Konantz, M., Oberländer, M., Rudolph-Geiger, S., Teucke, M., Lanz, C., Raddatz, G., Osoegawa, K., Zhu, B., Rapp, A., Widaa, S., Langford, C., Yang, F., Schuster, S. C., Carter, N. P., Harrow, J., Ning, Z., Herrero, J., Searle, S. M. J., Enright, A., Geisler, R., Plasterk, R. H. A., Lee, C., Westerfield, M., de Jong, P. J., Zon, L. I., Postlethwait, J. H., Nüsslein-Volhard, C., Hubbard, T. J. P., Crollius, H. R., Rogers, J., and Stemple, D. L. (2013). The zebrafish reference genome sequence and its relationship to the human genome. *Nature*, 496:498–503.

[Huang and Neuhauss, 2008] Huang, Y.-Y. and Neuhauss, S. C. F. (2008). The optokinetic response in zebrafish and its applications. *Frontiers in bioscience : a journal and virtual library*, 13:1899–1916.

[Hubbard and Binder, 2016] Hubbard, J. A. and Binder, D. K. (2016). Chapter 1 - history of astrocytes.

[Hunter et al., 2013] Hunter, P. R., Lowe, A. S., Thompson, I. D., and Meyer, M. P. (2013). Emergent properties of the optic tectum revealed by population analysis of direction and orientation selectivity. *Journal of Neuroscience*, 33:13940–13945.

[Jennings et al., 2017] Jennings, A., Tyurikova, O., Bard, L., Zheng, K., Semyanov, A., Henneberger, C., and Rusakov, D. A. (2017). Dopamine elevates and lowers astroglial

ca2+ through distinct pathways depending on local synaptic circuitry. *Glia*, 65:447–459.

[Jouary et al., 2016] Jouary, A., Haudrechy, M., Candelier, R., and Sumbre, G. (2016). A 2d virtual reality system for visual goal-driven navigation in zebrafish larvae. *Scientific reports*, 6.

[Jourdain et al., 2007] Jourdain, P., Bergersen, L. H., Bhaukaurally, K., Bezzi, P., Santello, M., Domercq, M., Matute, C., Tonello, F., Gundersen, V., and Volterra, A. (2007). Glutamate exocytosis from astrocytes controls synaptic strength. *Nature Neuroscience 2007 10:3*, 10:331–339.

[Jurisch-Yaksi et al., 2020] Jurisch-Yaksi, N., Yaksi, E., and Kizil, C. (2020). Radial glia in the zebrafish brain: Functional, structural, and physiological comparison with the mammalian glia. *Glia*, 68:2451–2470.

[Kang et al., 2013] Kang, N., Peng, H., Yu, Y., Stanton, P. K., Guilarte, T. R., and Kang, J. (2013). Astrocytes release d-serine by a large vesicle. *Neuroscience*, 240:243.

[Karlsson et al., 2001] Karlsson, J., Hofsten, J. V., and Olsson, P. E. (2001). Generating transparent zebrafish: A refined method to improve detection of gene expression during embryonic development. *Marine Biotechnology*, 3:522–527.

[Kartvelishvily et al., 2006] Kartvelishvily, E., Shleper, M., Balan, L., Dumin, E., and Wolosker, H. (2006). Neuron-derived d-serine release provides a novel means to activate n-methyl-d-aspartate receptors. *The Journal of biological chemistry*, 281:14151–14162.

[Katz et al., 2018] Katz, M., Corson, F., Iwanir, S., Biron, D., and Shaham, S. (2018). Glia modulate a neuronal circuit for locomotion suppression during sleep in c. elegans. *Cell Reports*, 22:2575–2583.

[Kawashima et al., 2016] Kawashima, T., Zwart, M. F., Yang, C.-T., Mensh, B. D., and Ahrens, M. B. (2016). The serotonergic system tracks the outcomes of actions to mediate short-term motor learning. *Cell*, 167:933–946.e20.

[Kettenmann and Verkhratsky, 2008] Kettenmann, H. and Verkhratsky, A. (2008). Neuroglia: the 150 years after. *Trends in Neurosciences*, 31:653–659.

[Khakh and McCarthy, 2015] Khakh, B. S. and McCarthy, K. D. (2015). Astrocyte calcium signaling: From observations to functions and the challenges therein. *Cold Spring Harbor Perspectives in Biology*, 7.

[Kofuji and Araque, 2021a] Kofuji, P. and Araque, A. (2021a). Astrocytes and behavior. *Annual review of neuroscience*, 44:49–67.

[Kofuji and Araque, 2021b] Kofuji, P. and Araque, A. (2021b). G-protein-coupled receptors in astrocyte-neuron communication. *Neuroscience*, 456:71–84.

[Kohro et al., 2020] Kohro, Y., Matsuda, T., Yoshihara, K., Kohno, K., Koga, K., Katsuragi, R., Oka, T., Tashima, R., Muneta, S., Yamane, T., Okada, S., Momokino, K., Furusho, A., Hamase, K., Oti, T., Sakamoto, H., Hayashida, K., Kobayashi, R., Horii, T., Hatada, I., Tozaki-Saitoh, H., Mikoshiba, K., Taylor, V., Inoue, K., and Tsuda, M. (2020). Spinal astrocytes in superficial laminae gate brainstem descending control of mechanosensory hypersensitivity. *Nature neuroscience*, 23:1376–1387.

[Kozlov et al., 2006] Kozlov, A. S., Angulo, M. C., Audinat, E., and Charpak, S. (2006). Target cell-specific modulation of neuronal activity by astrocytes. *Proceedings of the National Academy of Sciences*, 103:10058–10063.

[Kroehne et al., 2011] Kroehne, V., Freudenreich, D., Hans, S., Kaslin, J., and Brand, M. (2011). Regeneration of the adult zebrafish brain from neurogenic radial glia-type progenitors. *Development (Cambridge, England)*, 138:4831–4841.

[Kwak et al., 2020] Kwak, H., Koh, W., Kim, S., Song, K., Shin, J. I., Lee, J. M., Lee, E. H., Bae, J. Y., Ha, G. E., Oh, J. E., Park, Y. M., Kim, S., Feng, J., Lee, S. E., Choi, J. W., Kim, K. H., Kim, Y. S., Woo, J., Lee, D., Son, T., Kwon, S. W., Park, K. D., Yoon, B. E., Lee, J., Li, Y., Lee, H., Bae, Y. C., Lee, C. J., and Cheong, E. (2020). Astrocytes control sensory acuity via tonic inhibition in the thalamus. *Neuron*, 108:691–706.e10.

[Lalo et al., 2011] Lalo, U., Pankratov, Y., Parpura, V., and Verkhratsky, A. (2011). Ionotropic receptors in neuronal–astroglial signalling: What is the role of "excitable" molecules in non-excitable cells. *Biochimica et Biophysica Acta (BBA) - Molecular Cell Research*, 1813:992–1002.

[Lee et al., 2010] Lee, S., Yoon, B. E., Berglund, K., Oh, S. J., Park, H., Shin, H. S., Augustine, G. J., and Lee, C. J. (2010). Channel-mediated tonic gaba release from glia. *Science (New York, N.Y.)*, 330:790–796.

[Lia et al., 2021] Lia, A., Henriques, V. J., Zonta, M., Chiavegato, A., Carmignoto, G., Gómez-Gonzalo, M., and Losi, G. (2021). Calcium signals in astrocyte microdomains, a decade of great advances. *Frontiers in Cellular Neuroscience*, 15:177.

[Lin and Schnitzer, 2016] Lin, M. Z. and Schnitzer, M. J. (2016). Genetically encoded indicators of neuronal activity. *Nature neuroscience*, 19:1142–1153.

[Lines et al., 2020] Lines, J., Martin, E. D., Kofuji, P., Aguilar, J., and Araque, A. (2020). Astrocytes modulate sensory-evoked neuronal network activity. *Nature Communications 2020 11:1*, 11:1–12.

[Lister et al., 1999] Lister, J. A., Robertson, C. P., Lepage, T., Johnson, S. L., and Raible, D. W. (1999). Nacre encodes a zebrafish microphthalmia-related protein that regulates neural-crest-derived pigment cell fate. *Development*, 126:3757–3767.

[Lojowska et al., 2015] Lojowska, M., Gladwin, T. E., Hermans, E. J., and Roelofs, K. (2015). Freezing promotes perception of coarse visual features. *Journal of experimental psychology. General*, 144:1080–1088.

[Lyons and Talbot, 2015] Lyons, D. A. and Talbot, W. S. (2015). Glial cell development and function in zebrafish. *Cold Spring Harbor Perspectives in Biology*, 7.

[Malarkey et al., 2008] Malarkey, E. B., Ni, Y., and Parpura, V. (2008). Ca2+ entry through trpc1 channels contributes to intracellular ca2+ dynamics and consequent glutamate release from rat astrocytes. *Glia*, 56:821–835.

[Marques et al., 2018] Marques, J. C., Lackner, S., Félix, R., and Orger, M. B. (2018). Structure of the zebrafish locomotor repertoire revealed with unsupervised behavioral clustering. *Current biology : CB*, 28:181–195.e5.

[Martín et al., 2007] Martín, E. D., Fernández, M., Perea, G., Pascual, O., Haydon, P. G., Araque, A., and Ceña, V. (2007). Adenosine released by astrocytes contributes to hypoxia-induced modulation of synaptic transmission. *Glia*, 55:36–45.

[Matos et al., 2018] Matos, M., Bosson, A., Riebe, I., Reynell, C., Vallée, J., Laplante, I., Panatier, A., Robitaille, R., and Lacaille, J. C. (2018). Astrocytes detect and upregulate transmission at inhibitory synapses of somatostatin interneurons onto pyramidal cells. *Nature communications*, 9.

[Mazaud et al., 2021] Mazaud, D., Capano, A., and Rouach, N. (2021). The many ways astroglial connexins regulate neurotransmission and behavior. *Glia*, 69:2527–2545.

[Mederos and Perea, 2019] Mederos, S. and Perea, G. (2019). Gabaergic-astrocyte signaling: A refinement of inhibitory brain networks. *Glia*, 67:1842.

[Meriney and Fanselow, 2019] Meriney, S. D. and Fanselow, E. E. (2019). Ionotropic receptors. *Synaptic Transmission*, pages 215–243.

[Min and Nevian, 2012] Min, R. and Nevian, T. (2012). Astrocyte signaling controls spike timing–dependent depression at neocortical synapses. *Nature Neuroscience 2012 15:5*, 15:746–753.

[Mirat et al., 2013] Mirat, O., Sternberg, J. R., Severi, K. E., and Wyart, C. (2013). Zebrazoom: An automated program for high-throughput behavioral analysis and categorization. *Frontiers in Neural Circuits*, 7.

[Mu et al., 2019] Mu, Y., Bennett, D. V., Rubinov, M., Narayan, S., Yang, C.-T., Tanimoto, M., Mensh, B. D., Looger, L. L., and Ahrens, M. B. (2019). Glia accumulate evidence that actions are futile and suppress unsuccessful behavior.

[Muto et al., 2013] Muto, A., Ohkura, M., Abe, G., Nakai, J., and Kawakami, K. (2013). Real-time visualization of neuronal activity during perception. *Current biology : CB*, 23:307–311.

[Müller and Kettenmann, 1995] Müller, T. and Kettenmann, H. (1995). Physiology of bergmann glial cells. *International review of neurobiology*, 38:341–350.

[Nagai et al., 2019] Nagai, J., Rajbhandari, A. K., Gangwani, M. R., Hachisuka, A., Coppola, G., Masmanidis, S. C., Fanselow, M. S., and Khakh, B. S. (2019). Hyperactivity with disrupted attention by activation of an astrocyte synaptogenic cue. *Cell*, 177:1280–1292.e20.

[Nagai et al., 2021] Nagai, J., Yu, X., Papouin, T., Cheong, E., Freeman, M. R., Monk, K. R., Hastings, M. H., Haydon, P. G., Rowitch, D., Shaham, S., and Khakh, B. S. (2021). Behaviorally consequential astrocytic regulation of neural circuits. *Neuron*, 109:576–596.

[Navarrete and Araque, 2008] Navarrete, M. and Araque, A. (2008). Endocannabinoids mediate neuron-astrocyte communication. *Neuron*, 57:883–893.

[Navarrete et al., 2012] Navarrete, M., Perea, G., de Sevilla, D. F., Gómez-Gonzalo, M., Núñez, A., Martín, E. D., and Araque, A. (2012). Astrocytes mediate in vivo cholinergic-induced synaptic plasticity. *PLOS Biology*, 10:e1001259.

[Nedergaard et al., 2004] Nedergaard, M., Liu, Q. S., Xu, Q., and Kang, J. (2004). Astrocyte activation of presynaptic metabotropic glutamate receptors modulates hippocampal inhibitory synaptic transmission. *Neuron glia biology*, 1:307–316.

[Neuhauss et al., 1999] Neuhauss, S. C., Biehlmaier, O., Seeliger, M. W., Das, T., Kohler, K., Harris, W. A., and Baier, H. (1999). Genetic disorders of vision revealed by a behavioral screen of 400 essential loci in zebrafish. *The Journal of neuroscience : the official journal of the Society for Neuroscience*, 19:8603–8615.

[Nevin et al., 2010] Nevin, L. M., Robles, E., Baier, H., and Scott, E. K. (2010). Focusing on optic tectum circuitry through the lens of genetics. *BMC biology*, 8.

[Nguyen and Connor, 2019] Nguyen, P. V. and Connor, S. A. (2019). Noradrenergic regulation of hippocampus-dependent memory. *Central nervous system agents in medicinal chemistry*, 19:187–196.

[Niell and Smith, 2005] Niell, C. M. and Smith, S. J. (2005). Functional imaging reveals rapid development of visual response properties in the zebrafish tectum. *Neuron*, 45:941–951.

[Niklaus et al., 2017] Niklaus, S., Cadetti, L., Berg-Maurer, C. M. V., Lehnherr, A., Hotz, A. L., Forster, I. C., Gesemann, M., and Neuhauss, S. C. (2017). Shaping of signal transmission at the photoreceptor synapse by eaat2 glutamate transporters. *eNeuro*, 4.

[Nimmerjahn et al., 2009] Nimmerjahn, A., Mukamel, E. A., and Schnitzer, M. J. (2009). Motor behavior activates bergmann glial networks. *Neuron*, 62:400–412.

[Noriega-Prieto and Araque, 2021] Noriega-Prieto, J. A. and Araque, A. (2021). Sensing and regulating synaptic activity by astrocytes at tripartite synapse. *Neurochemical research*, 46:2580–2585.

[Oberheim et al., 2012] Oberheim, N. A., Goldman, S. A., and Nedergaard, M. (2012). Heterogeneity of astrocytic form and function. *Methods in molecular biology (Clifton, N.J.)*, 814:23.

[Oberheim et al., 2009] Oberheim, N. A., Takano, T., Han, X., He, W., Lin, J. H., Wang, F., Xu, Q., Wyatt, J. D., Pilcher, W., Ojemann, J. G., Ransom, B. R., Goldman, S. A., and Nedergaard, M. (2009). Uniquely hominid features of adult human astrocytes. *The Journal of Neuroscience*, 29:3276.

[Oe et al., 2020] Oe, Y., Wang, X., Patriarchi, T., Konno, A., Ozawa, K., Yahagi, K., Hirai, H., Tian, L., McHugh, T. J., and Hirase, H. (2020). Distinct temporal integration of noradrenaline signaling by astrocytic second messengers during vigilance. *Nature communications*, 11.

[Ohno-Shosaku and Kano, 2014] Ohno-Shosaku, T. and Kano, M. (2014). Endocannabinoid-mediated retrograde modulation of synaptic transmission. *Current opinion in neurobiology*, 29:1–8.

[Orts-Del'Immagine et al., 2022] Orts-Del'Immagine, A., Dhanasekar, M., Lejeune, F. X., Roussel, J., and Wyart, C. (2022). A norepinephrine-dependent glial calcium wave travels in the spinal cord upon acoustovestibular stimuli. *Glia*, 70:491–507.

[Palygin et al., 2010] Palygin, O., Lalo, U., Verkhratsky, A., and Pankratov, Y. (2010). Ionotropic nmda and p2x1/5 receptors mediate synaptically induced ca2+ signalling in cortical astrocytes. *Cell calcium*, 48:225–231.

[Panatier et al., 2011] Panatier, A., Vallée, J., Haber, M., Murai, K. K., Lacaille, J. C., and Robitaille, R. (2011). Astrocytes are endogenous regulators of basal transmission at central synapses. *Cell*, 146:785–798.

[Panier et al., 2013] Panier, T., Romano, S. A., Olive, R., Pietri, T., Sumbre, G., Candelier, R., and Debregeas, G. (2013). Fast functional imaging of multiple brain regions in intact zebrafish larvae using selective plane illumination microscopy. *Frontiers in Neural Circuits*, 7:1–11.

[Pankratov and Lalo, 2015] Pankratov, Y. and Lalo, U. (2015). Role for astroglial α1-adrenoreceptors in gliotransmission and control of synaptic plasticity in the neocortex. *Frontiers in Cellular Neuroscience*, 9:1–11.

[Pannasch and Rouach, 2013] Pannasch, U. and Rouach, N. (2013). Emerging role for astroglial networks in information processing: from synapse to behavior. *Trends in neurosciences*, 36:405–417.

[Parichy, 2015] Parichy, D. M. (2015). Advancing biology through a deeper understanding of zebrafish ecology and evolution. *eLife*, 4:1–11.

[Park et al., 2015] Park, H., Han, K. S., Seo, J., Lee, J., Dravid, S. M., Woo, J., Chun, H., Cho, S., Bae, J. Y., An, H., Koh, W., Yoon, B. E., Berlinguer-Palmini, R., Mannaioni, G., Traynelis, S. F., Bae, Y. C., Choi, S. Y., and Lee, C. J. (2015). Channel-mediated astrocytic glutamate modulates hippocampal synaptic plasticity by activating postsynaptic nmda receptors. *Molecular brain*, 8.

[Pascual et al., 2005] Pascual, O., Casper, K. B., Kubera, C., Zhang, J., Revilla-Sanchez, R., Sul, J. Y., Takano, H., Moss, S. J., McCarthy, K., and Haydon, P. G. (2005). Astrocytic purinergic signaling coordinates synaptic networks. *Science (New York, N.Y.)*, 310:113–116.

[Patterson et al., 2013] Patterson, B. W., Abraham, A. O., MacIver, M. A., and McLean, D. L. (2013). Visually guided gradation of prey capture movements in larval zebrafish. *The Journal of experimental biology*, 216:3071–3083.

[Paukert et al., 2014] Paukert, M., Agarwal, A., Cha, J., Doze, V. A., Kang, J. U., and Bergles, D. E. (2014). Norepinephrine controls astroglial responsiveness to local circuit activity. *Neuron*, 82:1263–1270.

[Pelluru et al., 2016] Pelluru, D., Konadhode, R. R., Bhat, N. R., and Shiromani, P. J. (2016). Optogenetic stimulation of astrocytes in the posterior hypothalamus increases sleep at night in c57bl/6j mice. *The European journal of neuroscience*, 43:1298–1306.

[Perea and Araque, 2005] Perea, G. and Araque, A. (2005). Properties of synaptically evoked astrocyte calcium signal reveal synaptic information processing by astrocytes. *Journal of Neuroscience*, 25:2192–2203.

[Perea et al., 2009] Perea, G., Navarrete, M., and Araque, A. (2009). Tripartite synapses: astrocytes process and control synaptic information. *Trends in Neurosciences*, 32:421–431.

[Perez-Catalan et al., 2021] Perez-Catalan, N. A., Doe, C. Q., and Ackerman, S. D. (2021). The role of astrocyte-mediated plasticity in neural circuit development and function. *Neural Development 2021 16:1*, 16:1–14.

[Petravicz et al., 2014] Petravicz, J., Boyt, K. M., and McCarthy, K. D. (2014). Astrocyte ip3r2-dependent ca2+ signaling is not a major modulator of neuronal pathways governing behavior. *Frontiers in Behavioral Neuroscience*, 8:1–13.

[Pinto-Duarte et al., 2019] Pinto-Duarte, A., Roberts, A. J., Ouyang, K., and Sejnowski, T. J. (2019). Impairments in remote memory caused by the lack of type 2 ip 3 receptors. *Glia*, 67:1976–1989.

[Pologruto et al., 2003] Pologruto, T. A., Sabatini, B. L., and Svoboda, K. (2003). Scanimage: Flexible software for operating laser scanning microscopes. *BioMedical Engineering OnLine*, 2:13.

[Ponce-Alvarez et al., 2018] Ponce-Alvarez, A., Jouary, A., Privat, M., Deco, G., and Sumbre, G. (2018). Whole-brain neuronal activity displays crackling noise dynamics. *Neuron*, 100:1446–1459.e6.

[Portugues and Engert, 2009] Portugues, R. and Engert, F. (2009). The neural basis of visual behaviors in the larval zebrafish. *Current opinion in neurobiology*, 19:644–647.

[Pérez-Schuster et al., 2016] Pérez-Schuster, V., Kulkarni, A., Nouvian, M., Romano, S. A., Lygdas, K., Jouary, A., Dippopa, M., Pietri, T., Haudrechy, M., Candat, V., Boulanger-Weill, J., Hakim, V., and Sumbre, G. (2016). Sustained rhythmic brain activity underlies visual motion perception in zebrafish. *Cell Reports*, 17:1098–1112.

[Rajadhyaksha and Manghani, 2002] Rajadhyaksha, M. S. and Manghani, D. (2002). Glial cells: The other cells of the nervous system. *Resonance 2002 7:4*, 7:20–26.

[Rakic, 2009] Rakic, P. (2009). Radial glial cells: Brain functions. *Encyclopedia of Neuroscience*, pages 15–21.

[Robin et al., 2018] Robin, L. M., da Cruz, J. F. O., Langlais, V. C., Martin-Fernandez, M., Metna-Laurent, M., Busquets-Garcia, A., Bellocchio, L., Soria-Gomez, E., Papouin, T., Varilh, M., Sherwood, M. W., Belluomo, I., Balcells, G., Matias, I., Bosier,

B., Drago, F., Eeckhaut, A. V., Smolders, I., Georges, F., Araque, A., Panatier, A., Oliet, S. H. R., and Marsicano, G. (2018). Astroglial cb 1 receptors determine synaptic d-serine availability to enable recognition memory. *Neuron*, 98:935–944.e5.

[Robles et al., 2013] Robles, E., Filosa, A., and Baier, H. (2013). Precise lamination of retinal axons generates multiple parallel input pathways in the tectum. *Journal of Neuroscience*, 33:5027–5039.

[Roeser and Baier, 2003] Roeser, T. and Baier, H. (2003). Visuomotor behaviors in larval zebrafish after gfp-guided laser ablation of the optic tectum. *The Journal of neuroscience : the official journal of the Society for Neuroscience*, 23:3726–3734.

[Romano et al., 2015] Romano, S. A., Pietri, T., Pérez-Schuster, V., Jouary, A., Haudrechy, M., and Sumbre, G. (2015). Spontaneous neuronal network dynamics reveal circuit's functional adaptations for behavior. *Neuron*, 85:1070–1085.

[Romano et al., 2017] Romano, S. A., Pérez-Schuster, V., Jouary, A., Boulanger-Weill, J., Candeo, A., Pietri, T., and Sumbre, G. (2017). An integrated calcium imaging processing toolbox for the analysis of neuronal population dynamics. *PLoS computational biology*, 13:e1005526.

[Rose et al., 2018] Rose, C. R., Felix, L., Zeug, A., Dietrich, D., Reiner, A., and Henneberger, C. (2018). Astroglial glutamate signaling and uptake in the hippocampus. *Frontiers in Molecular Neuroscience*, 10:451.

[Rouach et al., 2008] Rouach, N., Koulakoff, A., Abudara, V., Willecke, K., and Giaume, C. (2008). Astroglial metabolic networks sustain hippocampal synaptic transmission. *Science (New York, N.Y.)*, 322:1551–1555.

[Santello et al., 2012] Santello, M., Calì, C., and Bezzi, P. (2012). Gliotransmission and the tripartite synapse. *Advances in Experimental Medicine and Biology*, 970:307–331.

[Sara, 2009] Sara, S. J. (2009). The locus coeruleus and noradrenergic modulation of cognition. *Nature reviews. Neuroscience*, 10:211–223.

[Savtchouk and Volterra, 2018] Savtchouk, I. and Volterra, A. (2018). Gliotransmission: Beyond black-and-white. *The Journal of neuroscience : the official journal of the Society for Neuroscience*, 38:14–25.

[Schwarz et al., 2017] Schwarz, Y., Zhao, N., Kirchhoff, F., and Bruns, D. (2017). Astrocytes control synaptic strength by two distinct v-snare-dependent release pathways. *Nature neuroscience*, 20:1529–1539.

[Shemesh et al., 2020] Shemesh, O. A., Linghu, C., Piatkevich, K. D., Goodwin, D., Celiker, O. T., Gritton, H. J., Romano, M. F., Gao, R., Yu, C.-C. J., Tseng, H.-A., Bensussen, S., Narayan, S., Yang, C.-T., Freifeld, L., Siciliano, C. A., Gupta, I., Wang, J., Pak, N., Yoon, Y.-G., Ullmann, J. F. P., Guner-Ataman, B., Noamany, H., Sheinkopf, Z. R., Park, W. M., Asano, S., Keating, A. E., Trimmer, J. S., Reimer, J., Tolias, A. S., Bear, M. F., Tye, K. M., Han, X., Ahrens, M. B., and Boyden, E. S. (2020). Precision calcium imaging of dense neural populations via a cell-body-targeted calcium indicator. *Neuron*, 107:470–486.e11.

[Shigetomi et al., 2018] Shigetomi, E., Hirayama, Y. J., Ikenaka, K., Tanaka, K. F., and Koizumi, S. (2018). Role of purinergic receptor p2y1 in spatiotemporal ca2+ dynamics in astrocytes. *Journal of Neuroscience*, 38:1383–1395.

[Shigetomi et al., 2013] Shigetomi, E., Jackson-Weaver, O., Huckstepp, R. T., O'Dell, T. J., and Khakh, B. S. (2013). Trpa1 channels are regulators of astrocyte basal calcium levels and long-term potentiation via constitutive d-serine release. *Journal of Neuroscience*, 33:10143–10153.

[Shimizu et al., 2015] Shimizu, Y., Ito, Y., Tanaka, H., and Ohshima, T. (2015). Radial glial cell-specific ablation in the adult zebrafish brain. *genesis*, 53:431–439.

[Slezak et al., 2019] Slezak, M., Kandler, S., Veldhoven, P. P. V., den Haute, C. V., Bonin, V., and Holt, M. G. (2019). Distinct mechanisms for visual and motor-related astrocyte responses in mouse visual cortex. *Current biology : CB*, 29:3120–3127.e5.

[Sonoda et al., 2018] Sonoda, K., Matsui, T., Bito, H., and Ohki, K. (2018). Astrocytes in the mouse visual cortex reliably respond to visual stimulation. *Biochemical and biophysical research communications*, 505:1216–1222.

[Steiner et al., 2019] Steiner, E., Tata, M., and Frisén, J. (2019). A fresh look at adult neurogenesis. *Nature Medicine*, 25:542–543.

[Stobart et al., 2018] Stobart, J. L., Ferrari, K. D., Barrett, M. J. P., Glück, C., Stobart, M. J., Zuend, M., and Weber, B. (2018). Cortical circuit activity evokes rapid astrocyte calcium signals on a similar timescale to neurons. *Neuron*, 98:726–735.e4.

[Sun et al., 2013] Sun, W., McConnell, E., Pare, J. F., Xu, Q., Chen, M., Peng, W., Lovatt, D., Han, X., Smith, Y., and Nedergaard, M. (2013). Glutamate-dependent neuroglial calcium signaling differs between young and adult brain. *Science (New York, N.Y.)*, 339:197–200.

[Temizer et al., 2015] Temizer, I., Donovan, J. C., Baier, H., and Semmelhack, J. L. (2015). A visual pathway for looming-evoked escape in larval zebrafish. *Current Biology*, 25:1823–1834.

[Thompson et al., 2016] Thompson, A. W., Vanwalleghem, G. C., Heap, L. A., and Scott, E. K. (2016). Functional profiles of visual-, auditory-, and water flow-responsive neurons in the zebrafish tectum. *Current Biology*, 26:743–754.

[Ung et al., 2021] Ung, K., Huang, T. W., Lozzi, B., Woo, J., Hanson, E., Pekarek, B., Tepe, B., Sardar, D., Cheng, Y. T., Liu, G., Deneen, B., and Arenkiel, B. R. (2021). Olfactory bulb astrocytes mediate sensory circuit processing through sox9 in the mouse brain. *Nature Communications 2021 12:1*, 12:1–15.

[Ung et al., 2020] Ung, K., Tepe, B., Pekarek, B., Arenkiel, B. R., and Deneen, B. (2020). Parallel astrocyte calcium signaling modulates olfactory bulb responses. *Journal of neuroscience research*, 98:1605.

[Verdugo et al., 2019] Verdugo, C. D., Myren-Svelstad, S., Aydin, E., Hoeymissen, E. V., Deneubourg, C., Vanderhaeghe, S., Vancraeynest, J., Pelgrims, R., Cosacak, M. I., Muto, A., Kizil, C., Kawakami, K., Jurisch-Yaksi, N., and Yaksi, E. (2019). Glia-neuron interactions underlie state transitions to generalized seizures. *Nature communications*, 10.

[Verkhratsky et al., 2019a] Verkhratsky, A., Ho, M. S., and Parpura, V. (2019a). Evolution of neuroglia. *Advances in Experimental Medicine and Biology*, 1175:15–44.

[Verkhratsky et al., 2019b] Verkhratsky, A., Ho, M. S., Vardjan, N., Zorec, R., and Parpura, V. (2019b). General pathophysiology of astroglia. *Advances in Experimental Medicine and Biology*, 1175:149–179.

[Verkhratsky et al., 2019c] Verkhratsky, A., Ho, M. S., Zorec, R., and Parpura, V. (2019c). The concept of neuroglia. *Advances in Experimental Medicine and Biology*, 1175:1–13.

[Verkhratsky and Steinhäuser, 2000] Verkhratsky, A. and Steinhäuser, C. (2000). Ion channels in glial cells. *Brain research. Brain research reviews*, 32:380–412.

[Verkhratsky et al., 2017] Verkhratsky, A., Zorec, R., and Parpura, V. (2017). Stratification of astrocytes in healthy and diseased brain. *Brain pathology (Zurich, Switzerland)*, 27:629–644.

[von Bartheld et al., 2016] von Bartheld, C. S., Bahney, J., and Herculano-Houzel, S. (2016). The search for true numbers of neurons and glial cells in the human brain: A review of 150 years of cell counting. *The Journal of comparative neurology*, 524:3865.

[Wahis and Holt, 2021] Wahis, J. and Holt, M. G. (2021). Astrocytes, noradrenaline, α1-adrenoreceptors, and neuromodulation: Evidence and unanswered questions. *Frontiers in Cellular Neuroscience*, 15.

[Wang et al., 2012] Wang, F., Smith, N. A., Xu, Q., Fujita, T., Baba, A., Matsuda, T., Takano, T., Bekar, L., and Nedergaard, M. (2012). Astrocytes modulate neural network activity by ca²+-dependent uptake of extracellular k+. *Science signaling*, 5.

[Wang et al., 2006] Wang, X., Lou, N., Xu, Q., Tian, G. F., Peng, W. G., Han, X., Kang, J., Takano, T., and Nedergaard, M. (2006). Astrocytic ca2+ signaling evoked by sensory stimulation in vivo. *Nature neuroscience*, 9:816–823.

[Winters and Vaughan, 2021] Winters, B. L. and Vaughan, C. W. (2021). Mechanisms of endocannabinoid control of synaptic plasticity. *Neuropharmacology*, 197.

[Witcher et al., 2007] Witcher, M. R., Kirov, S. A., and Harris, K. M. (2007). Plasticity of perisynaptic astroglia during synaptogenesis in the mature rat hippocampus. *Glia*, 55:13–23.

[Woo et al., 2018] Woo, J., Min, J. O., Kang, D. S., Kim, Y. S., Jung, G. H., Park, H. J., Kim, S., An, H., Known, J., Kim, J., Shim, I., Kim, H. G., Lee, C. J., and Yoon, B. E. (2018). Control of motor coordination by astrocytic tonic gaba release through modulation of excitation/inhibition balance in cerebellum. *Proceedings of the National Academy of Sciences of the United States of America*, 115:5004–5009.

[Xin et al., 2018] Xin, W., Schuebel, K. E., wing Jair, K., Cimbro, R., Biase, L. M. D., Goldman, D., and Bonci, A. (2018). Ventral midbrain astrocytes display unique physiological features and sensitivity to dopamine d2 receptor signaling. *Neuropsychopharmacology 2018 44:2*, 44:344–355.

[Yarishkin et al., 2015] Yarishkin, O., Lee, J., Jo, S., Hwang, E. M., and Lee, C. J. (2015). Disinhibitory action of astrocytic gaba at the perforant path to dentate gyrus granule neuron synapse reverses to inhibitory in alzheimer's disease model. *Experimental Neurobiology*, 24:211–218.

[Zada et al., 2019] Zada, D., Bronshtein, I., Lerer-Goldshtein, T., Garini, Y., and Appelbaum, L. (2019). Sleep increases chromosome dynamics to enable reduction of accumulating dna damage in single neurons. *Nature Communications 2019 10:1*, 10:1–12.

[Zhang et al., 2003] Zhang, J. M., Wang, H. K., Ye, C. Q., Ge, W., Chen, Y., Jiang, Z. L., Wu, C. P., Poo, M. M., and Duan, S. (2003). Atp released by astrocytes mediates glutamatergic activity-dependent heterosynaptic suppression. *Neuron*, 40:971–982.

[Zhou et al., 2019] Zhou, B., Zuo, Y. X., and Jiang, R. T. (2019). Astrocyte morphology: Diversity, plasticity, and role in neurological diseases. *CNS Neuroscience Therapeutics*, 25:665–673.

RÉSUMÉ

De récentes recherches suggèrent que l'activité cérébrale et les comportements complexes sont contrôlés non seulement par l'activité neuronale, mais plutôt par l'interaction entre le réseau neuro-astrocytaire et leur rôle dans la modulation de la perception est inconnu. Pour explorer ces interactions dans le traitement visuel, nous avons utilisé la microscopie à deux photons pour imager des larves de poisson zèbre transgéniques exprimant GCaMP sous le contrôle d'un promoteur glial, pour étudier la dynamique Ca^{2+} des cellules gliales radiales dans le toit optique. Nous avons constaté que l'activité Ca^{2+} des cellules gliales radiales individuelles se synchronise juste après la fin d'un comportement d'échappement. Cette activité synchrone est médiée par le Locus Coeruleus, la principale source de norepinéphrine du cerveau. La synchronisation des cellules gliales radiales tectales se produit dans une couche spécifique du toit optique et module spécifiquement la sélectivité directionnelle des neurones tectaux et leurs corrélations fonctionnelles à longue distance. Ces résultats mettent en lumière le rôle pertinent de l'interaction des cellules gliales radiales tectales dans la modulation du traitement visuel neuronal.

MOTS CLÉS

Larve de poisson zèbre, La Glie Radiale, Le Toit optique.

ABSTRACT

Recent evidence suggest that brain computations and complex behaviours are controlled no only by neuron activity rather by the interaction between neuron-astrocyte network and their role perception modulating is unknown. To explore these interactions in visual processing, we used two-photon microscopy to image transgenic zebrafish larvae expressing GCaMP under the control of a glia promoter, to study Ca^{2+} dynamics of radial glia cells in the optic tectum. We found that the Ca^{2+} activity of individual Radial Glial Cells synchronizes just after the end of an escape behaviour. This synchronous activity is mediated by the locus Coeruleus, the main brain’s source of norepinephrine. Tectal Radial Glial Cells synchronization occurs in a specific layer of the Optic Tectum.Optic Tectum. and specifically modulates the direction selectivity of tectal neurons and their long-distance functional correlations. These results shed light on the relevant role of tectal Radial Glial Cells s interaction in the modulation of neuronal visual processing.

KEYWORDS

Zebrafish Larva, Radial Glia Cell, The Optic Tectum.